SURFACE CHARACTERIZATION OF BIOMASS BY IMAGING MASS SPECTROMETRY

A Dissertation
Presented to
The Academic Faculty

by

Seokwon Jung

In Partial Fulfillment
of the Requirements for the Degree
Doctor of Philosophy in the
School of Chemistry and Biochemistry

Georgia Institute of Technology
December 2012

SURFACE CHARACTERIZATION OF BIOMASS BY IMAGING MASS SPECTROMETRY

Approved by:

Dr. Art J. Ragauskas, Advisor
School of Chemistry and Biochemistry
Georgia Institute of Technology

Dr. Charles L. Liotta
School of Chemistry and Biochemistry
Georgia Institute of Technology

Dr. David M. Collard
School of Chemistry and Biochemistry
Georgia Institute of Technology

Dr. Stefan France
School of Chemistry and Biochemistry
Georgia Institute of Technology

Dr. Yulin Deng
School of Chemical and Biomolecular Engineering
Georgia Institute of Technology

Date Approved: November 06, 2012

ACKNOWLEGMENTS

I would like to express my respectful gratitude to Professor Art J. Ragauskas for his guidance, mentorship, and financial support throughout my graduate career. Under Dr. Ragauskas' guidance, I have learned and accomplished far more than I had imagined at the beginning of my studies. In addition, I also would like to thank my committee members, Prof. Charles Liotta, Prof. David Collard, Prof. Yulin Deng, and Prof. Stefan France, for their patience, encouragement, and advice.

I would like to thank members of the Ragauskas group, past and present, for their friendship, helpful discussions, and collaborations. My special sincere thanks go to Dr. Marcus Foston, Dr. Poulomi Sannigrahi, Dr. Yunqiao Pu, and Dr. Rajalaxmi Dash, and Fan Hu. I am also thankful to Dr. Cam Tyson and Michele Yager for their guidance and supports. I would also like to thank Dr. M. Cameron Sullards, Dr. Yanfeng Chen at Mass Spec Lab and Walter Henderson School at Microelectronic Center, Georgia Institute of Technology for their guidance and discussions. I would also like to thank collaborators at BioEnergy Science Center: Dr. Laurene Tetard, Prof. Heather McKenzie, and Dr. Brian Davison for their tremendous efforts, discussions, and cooperation with me. I also acknowledge the financial support from BioEnergy Science Center at U.S. Department of Energy.

Most importantly, the love and support of my wife Eunkyung, my son Jihoon, my parents, my family, and my friends have provided balance to my life and made my commitment to science possible.

TABLE OF CONTENTS

Page

LIST OF TABLES

Page

LIST OF FIGURES

Page

LIST OF ABBREVATIONS

2D	2-Dimensional
3D	Three-dimensional
AFEX	Ammonia fiber explosion
AFM	Atomic force microscopy
AGX	(Arabino)glucuronoxylan
C	Cellulose
CARS	Coherent anti-Stokes Raman scattering
CC	Cell corner
CHCA	α-Cyano-4-hydroxy-cinnamic acid
CP/MAS	Cross polarization/magic angle spinning
CrI	Crystallinity index
DAP	Dilute acid pretreatment
DHB	2, 5-Dihydroxybenzoic acid
DI	Deionized
DP	Degree of polymerization
DP_n	Number-average degree of polymerization
DP_w	Weight-average degree of polymerization
EM	Electron microscopy
ET	Electron tomography
G	Guaiacyl or coniferyl alcohol
GPC	Gel permeation chromatography
H	*p*-Hydroxyphenyl unit,or *p*-coumaryl alcohol
HMF	5-Hydroxymethyl furfural
HPAEC-PAD	High-performance anion-exchange chromatography with pulsed amperometric detection
HPLC	High-performance liquid chromatography
HW	Hardwood
IMS	Imaging mass spectrometry

IR	Infrared
LCCs	Lignin-carbohydrate complexes
LHW	Liquid hot water
LIMG	Liquid metal ion gun
m/z	Mass-to-charge ratio
MALDI	Matrix-assisted laser desorption/ionization
MCC	Microcrystalline cellulose
ML	Middle lamella
M_n	Number-average molecular weight
MPa	Mega Pascal pressure unit
MS	Mass spectrometry
MSAFM	Mode-synthesizing atomic force microscopy
MW	Molecular weight
M_w	Weight average of molecular weight
Nd:YAG	Neodymium-doped Yttrium aluminum garnet
NMR	Nuclear magnetic resonance
NW	Normal unstressed stems
OW	Stems under tension on the compressed side
PI	Primary ion
PTA	*Populus tremula* x *alba*
ROI	Regions of interest
S	Syringyl unit,or sinapyl alcohol
SA	Sinapinic acid
SCW, S1, S2, S3	Secondary cell wall layer
sDAP	severe Dilute acid pretreatment
SEM	Scanning electron microscopy
SIMS	Secondary ion mass spectrometry
SRS	Stimulated Raman scattering
SW	Softwood
TA solution	10% Acetonitrile and 0.1% trifluoroacetic acid (v/v) in DI water

TEM	Transmission electron microscopy
TOF	Time-of-flight
TW	Stems under tension on the elongated side
UV	Ultraviolet
X	Xylan

SUMMARY

Bioethanol has been highlighted as an alternative renewable energy source, which plays significant roles in reducing greenhouse gas emission and ensuring fuel security. Recently, lignocellulosic biomass (e.g., non food-based agricultural resides and forestry wastes) has been promoted for use as a source of bioethanol instead of food-based materials (e.g., corn and sugar cane), however to fully realize these benefits an improved understanding of lignocellulosic recalcitrance must be developed. Therefore, enhanced characterization methodology is required to measure the chemistry, structure, and interactions of the biomass components and it can contribute to understanding biomass recalcitrance.

In this dissertation, imaging mass spectrometry (IMS) is applied for biomass to characterize the surface upon pretreatment processes. For methodologies development, time of flight secondary mass spectrometry (TOF-SIMS) and matrix-assisted laser desorption/ionization (MALDI) are used for biomass characterization. Juvenile hybrid poplar stem grown in a greenhouse were used as a model substrate.

The first part of this thesis focuses on the development of sample preparation for surface analysis by IMS. A cross sectioned sample is then treated under various methods such as dilute sulfuric acid pretreatment, flowthrough pretreatment, and cellulose isolation. To determine the different chemistry between surface and bulk upon dilute acid pretreatment in batch reactor, TOF-SIMS is firstly applied to characterize the surface of the pretreated

poplar stem in Chapter 5. TOF-SIMS probes the surface of cross sectioned poplar samples, providing two-dimensional (2D) molecular images of major components (i.e., cellulose, hemicelluloses, and lignin) and their relative ion counts. 2D molecular images present the lateral distribution of major components before and after dilute acid pretreatment while the comparison of the relative ions provides semi-quantitative information on the surface. Thereafter, these surface data are compared to bulk chemical composition by sugar analysis in order to prove different chemistry between surface and bulk.

The second part is focused on tracking the lateral lignin distribution on the surface of poplar stem using TOF-SIMS technique developed earlier. Cross sectioned poplar stems are flowthrough pretreated under different conditions, providing different bulk lignin contents. Flowthrough pretreatment provides a number of advantages such as the removal of pretreatment products prior to quenching process thus avoiding precipitation of products. To understand lignin changes at cell wall layers, high resolution TOF-SIMS imaging process is optimized under burst mode. As a result, 2D lignin ion images present the lateral distribution under submicron scale, providing a lignin localized area in cell corner after flowthrough pretreatment. Semi-quantitative information also presents an evidence of different chemistry between surface and bulk upon flowthrough pretreatment process.

The third part is focused on the development of three-dimensional (3D) molecular imaging method using TOF-SIMS. Extending the usefulness of TOF-SIMS for biomass

recalcitrance, a 3D molecular imaging is firsly introduced to biomass by acquiring multiple 2D images in a stack. This is accomplished by reconstruction, stacking the 2D molecular images layer by layer. Consequentially 3D molecular image provides both later and vertical distirbituion of characteristic species from surface to sub-surface. This spatial molecular information can be used to directly determine the chemical change between surface and bulk without relative comparison of other data such as bulk sugar profile. Stress-induced tension wood in poplar stem is used as a model substrate. Tension wood is not only defined by the presence of this gelatinous (G-) layer but also is ideal for demonstrations of chemical imaging because this cellulose rich area can be readily distinguished from the more chemically complex surroundings.

The last part of this thesis is focused on the development and optimization of MALDI-MS/IMS method for insoluble cellulose. MALDI has a capability to detect large molecules (theoretically unlimited) while SIMS can only detect relatively lower mass species. This feature allows detecting different molecular size of cellulose oligomers. Microcrystalline cellulose is used to optimize a cellulose detection protocol such as matrix application. Thereafter, cellulose poplar isolated from holocellulose poplar is introduced to MALDI-MS. To visualize lateral distribution of different DP of cellulose on the surface of poplar stem, a cross-section of cellulose poplar is used. Series of cellulose oligomers in poplar stem are firstly generated using MALDI-IMS.

CHAPTER 1

INTRODUCTION

Due to the uncertainty of future fossil-based fuel reserves, increasing of energy consumption and greenhouse gas emission, alternative renewable energy sources such as biofuel and solar cell energy have been highlighted.[1-2] Biofuel, a promising renewable energy source, has been promoted to replace a primary energy source (i.e., fossil fuel) since it can reduce greenhouse gas emission and contribute to energy security.[3] For this reason, many countries worldwide have set the goal to increase biofuel consumption, especially for transportation fuel. For example, The U.S. Department of Energy has made a plan to replace 30% of petroleum-based liquid transportation fuel with biofuels by 2025. The European Union has also proposed a genuine action plan aimed at increasing the share of biofuels to more than 20 % of European petrol and diesel consumption by 2020.[4-6]

Second-generation biofuel produced from biomass is more sustainable compared to first-generation biofuel made up of food commodities (e.g., corn and sugar cane).[7-8] With respect to biofuel production, the term biomass generally refers to non food-based lignocellulosic feedstocks available from plants and plant-derived materials.[9] These resources are ultimately renewable and sustainable. Therefore, biofuel production produced from lignocellulosic biomass is very attractive; however, it still has economic and technical obstacles.[10-11]

Lignocellulosic biomass has a physically rigid and chemically complex structure which is mainly composed of cellulose, hemicelluloses, and lignin polymers.[1,12-14] The natural resistance of the plant cell wall has evolved for survival to resist the microbial and enzymatic deconstruction of cellulose, referred to as biomass recalcitrance with respect to biofuel production. Biomass recalcitrance is largely responsible for high cost of lignocellulose conversion due to additional time, additives, and processes whereas corn and sugar cane are directly fermented to ethanol.[3,15] To achieve sustainable energy production, a significant technical improvement along with understanding the chemical and structural properties is required for the commercialization of second-generation biofuel.[3,16-18]

Biomass recalcitrance is gradually decreasing with the application of advanced technologies, such as altering plant substrate characteristics via genetic manipulation, improving pretreatment efficacy, and developing microorganisms/enzymes for high-yield sugar release.[19-23] With many recent approaches aimed at reducing biomass recalcitrance, advanced analytical tools have also been required in order to achieve detailed information since the limited chemical and/or physical information have been acquired via conventional wet chemical techniques.[24-25] For example, a new imaging technique showing topochemical distribution of major components in plant cell wall can provide new insights into biomass recalcitrance.

Imaging mass spectrometry (IMS) is a powerful and versatile tool for visualizing chemical topography on the surface of a sample. A key advantage of IMS using time-of-

flight secondary ion mass spectrometry (TOF-SIMS) or matrix-assisted laser desorption/ionization (MALDI) is the ability to probe the major components directly from the surface of the plant cell wall. Consequently, we can understand the spatial distribution of the interesting species and their changes upon chemical and/or biological applications, whereas conventional bulk analysis such as high-performance liquid chromatography (HPLC) averages over a large spatial dimension, losing critical information about differences in chemical heterogeneity as a function of spatial and lateral position in the cell wall.

The primary goal of this thesis is to gain fundamental knowledge about the surface of the plant cell wall, which is to be integrated into understanding biomass recalcitrance. IMS is well-suited to understand detailed spatial and lateral changes of major components in biomass, but it has been seldom used for the plant cell wall characterization. First, the methodology from sample preparation to instrument optimization for lignocellulosic biomass, especially poplar stem was developed (Chapter 5, 7, and 8). Then, a hypothesis that there was different chemistry between surface and bulk biomass before and after pretreatment process was formulated. To logically test the hypothesis, TOF-SIMS for the surface characterization of dilute acid pretreated poplar sample was employed and compared to the bulk analysis data (Chapter 5). TOF-SIMS methodology successfully developed for biomass was applied for hydrothermal pretreated poplar samples and different chemistry between surface and bulk was observed after the pretreatment (Chapter 6). To obtain spatially resolved chemical information from the surface to sub-surface (i.e., bulk), three-dimensional TOF-SIMS analysis for poplar sample has been

firstly applied (Chapter 7). In addition, MALDI-IMS methodology to observe different size of cellulose oligomers on the surface of the poplar stem was successfully developed (Chapter 8).

CHAPTER 2

LITERATURE REVIEW A: LIGNOCELLULOSES FOR BIOETHANOL

2.1 Lignocellulosic Bioethanol

Bioethanol is a liquid biofuel produced from different source of feedstocks and conversion technologies. Currently, bioethanol using first-generation feedstocks (i.e., food-based sources) is predominantly produced, adversely affecting global food supply or encroaching on other important land uses.[1] With a significant improvement of biotechnology, lignocellulosic biomass referred to as second-generation feedstocks (i.e., non food-based sources) has been recognized as a potential sustainable source of mixed sugars for fermentation to biofuels. Lignocellulosic biomass represents one of the most abundant, renewable, and sustainable resource on the planet, but it requires more complex processes for bioethanol production and overcoming biomass recalcitrance for cost-effective production (Figure 1).[10]

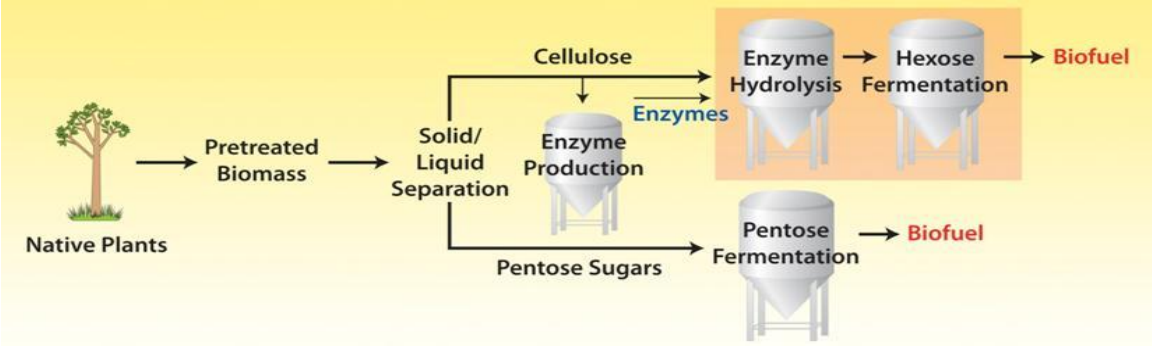

Figure 1 Bioethanol production processes using biomass.[26]

Conventional processes for producing lignocellulosic ethanol are typically divided into four steps: pretreatment, enzymatic cellulose hydrolysis (saccharification), fermentation, and distillation.[9] Firstly, lignocellulosic biomass is pretreated in order to alter cellular structure of the lignocelluloses. The pretreated biomass is amenable to be accessed by cellulolytic enzymes for cellulose hydrolysis to glucose. Subsequently, simple sugars are fermented to ethanol followed by a distillation process which is separating and purifying ethanol to meet fuel specifications.

2.2 Lignocellulosic Biomass

Lignocellulosic biomass has been recently highlighted as a potential resource for bioethanol production since it represents the most abundant form of carbon on Earth (~ annual production at 10^{10} million tons).[27] Lignocellulosic biomass is a fully renewable bioresources obtained from both forest and agricultural ecosystems categorized in Figure 2.[28] The forest-derived resources include forest residues from harvesting or land conversion, unused mills from wood or pulp processing, urban wood wastes, and construction/ demolition debris. The agriculture-derived resources include crop residues, perennial energy crops (e.g., switchgrass) and woody crops cultivated in cropland. In United States, forest lands and timberlands have the potential to sustainably produce close to 370 million dry tons of biomass annually.[29] This estimate includes the residues generated in the manufacture of various forest products and the residues generated in the use of manufactured forest products. It also includes the harvest of wood for various residential and commercial space-heating applications. With the exception of urban wood residues, most of these sources of forest biomass are currently being utilized. Two

potential large sources of forest biomass not currently being used are logging/other removal residues, and fuel treatment thinnings.[29] These sources can sustainably contribute over 120 million dry tons annually. The logging and other removal residues can be recovered following commercial harvest and land clearing operations. Fuel treatment thinnings can also be recovered with efforts to reduce forest fire hazards. Agricultural lands can provide nearly 1 billion dry tons of sustainably collectable biomass, which continue to meet food, feed and export demands.[29] This estimate includes 446 million dry tons of crop residues, 377 million dry tons of perennial crops, 87 million dry tons of grains used for biofuels, and 87 million dry tons of animal manures, process residues, and other residues generated in the consumption food products. The perennial crops are dedicated primarily for bioenergy and bio-based products and will likely include a combination of grasses and woody crops.

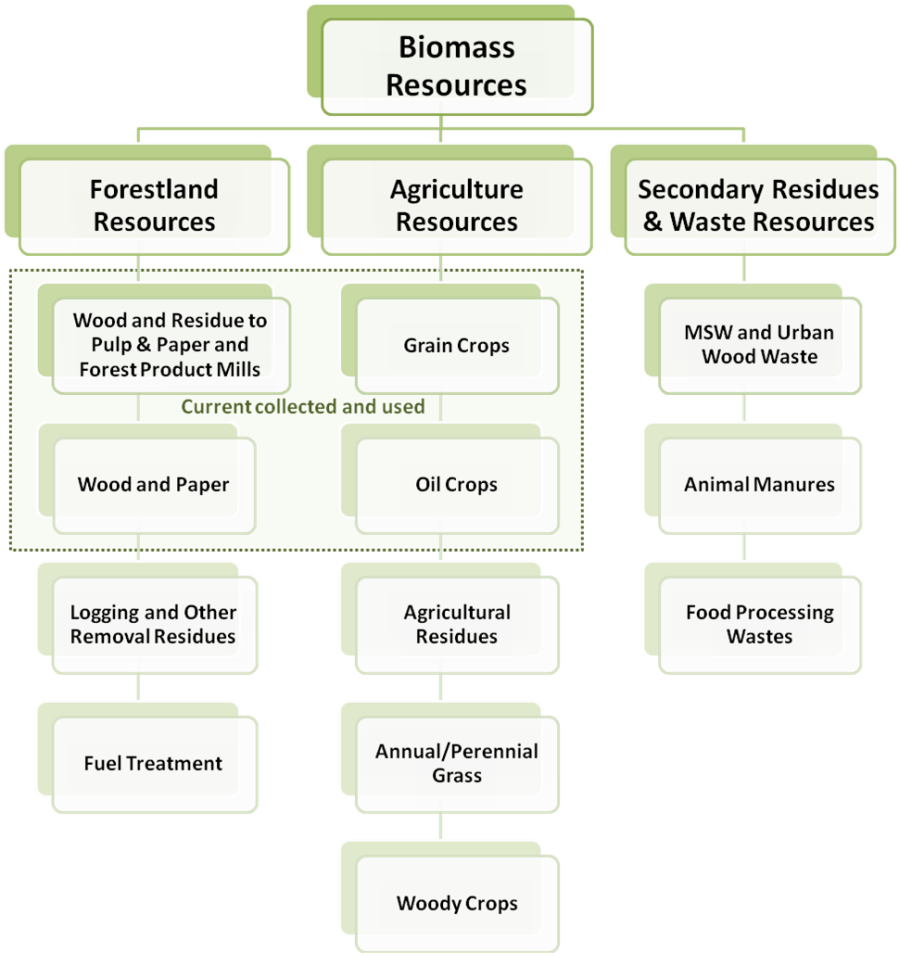

Figure 2 Biomass resources categories.[28]

2.2.1 Anatomical structure of lignocellulose

Lignocelluloses are made up of the plant cell wall as a basic unit positioned outside the cell membrane in order for structural support and core protection.[13] The plant cell wall is a highly complex and dynamic structure, consisting of cross-linked networks of polysaccharides and lignin.[30] The primary cell wall solely protects the cell during growth stages, and the secondary cell wall is synthesized at the outer layer of the primary cell wall once the cell growth is terminated.[14,31] After that, the cell walls are gradually thickened as major components (i.e., cellulose, hemicelluloses, and lignin) are

progressively growing inside cell walls. Finally, protoplasm is lost and the cell walls form cellulose microfibrils interconnected with hemicelluloses (e.g., xylan and xyloglucan) and lignin at nanometer scale. Then, cellulose microfibrils in the secondary cell wall are densely packed and highly ordered compared to that in the primary cell wall. The secondary cell wall is further divided into three layers partially based on the orientation of microfibrils: S1, S2, and S3 (Figure 3).[32] Thicker middle layer (S2) represents a steep and uniform angle in microfibrils while the outer (S1) and inner (S3) have a cross-helical orientation.[14] A single cell containing primary and secondary cell wall is separated with adjacent cells by intercellular substance referred to as middle lamella. Middle lamella makes up the outer cell wall, sharing with adjacent cells shown in Figure 3.[32] Among cell wall multilayers, the secondary cell walls typically account for more than 95% by the weight of the cell wall materials.[13]

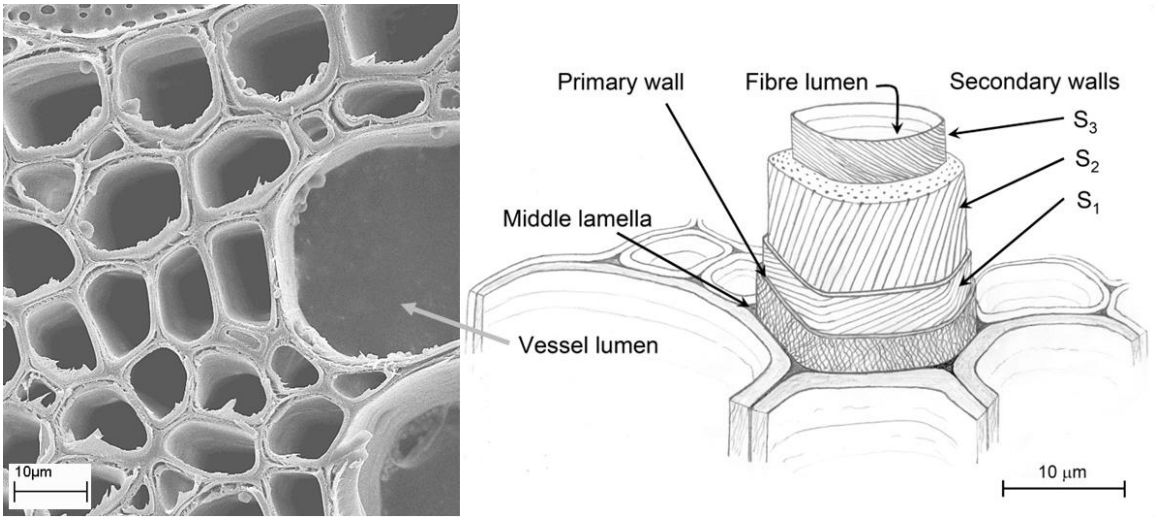

Figure 3 Electron microscope and schematic diagram of wood cell wall structure.[32]

2.2.2 Molecular composition of lignocellulose

Lignocelluloses are composite and complex materials which are largely divided into major (e.g., polysaccharides and lignin) and minor components (e.g., extractives and mineral substances) shown in Figure 4. Dry wood typically consists of 40-45% cellulose, 20-30% hemicelluloses, and 20-32% lignin. Other constituents of lignocellulose are extractives (< 10%) and ash (< 1%). Major molecular components are cellulose, hemicelluloses and lignin where they are physically or chemically connected each other. Contents of major components in lignocelluloses are strongly based on biological species, growth stage, and cell type in nature (Table 1).[9] In general, softwood has higher lignin content than hardwood.

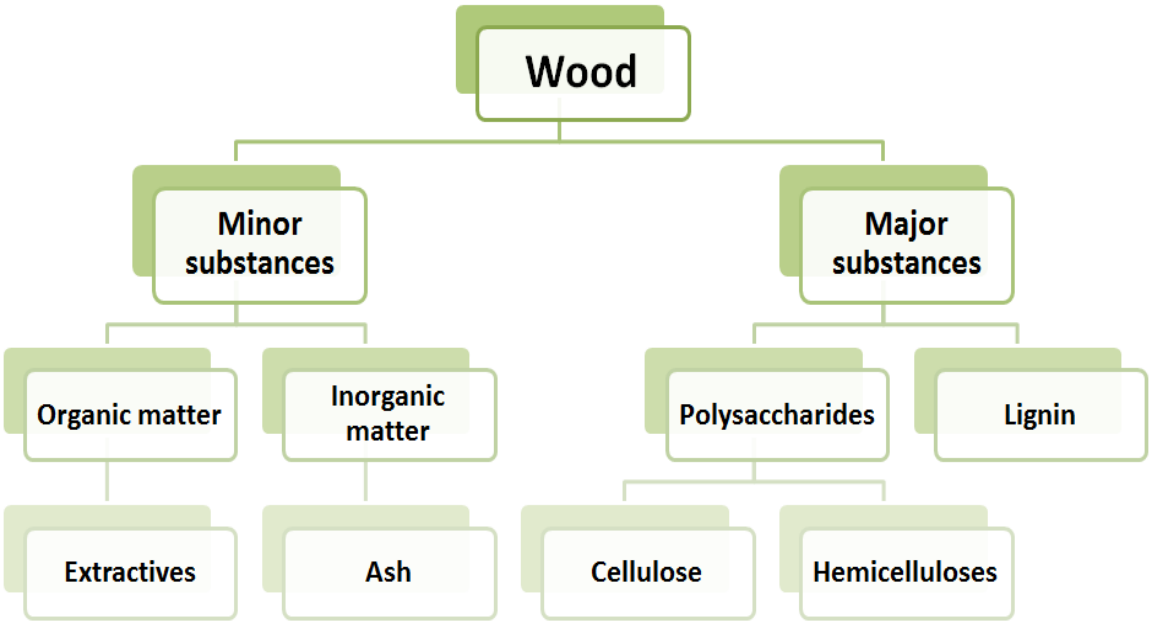

Figure 4 Chemical composition of the cell wall.

Table 1 Composition of some lignocellulose sources (% dry weight).[9,33]

Biomass or waste	Cellulose	Hemicelluloses	Lignin
Tree			
Poplar	45-50	17-19	18-26
Eucalyptus	50	13	28
Pine (spruce)	44	23	28
Salix (hardwood)	43	22	26
Grasses			
Switchgrass	31-45	20-30	12-18
Bemuda grass	25	36	6
Rye grasses	25-40	35-50	10-30
Food/agriculture waste			
Corn cobs	45	35	15
Corn stover	38-40	22-28	18-23
Corn fiber	14	17	8
Wheat straw	30-38	21-50	15-23
Rice husk	24	27	13
Bagasse	38	27	20
Nut shells	25-30	25-30	30-40

2.2.2.1 Cellulose

Cellulose is a main component of lignocellulose consisted of approximately 40~50% of total dry weight. Cellulose is an unbranched homopolysaccharide composed of β-D-glucopyranose units which are linked by β-(1→4)-glycosidic linkage (Figure 5).

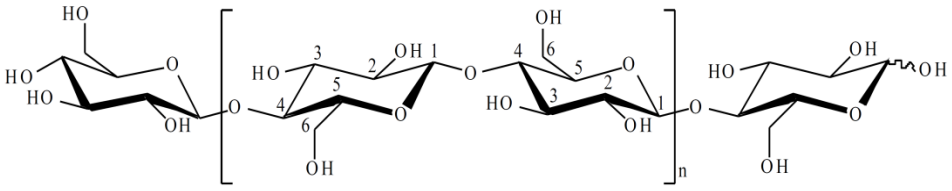

Figure 5 Molecular structure of cellulose.

Size of the cellulose molecule is typically defined by the average number of monomer units referred to as degree of polymerization (DP). DP of cellulose can be determined by various analytical methods such as gel permeation chromatography (GPC), light scattering intrinsic viscosity measurements and viscometric methods. In nature, cellulose chains have a degree of polymerization (DP) in the range of 200 to 27000 shown in Table 2.[13] Native cellulose in wood has a degree of polymerization (DP) of approximately 5000 glucopyranose units and it is around 15000 for native cellulose in cotton. Native cellulose DP is reduced during purification procedures reported by Bledzki et al.[34] For example, a DP of 14000 in native cellulose was reduced to ~2500. A DP of cellulose is very depending on its origin, isolation method, and even the part of plant/fiber. For example, valonia fibers show DP of 25000 to 27000, while cotton fibers present a DP of 14000 to 20000. Cellulose DP value profoundly influences the mechanical, solution, biological, and physiological properties of cellulose in many cases.[35]

Table 2 Degree of polymerization of some celluloses.[13,36]

Cellulose	Degree of polymerization
Cotton	8000 – 15000
Purified Cotton Linters	1000 – 3000
Commercial Wood Pulps	600 – 1500
Regenerated Cellulose	200 – 600
Rayon	300
Bagasse	700 -900
Alamo switchgrass	1891
Poplar	2200 - 250

Cellulose also has a strong tendency to form intra- and intermolecular hydrogen bonds, resulting in the formation of a crystalline structure (Figure 6).[37-40] The hydrogen bonds contribute to stiffen the straight chain and promote aggregation into the crystalline structure.

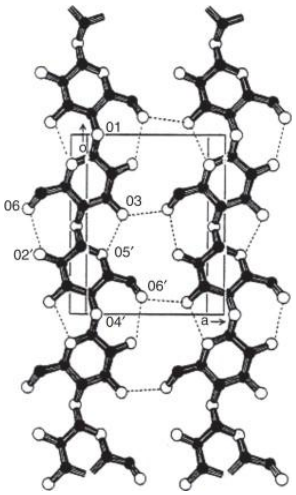

Figure 6 Inter- and intra-molecular hydrogen bond system of cellulose I.[41]

Cellulose contains highly ordered (crystalline) regions and less ordered (amorphous) regions. There are largely four types of crystalline allomorphs of cellulose: cellulose I, II, III, and IV, which are typically measured by wide-angle X-ray scattering (WAXS) patterns and CP/MAS ^{13}C NMR spectrum.[42-43] Para-crystalline cellulose is less ordered than crystalline cellulose I_α and I_β, but more ordered than the amorphous region.[44] Amorphous cellulose can also be divided into two non-crystalline forms: accessible fibril surface and inaccessible fibril surface.[44-45] The degree of cellulose crystallinity is determined as a ratio of weight fraction of the crystalline regions. A structure of cellulose I has been proposed that a unit cell of the crystal lattice is a monoclinic unit with the space group $P2_1$, consisting of two anti-parallel cellobiose chain segments shown in Figure 7.[46]

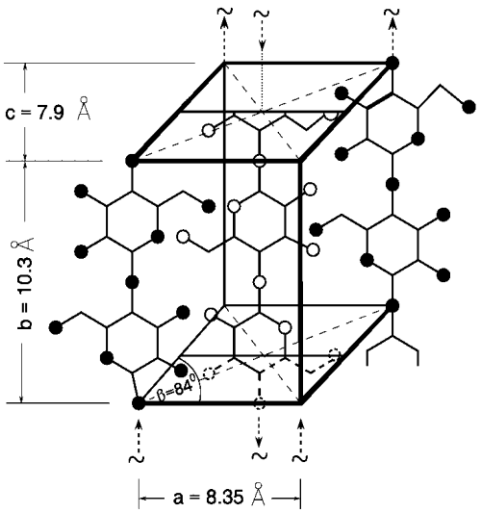

Polymorph	a-axis (Å)	b-axis (Å)	c-axis (Å)	γ-axis (Å)
Cellulose I	7.87	8.17	10.34	96.4
Cellulose II	9.08	7.92	10.34	117.3
Cellulose III	9.9	7.74	10.3	122
Cellulose IV	7.9	8.11	10.3	90

Figure 7 Unit cell of cellulose I and the dimensions of various cellulose allomorphs.[42,47]

Cellulose I, the most abundant form in nature, has two distinct crystalline forms based on hydrogen bonding pattern at glycosidic linkages: cellulose I_α and cellulose I_β.[48-50] Cellulose I_α known as a triclinic (*t*) P1 structure has one cellulose chain per unit cell, whereas cellulose I_β known as a monoclinic (*m*) $P2_1$ structure has two cellulose chains per unit cell. Generally, cellulose I_α is the predominant form in bacteria and algae and Cellulose I_β predominantly exists in higher plants. The abundance of I_α or I_β polymorphs in lignocellulosic material may affect the reactivity of cellulose because meta-stable cellulose I_α is more reactive than cellulose I_β. Other types of crystalline cellulose can be obtained by modifying cellulose I such as mercerization and regeneration for cellulose II, ammonia treatment for cellulose III, or heating for cellulose IV (Figure 8).[46,48] During modification processes, dimension of unit cell is also changed (Figure 7).

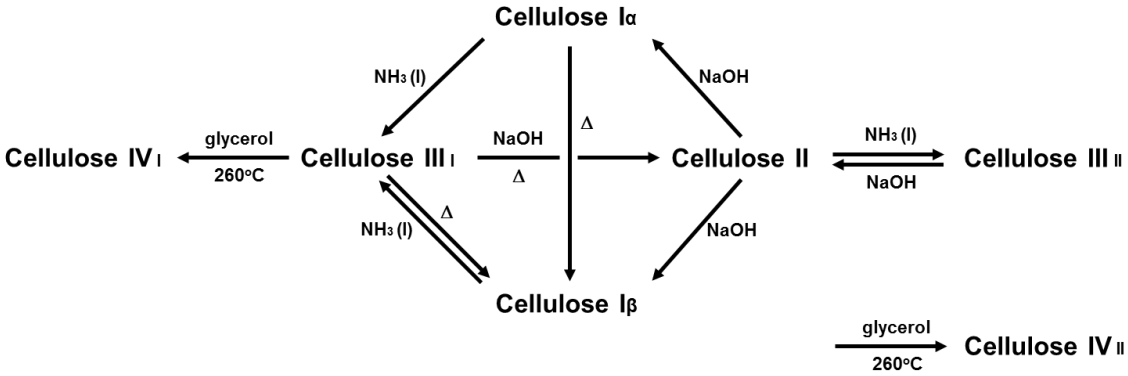

Figure 8 Transformation of cellulose into its various polymorphs.[46]

Cellulose crystallinity in lignocellulosic materials varies according to its origin and acquiring process. For example, cellulose crystallinity in hybrid *Populus* measured by CP/MAS ^{13}C NMR is ~63% very similar to loblolly pine shown in Table 3.[51-52] Differently, *Populus* contains ~20% less accessible amorphous region compared to that in

loblolly pine. Switchgrass is composed of relatively lower crystallinity (~44%) and higher inaccessible amorphous region (~51%) compared to *Populus* or loblolly pine.[53]

Table 3 Cellulose crystallinity (%) determined by CP/MAS ^{13}C NMR.[51-54]

Species	Crystallinity	Iα	Iα+β	Para-crystalline	Iβ	Accessible Fibril surfaces	Inaccessible Fibril surfaces
Populus[a]	63	5.0	14.2	31.1	19.8	10.2	18.3
Loblolly pine	63	0.1	30.7	24.8	6.9	33.1	15.6
Switchgrass[b]	44	2.3	8.8	27.3	4.5	5.7	51.3

[a] *P. trichocarpa x deltoids*, [b] Alamo

The basic building unit of the cellulose skeleton is an elementary fibril which contains 36 β–D-glucan chains with a diameter of approximately 3.5 nm (Figure 9).[55-57] The dimension of elementary fibrils (e.g., unit-cell parameters and lattice planes) differs from the forms of crystalline structures. For example, three lattice planes are shared and correspond to I_α lattice planes $(110)_t$, $(010)_t$, and $(100)_t$, and I_β lattice planes $(200)_m$, $(110)_m$, and $(110)_m$, respectively.[58-59] The main difference between I_α and I_β is the relative displacement of the sheet (i.e., parallel stacking of cellulose chains) along the $(100)_t$ and $(200)_m$ planes, referred to as hydrogen-bonded plane, in the chain axis direction, respectively. The cellulose I_α is a relative displacement of $c/4$ between each subsequent hydrogen-bonded plane, while the cellulose I_β is between $c/4$ and $-c/4$. The elementary fibrils are aggregated together in the form of microfibril partially reducing the free energy of the surface.[60] The diameter of the microfibril varies from 2 to 20nm with the length in the micrometer scale depending on its origin.[61]

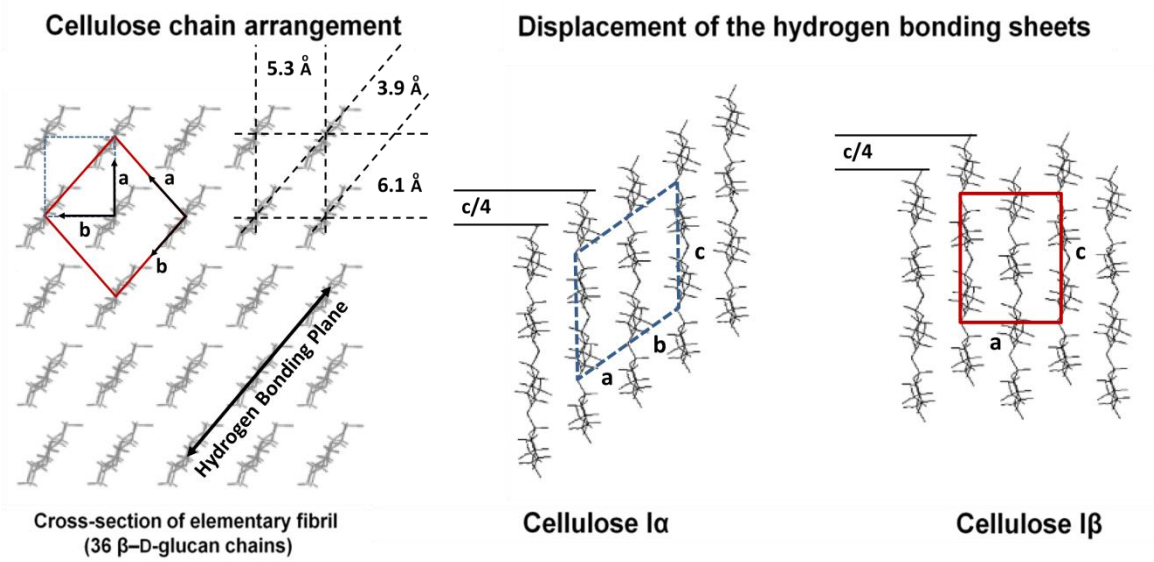

Figure 9 Cross section of the elementary fibril containing 36 glucan chains of the unit cells for cellulose I_{α} and I_{β}.[50]

2.2.2.2 Hemicelluloses

Hemicelluloses are typically branched heterogeneous polysaccharides mainly composed of pentoses (xylose, arabinose), hexoses (mannose, glucose, galactose), and/or uronic acids (glucuronic, galacturonic acids).[13] Other sugars such as rhamnose and fucose are also present in small amounts and the hydroxyl groups of sugars can be partially substituted with acetyl groups. Most hemicelluloses are relatively low molecular weight with a DP of 50~300 in woods which may contain 15-30% of hemicellulose in hardwood or softwood. The hemicelluloses are broadly classified into four polysaccharide types based on structural differences in cell-wall (Figure 10)[62-63]:

(i) Mannans comprise galactomannan, glucomannan and galactoglucomannan. Galactomannans have β-1,4-mannose backbones with α-1,6-galactose branches; glucomannans contain both β-1,4-mannose and β-1,4-glucose backbones; and

galactoglucomannans have β-1,4-mannose and β-1,4-glucose backbones with α-1,6-galactose branches attached to the mannose backbone. For example, the secondary cell walls of conifers (i.e., softwoods) consist of galactoglucomannan 10–30% (w/w).

(ii) Mixed-linkage glucans comprise a backbone of glucose residues having both β-1,3 and β-1,4 linkages. For example, the primary cell walls of grasses contain 2–15% of mixed-linkage glucans.

(iii) Xylans have β-1,4-xylose backbones with arabinan and/or glucuronic acid as side chains. For example, the primary cell walls of glasses contain 20–40% glucuronoarabinoxylan, whereas the secondary cell walls contain 40–50% glucuronoarabinoxylan. In dicots (e.g., hardwoods), the secondary cell walls contain 20–30% glucuronoxylan.

(iv) Xyloglucan has a β-1,4-glucan backbone with xylose-containing branches which partially contain other monosaccharide such as galactose, arabinose and fucose. For example, the primary cell walls of conifers (i.e., softwoods) contain 10% xyloglucans and the primary cell walls of dicots (e.g., hardwoods) contain 20–25%.

Glucuronoxylans (MGX)

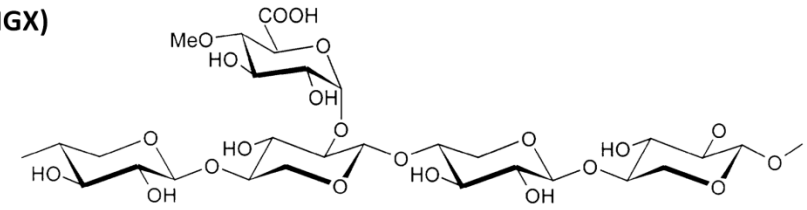

(Arabino)glucuronoxylan (AGX)

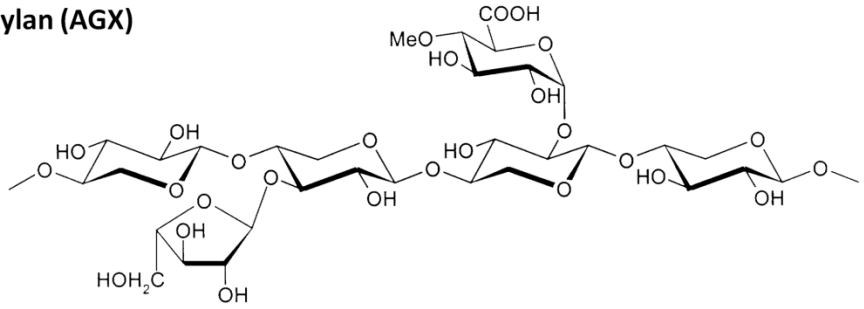

Xyloglucan (XG)

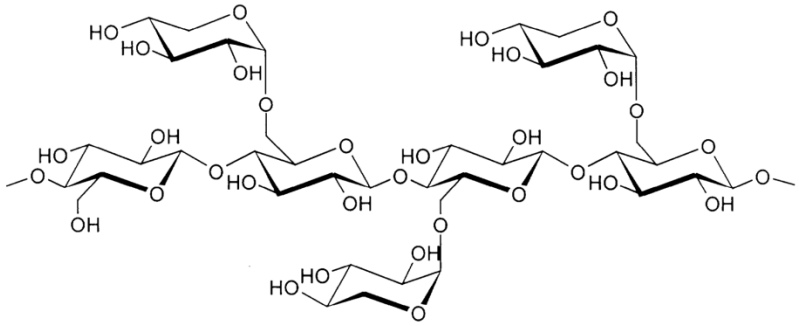

Glucomannans (GM)

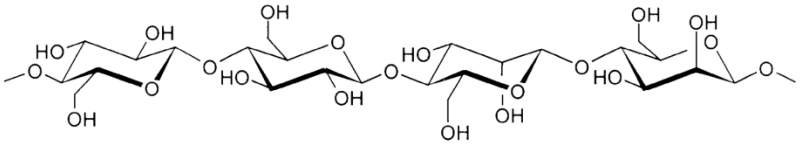

Galactomannans (GaM)

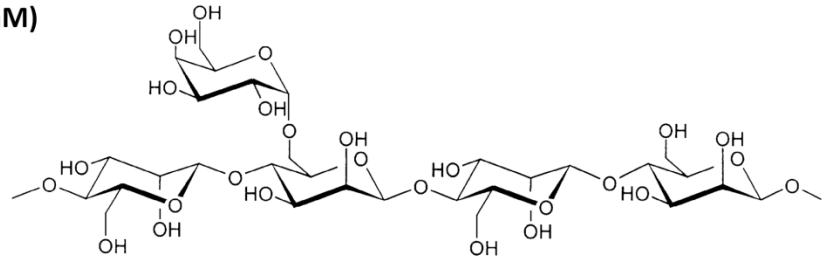

Mixed-linkage (1→3, 1→4)-D-glucan (*β*-glucan)

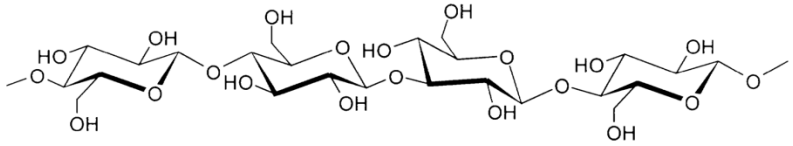

Figure 10 Molecular structure of hemicelluloses.[62]

The content and structure of each component generally differ between softwoods, and hardwoods. The main structural features of hemicelluloses in both softwood and hardwood are summarized in Table 4.[12] The main hemicellulose of hardwoods (e.g., poplar) is O-acetylated 4-O-methyl-glucuronic acid xylan or glucuronoxylan while that in softwood is galactoglucomannan or arbinoglucuronoxylan. In addition, the different ratio of hemicelluloses has been observed even at the cell wall layers (Table 5).[63] Xyloglucan is the most abundant hemicellulose structure in primary walls of dicots, whereas glucuronoxylan is predominant in the secondary cell wall of dicots. In commelinid monocots including grasses, glucuronoarabinoxylan is the major hemicellulose in both cell walls.

Table 4 The major hemicellulose components in softwood and hardwood.[12,64-66]

Wood type	Hemicellulose type	Amount (% on wood)	Compostion			DP
			Unit	Major ratio	Linkage	
SW	Galactoglucomannan	10-15	β-D-Man*p*	4	1→4	100
			β-D-Glc*p*	1	1→4	
			β-D-Gal*p*	0.1	1→6	
			Acetyl	1		
	Arabinoglucuronoxylan	7-10	β-D-Xyl*p*	10	1→4	100
			4-O-Me-α-D-Glc*p*A	2	1→2	
			β-L-Ara*f*	1.3	1→3	
HW	Glucuronoxylan	15-30	β-D-Xyl*p*	10	1→4	200
			4-O-Me-α-D-Glc*p*A	1	1→2	
			Acetyl	7		
	Glucomannan	2-5	β-D-Man*p*	1-2	1→4	200
			β-D-Glc*p*A	1	1→4	

Table 5 Occurrence of hemicelluloses in primary and secondary cell walls of plants.[63]

Amount of Polysaccharide in cell wall (% w/w)	Dicot walls		Grass walls		Conifer walls	
	Primary	Secondary	Primary	Secondary	Primary	Secondary
Xyloglucan	20-25	Minor	2-5	Minor	10	-[a]
Glucuronoxylan	-	20-30	-	-	-	-
Glucuronoarabinoxylan	5	-	20-40	40-50	2	5-15
(Gluco)mannan	3-5	2-5	2	0-5	-	-
Galactoglucomannan	-	0-3	-	-	+[b]	10-30
β-1,3 or 1,4-glucan	Absent	Absent	2-15	Minor	Absent	Absent

[a]- : absent or minor, [b]+ : present but quantitative data not available.

Other than cellulose and hemicelluloses, the cell wall also contains other carbohydrates such as sucrose, fructose, glucose and starch. These sugars categorized as soluble carbohydrate account for a much smaller amount of carbohydrate compared to cellulose and hemicelluloses. Their portions in biomass vary depending on their origin and source. For example, Sunburst switchgrass stem contains three times more sucrose than starch (2.86% to 0.88%) while switchgrass leave contains seven times more sucrose than starch (2.87% to 0.41%).[67] Differently, Cave-in-Rock switchgrass contains the concentrations of sucrose (2.7%), glucose (0.6%), fructose (0.6%) and starch (0.5%).[68]

2.2.2.3 Lignin

Lignin is the third macromolecule in lignocellulose and plays an important role as a matrix material which binds the polysaccharide microfibrils and fibers, resulting in increasing the strength and rigidity to the plant stem for vertical growth.[69] Lignin also plays an important biological function in the plant protection against foreign invasion by

impeding penetration of destructive enzymes through the cell wall.[13,70] Lignins are composed mainly of three phenylpropane monomers: *p*-hydroxyphenyl (H, *p*-coumaryl alcohol), guaiacyl (G, coniferyl alcohol), and syringyl (S, sinapyl alcohol) units in Figure 11.[71] Composition and content of lignin vary depending on its origin and type of lignocellulose. For example, gymnosperm (i.e., softwood) lignin is derived mostly from G-type monolignol while angiosperm (i.e., hardwood) lignin is derived mostly from G- and S-type monolignols with trace of H-type monolignol.[72-73] Grass lignin (e.g., switchgrass) is derived mostly from G- and S-type monolignols with significant amount of H-type monolignol. Grass also contains significant levels of *p*-coumaric and ferulic acid (Figure 12), which is involved in crosslinking to lignin and hemicellulose complex. The H and G contents of the lignin in Scots pine (softwood) are 2% and 98%, respectively, while the G and S contents in *Populus* (hardwood) are 41% and 59%, respectively. The H, S, and G contents of the lignin in switchgrass are 8%, 51% and 49%, respectively. Softwood generally contains about 25-35% lignin and hardwood contains 18-25% lignin.[73]

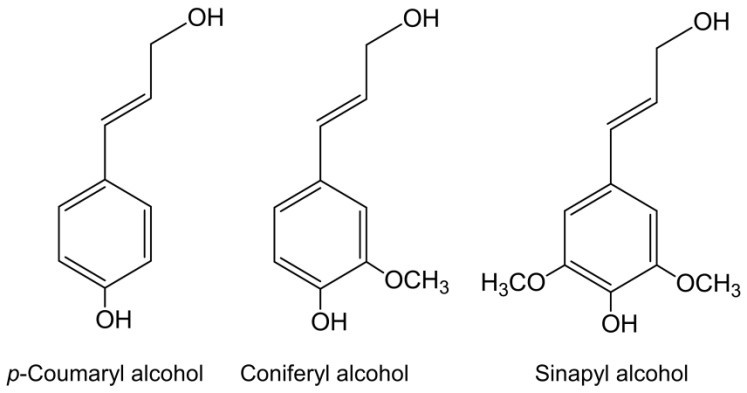

Figure 11 The three common monolignols.[74]

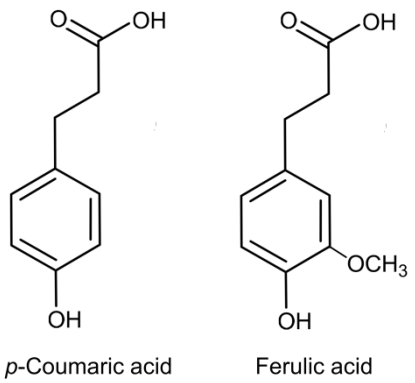

Figure 12 Structure of *p*-coumaric and ferulic acid.

Lignin precursors are polymerized via radical coupling reactions, resulting in three-dimensional complex, amorphous, and phenylpropanoid macromolecules.[71] Radial reaction is initiated by oxidation of the phenylpropane phenolic hydroxyl group, which forms a resonance stabilized quinine methide radical intermediate (Figure 13).[13] The radical electron occurs at different positions, allowing the several different inter monomer linkages via radical polymerization.

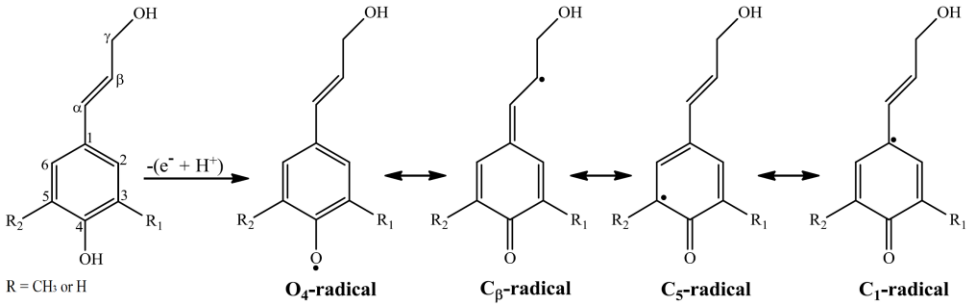

Figure 13 Resonance stabilized phenoxy radical during lignin biosynthesis.[13]

Thereby, many different types of inter monomer linkages are commonly found in both softwood and hardwood (Figure 14). For example, β-O-4 and β-5 linkages would lead to

a leaner polymer which is branched via subsequent nucleophilic attack by water, alcohol, or phenolic hydroxyl groups. Though the many possible coupling pathways between monolignol exist for producing macromolecule, the mechanism for biosynthetic regulation is not fully discovered yet. However, evidence of macromolecule in lignin has been empirically discovered. For example, typical proportions of lignin linkages in softwood and hardwood are summarized in Table 6. [13,75-76] Typical proportions of lignin linkages in poplar and switchgrass are also summarized in Table 7-8.[54,77]

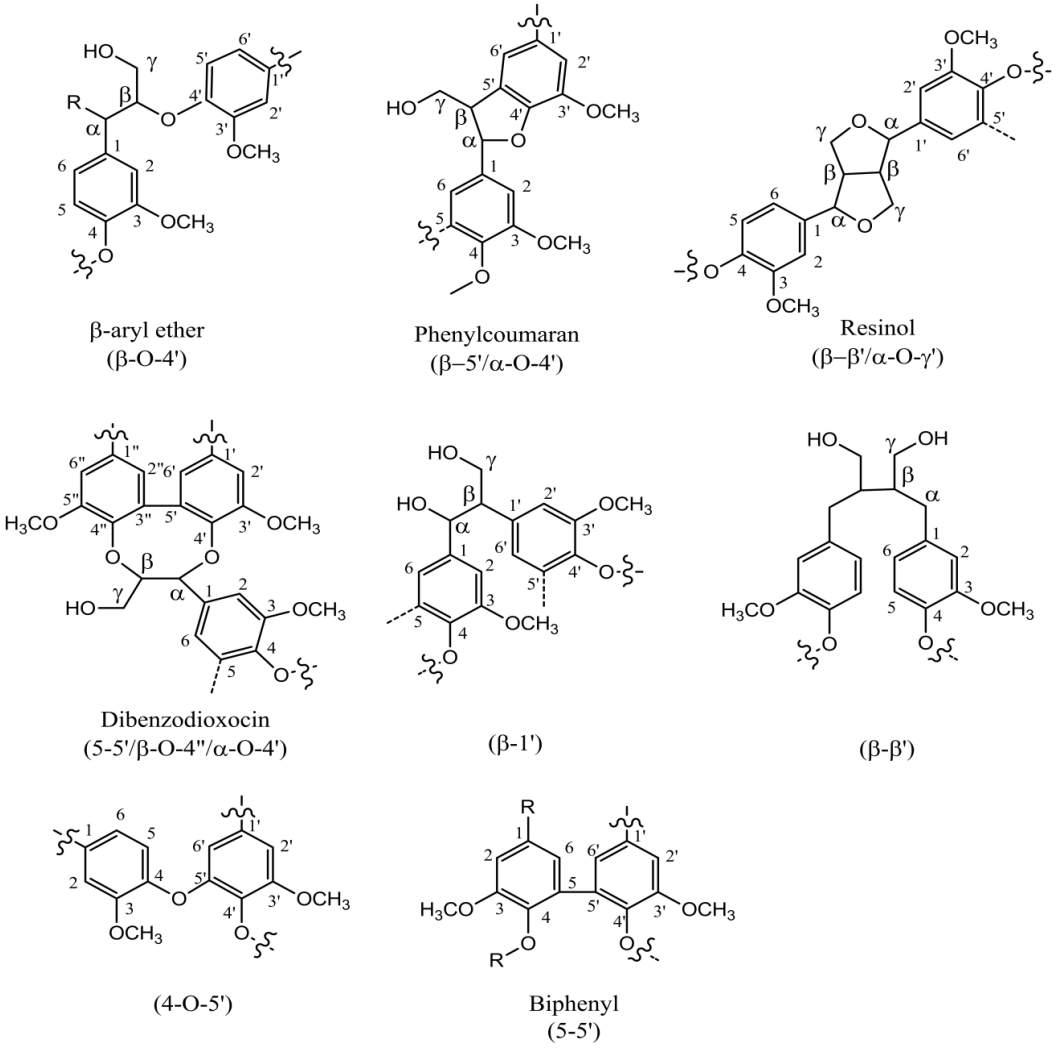

Figure 14 Common lignin linkages in softwood and hardwood lignin.[12, 72, 74]

Table 6 Proportions of different types of lignin linkages in softwood and hardwood.[13]

Linkage Type	Percentage of total linkages	
	Spruce lignin (%)	Eucalyptus lignin (%)
β-O-4'	45	61
α-O-4'	16	n.d.
β-β'	2	3
β-5'	9	3
5-5'	24-27	3
β-1'	1	2
4-O-5'	n.d.	9
Dibenzodioxocin	7	n.d.

Table 7 Proportions of different types of lignin linkages in poplar*.

Structure	Number per 100 Ar	
	P. Tremuloides Michx. 10-1	*P. Tremuloides* Michx. 16-2
β-1	10	9
Pinoresinol	8	9
Dibenzodioxcin	0	1
β-O-4	56	68
Methoxyl group	133	142
Side chain	306	304
p-hydroxyphenyl	11	10
Oxygenated aomatic	201	200

* Quantitative ^{13}C NMR data

Table 8 Proportions of different functional group of lignin linkages in switchgrass*.

Functional Group	Number per 100 Ar	
	Alamo	Kanlow
C=O in spirodienone unit	2	
C=O in aliphatic COOR	22	39
C=O in conjugated COOR	17	20
C_4 in H unit	107	7
C_3/C_4 in G unit, C_3/C_5 in S unit, C_α in cinnamate	171	
C_1 in G, S, H units, C_4 in S unit, $C_{2/6}$ in H unit	217	
C_6 in G unit	44	43
C_5 in G unit, $C_{3/5}$ in H unit, C_β in cinnamate	85	75
C_2 in G unit	44	40
C_2/C_6 in S unit	70	64
C_β in β-O-4, C_α in β-5 and β-β	35	
C_γ in β-5 and β-O-4 with C_α=O in G and S units	39	39
C_γ in β-O-4 without C_α=O Methoxy	99	91
C_β in β-β, C_β in β-5	10	13

* Quantitative ^{13}C NMR data

Many different types of lignin polymerization pathways result in a highly branched macromolecule. Weight average of molecular weight (Mw) of isolated lignin in softwood and hardwood has been estimated at ~20000 and slightly low, while polydispersity of lignin was calculated as 2.5 and 3.5, respectively.[13] Based on the inter linkage proportion and its structural analysis, a model structure of hardwood lignin has been proposed (Figure 16). [78-79]

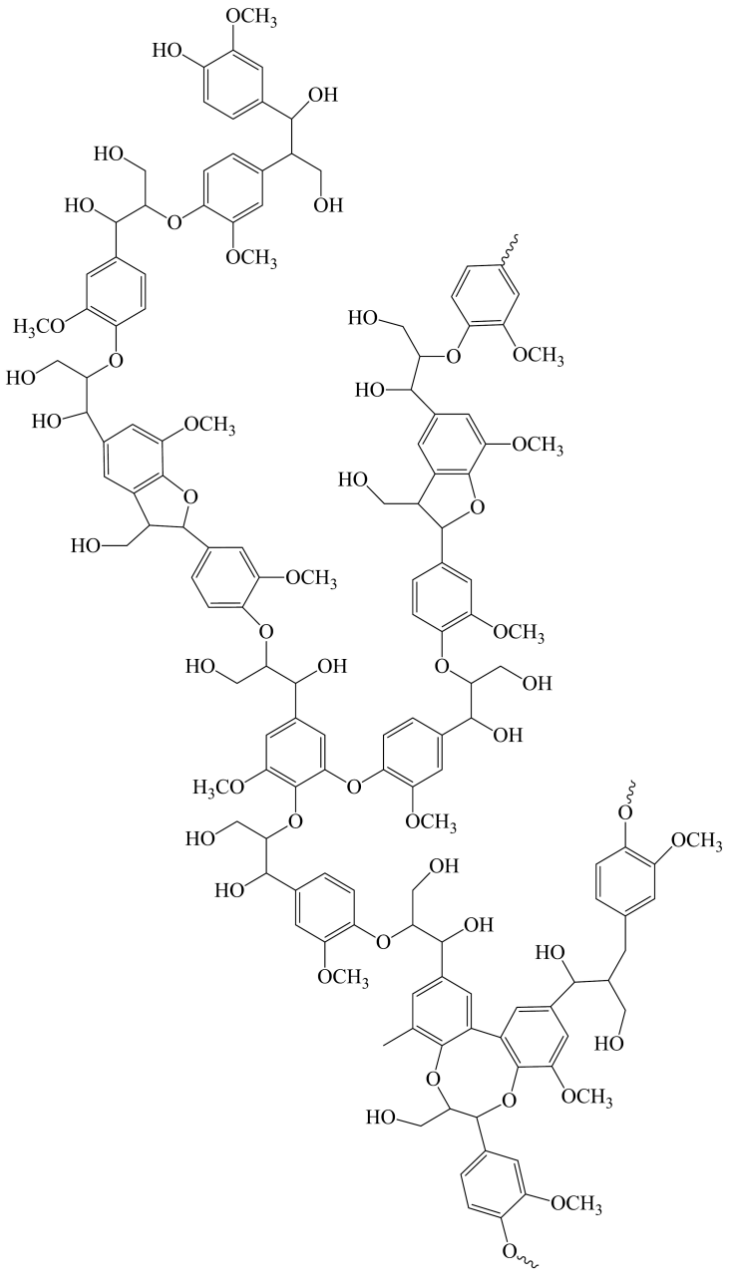

Figure 15 A structural model for softwood lignin.[78]

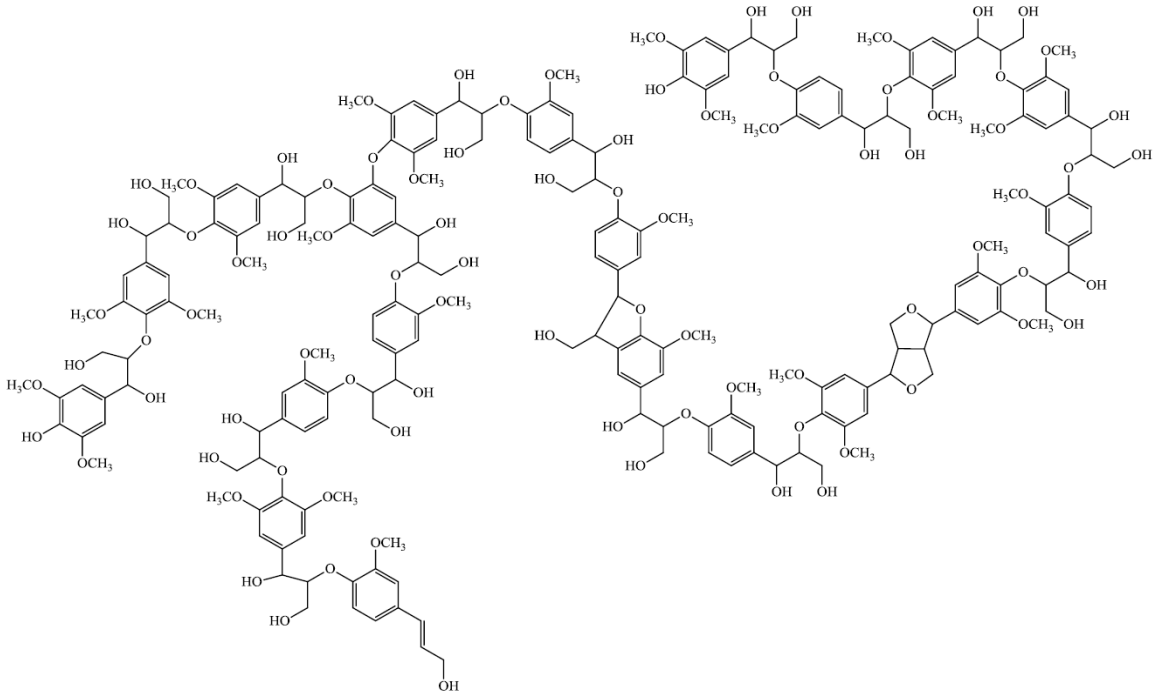

Figure 16 A structural model for hardwood lignin.[79]

2.2.2.4 Lignin-carbohydrate complex

Lignin-carbohydrate complexes (LCCs) are heterogeneous structures found in many plant species. Lignin is directly or indirectly bound covalently to carbohydrate which presents as a complex structure in biomass.[80] LCCs can be isolated as water-soluble entities and divided into three classes based on molecular weight. Lignin carbohydrate bonds are presumed to exist in higher molecular weight lignin fractions which are water insoluble. In softwood LCCs, carbohydrate portions are mainly composed of galactomannan, arabino-4-O-methylglucuronoxylan, and arabinogalactan which linked to lignin at benzyl positions.[81-82] However, hardwood and grass LCCs are exclusively composed of 4-O-methylglucuronoxylan and arabino-4-O-methylglucuronoxylan, respectively.[83] Four major types of native lignin-carbohydrate bonds have been proposed: benzyl ethers,

benzyl esters, phenyl glycosides, and recently, acetal linkages (Figure 17). Among many different types of LC bonds have been proposed, but most evidence exists for ether and ester linkages shown in Figure 17.[84-85]

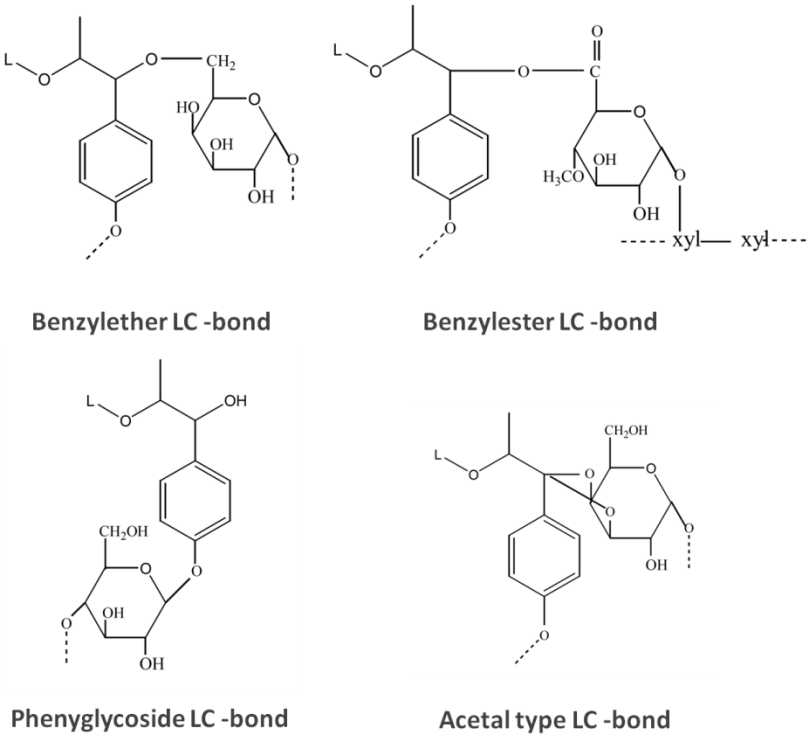

Figure 17 Proposed types of lignin carbohydrate linkages.

The biosynthetic pathway for the ether and ester types of lignin-polysaccharide covalent bonds has been proposed to involve a nucleophilic addition of the hemicelluloses to the quinone methide intermediate formed from the dehydrogenative polymerization of coniferyl alcohol.[13,86] From quantum mechanical calculations, the coupling between phenoxy radicals and β-radicals are most favored, therefore the β-O-4 linkage in lignin is the most abundant linkage. The formation of the β-O -4 linkage leads to a formation of a quinone methide-like structure as shown in.[86] The α-position is now an electrophile, and it can be attacked by water, alcohol, or carboxyl groups which lead to the formation of benzyl alcohols, benzyl ethers, and benzyl esters. The biosynthesis of ester and ether LCC linkages has been proposed, but the biosynthesis of glycosidic and acetal LCCs is not fully discovered yet.

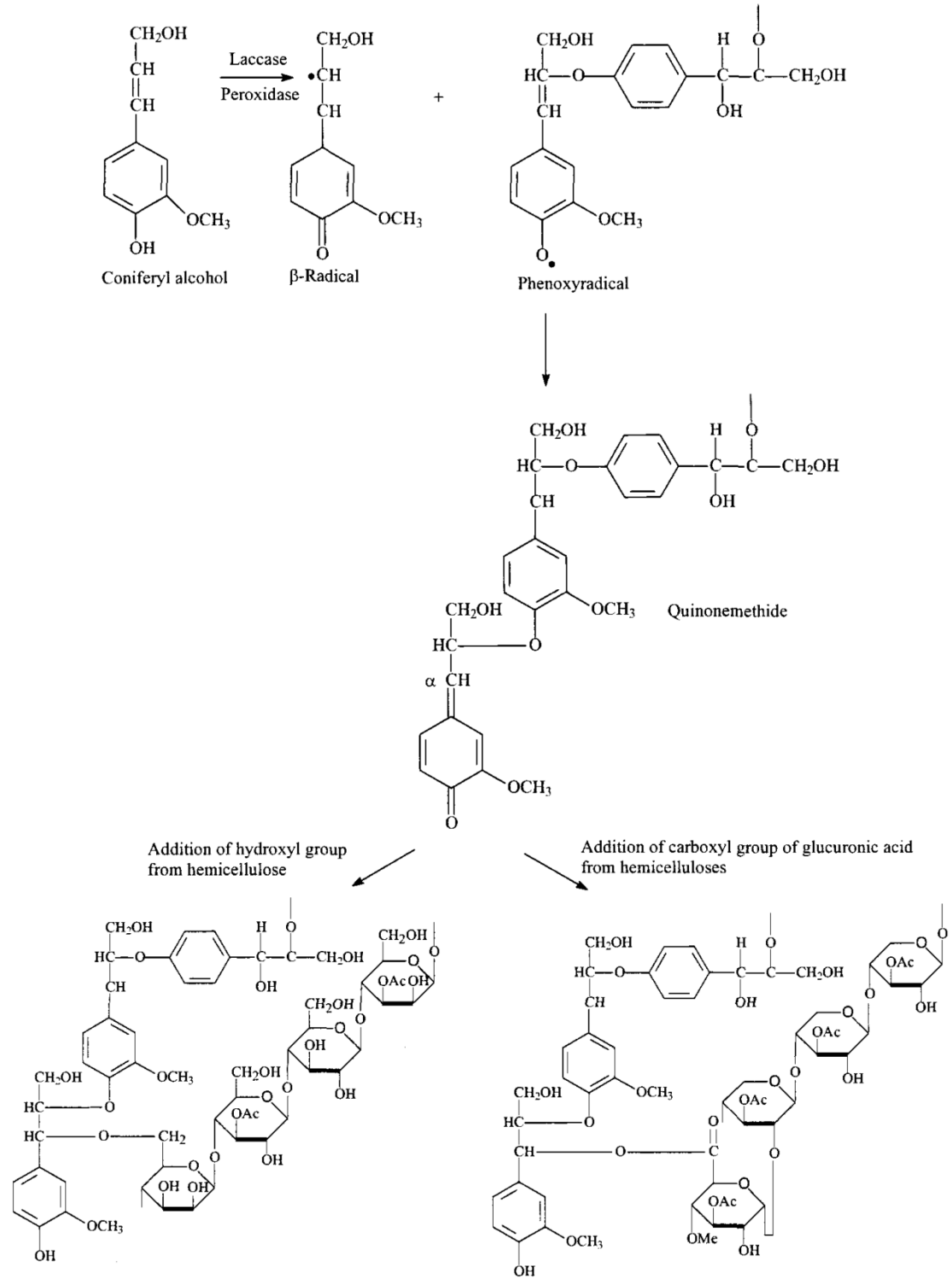

Figure 18 Biosynthesis of benzyl ether and benzyl ester LCCs.

2.3 Biomass recalcitrance and Pretreatments

2.3.1 Biomass recalcitrance

The inherent properties of lignocellulosic biomass make them resistant to deconstruction from microbes and enzymes, referred to as biomass recalcitrance.[3,15] The structural heterogeneity and complexity of plant cell wall made up of a matrix of cellulose and lignin bound by hemicellulose chains are believed to contribute to biomass recalcitrance, reducing and/or retarding cellulase accessibility (Figure 19).[3,26] To decrease the recalcitrance of biomass and make the cellulose in the lignocellulosic biomass more susceptible to digestion by cellulase enzymes, pretreatment is required.[87-88] Therefore, the primary goal of the pretreatment process is to remove lignin and hemicellulose, reduce the crystallinity of cellulose, and increase the porosity of the lignocellulosic materials.

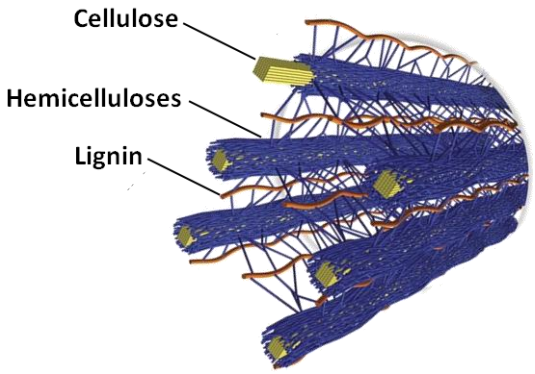

Figure 19 Schematic diagram of the secondary cell wall.[26]

Particularly the chemical and physical characteristics of plant cell wall are considered as major factors for biomass recalcitrance: particle size/surface area, cellulose crystallinity,

degree of polymerization (DP) of cellulose, hemicellulose/lignin/LCC content/structure, and degree of hemicellulose acetylation.[10,87-88] First, of the efficiency of enzymatic hydrolysis to glucose partially depend on the surface area of the lignocellulosic biomass because the reaction takes place under heterogeneous condition (e.g., solid biomass with liquid enzyme). Many studies reported that the larger surface area can positively affect the rate of enzymatic cellulose hydrolysis by increasing enzyme absorption.[89-90] However, surface area cannot solely explain biomass recalcitrance. For this reason, it often requires multistep pretreatment processes instead of a single pretreatment process such as milling or grinding. Second, cellulose crystallinity is strongly related to the rate of enzymatic cellulose hydrolysis because the strong inter- and intra-hydrogen bonding in crystalline cellulose resists enzyme attack.[91-93] Therefore, low-crystallinity regions of cellulose (e.g., amorphous regions) are the primary target for enzyme attack and readily digestible. Third, cellulose DP is also related to the rate of enzymatic cellulose hydrolysis because the number of reducing end per cellulose microfibrils has a higher chance to meet exoglucanases.[94-95] Therefore, the lower DP of cellulose influences higher activity of cellulose deconstruction. Finally, hemicelluloses and lignin content in lignocellulosic biomass are negatively correlated with the yield of enzymatic hydrolysis. Lignin partially acts as an inhibition compound and hemicelluloses make a physical barrier that restricts enzyme access to cellulose core.[93,96-99] Thus, removal of hemicelluloses exposes the cellulose surface and increases enzyme accessibility to the cellulose microfibrils.

2.3.2 Pretreatments

Pretreatment process in lignocellulosic biomass is for the structural breakdown of the plant cell, resulting in reducing biomass recalcitrance by decreasing degree of cellulose crystallinity, partially increasing the amorphous cellulose fraction, and solubilizing hemicelluloses and lignin (Figure 20).[21,87,100] Hence, the pretreatment process is considered as one solution for producing lignocellulosic bioethanol with low costs and high productivity. However, there is no universal pretreatment process to date because of the diverse nature of different biomass feedstocks.

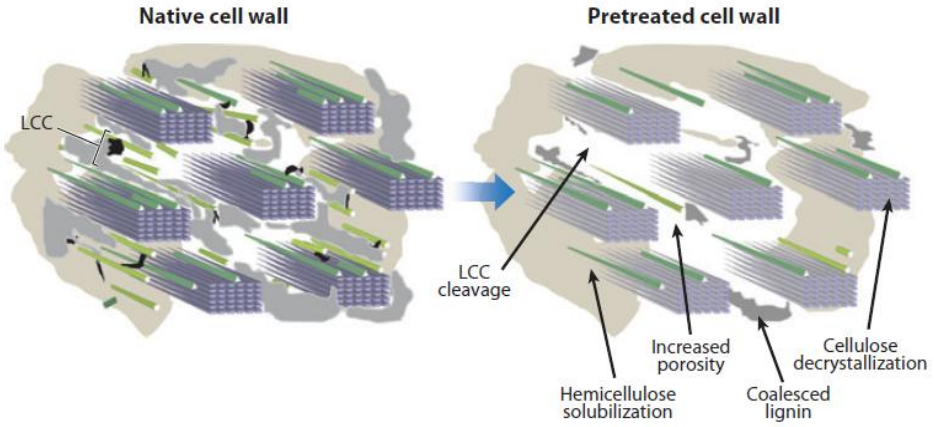

Figure 20 Schematic diagram of the effect of pretreatment on lignocellulosic materials.[101]

A large number of pretreatment approaches have been investigated on a wide variety of feedstock types, which are typically divided into physical, chemical and biological applications (Table 9).[21, 100] A combination of the different pretreatment methods such as physical and chemical pretreatments is frequently used in order to maximize pretreatment effects. Physical pretreatments (e.g., milling) typically enlarge the surface of

lignocellulosic biomass in order to increase enzyme absorption or further pretreatment accessibility, but the performance is economically poor. Biological pretreatment has been considered as an environmentally friendly approach because it requires low chemical and energy for enhancing enzymatic cellulose hydrolysis in lignocellulosic biomass. Biological pretreatments using microorganisms such as fungi can selectively degrade lignin, hemicellulose and very little of cellulose.[102] Lignin degradation by white-rot fungi occurs through the action of lignin-degrading enzymes such as peroxidases and laccases.[103] Therefore, it seems to be conceptually ideal pretreatment method, but the controllable, cost effective, and rapid system is not discovered to date. Chemical pretreatments are carried out to solubilize, in part, hemicelluloses and/or lignin, and are the most promising method to date.[87] Pretreatment method has to be selected based on the substrate and the desired end-product balancing with economic value. In this review, the selected leading pretreatment methods are briefly discussed: acid pretreatment, hydrothermal pretreatment, ammonia fiber explosion pretreatment, and organosolv pretreatment.

Table 9 Lignocellulose pretreatment methods and fractionation technologies.[21,100]

Pretreatment methods	Processes	
Physical Pretreatments	❑ Milling ❑ Hydrothermal ❑ Extrusion	❑ High pressure steaming ❑ Expansion ❑ Pyrolysis
Physicochemical & Chemical Pretreatments	❑ Explosion • Steam explosion • CO2 explosion • SO2 explosion • Ammonia fiber explosion (AFEX) ❑ Ionic liquid ❑ Oxidizing agents	❑ Acid • Sulfuric acid • Hydrochloric acid • Phosphoric acid • Sulfur dioxide ❑ Alkali • Sodium hydroxide • Ammonia • Ammonium sulfite
Biological Pretreatments	❑ Fungi	❑ Actinomycetes

2.3.2.1 Acid pretreatment

Acid pretreatment has been considered as one of most effective methods for rendering lignocellulosic biomass amenable to fermentation.[88,100] Dilute acid pretreatment effectively releases hemicelluloses, mostly xylan up to 90%, as forms of mono- or oligosaccharides and small amount of lignin under moderate condition (e.g., (0.5-2% H_2SO_4 at 121-160 ℃ for a few minutes).[104] Thereby, the cellulose is more accessible to enzyme, resulting in the significant improvement of enzymatic cellulose hydrolysis. Dilute sulfuric acid (H_2SO_4) is commonly used and widely effective for different types of biomass such as poplar, switchgrass, corn stover, and spruce.[105-110] However, this method requires pH neutralization and generates inhibition compounds for the downstream enzymatic hydrolysis.[111-113] The inhibition compounds are generated from sugar and lignin degradation to furfural, 5-hydroxymethyl furfural (HMF), and phenolic

compound (e.g., pseudo-lignin), which are mostly obtained under severe pretreatment condition.[113-115] For example, several studies have found that the acid-insoluble lignin content of dilute acid pretreated material is often higher than that of the starting material.[104] Sannigrahi et al. also reported that pseudo-lignin can be generated from carbohydrates without significant contribution from lignin during dilute acid pretreatment, especially under high severity pretreatment conditions.[116] In addition, equipment corrosion and acid recovery are additional drawbacks. To yield low inhibition compounds and high hemicelluloses/lignin recovery, it is necessary to optimize the pretreatment condition which is mathematically represented as the combined severity factor (log CS) calculated as:

$$R_0 = t \bullet \exp[(T_H - T_R)/14.75] \quad \textbf{(1)}$$

$$\log CS = \log R_0 - pH$$

where R_0 is the severity factor, t is the reaction time in minutes, T_H is the hydrolysis temperature in ℃, and T_R is a reference temperature. Reactor design also plays an important role like the selection of operating conditions. In order to maximize pretreatment efficiency different types of reactors have been introduced such as batch, continuous flow, percolation, and shrink-bed reactors.[117] For example, the batch reactor is used for low temperature batch process with high solids loading while the continuous flow reactor is used for high temperature reaction with low solid loading.[118] Different kinds of acid beside sulfuric acid have been applied as alternative methods to enhance cellulose hydrolysis such as triflulororacetic acid (TFA), hydrochloric acid, nitric acid, fumaric acid, and maleic acid.[119] For example, maleic, fumaric, or TFA acid pretreatment resulted in higher yield of hemicelluloses (similar to 70% yield from the

hemicellulose fraction) with less amount of the inhibition compounds at 150 ℃ at pH 1.65. TFA is considered as the mildest acid for pretreatment, leading to limited monosaccharide degradation among the acid pretreatment. However, TFA solvent is not generally used due to the high commercial price of solvents. Typical pretreatment methods and their features reported in the literature are described in Table 10.

2.3.2.2 Hydrothermal pretreatment: Steam explosion and Liquid hot water

Hydrothermal pretreatment (e.g., steam explosion or liquid hot water) is widely employed for lignocellulosic biomass which is subjected to pressurized steam or hot water for a certain period of time (e.g., 160-260 ℃ corresponding pressure 0.69-4.83 MPa for several seconds to a few minutes).[100] Hydrolysis reaction with no chemical additive is catalyzed by the release of *in situ* organic acids (i.e., acetic acid) generated from acetyl functional groups associated with hemicelluloses at high temperature.[100] This results in the breakdown of glycosidic linkages in hemicelluloses and of the β-O-4 ether bonds in lignin, solubilizing in liquid fraction as shown in Figure 21. Hydrothermal pretreatment provides reasonable hemicelluloses recovery and partial lignin depolymerization at moderate condition. In addition, hydrothermal pretreatment provides multiple benefits such as low yield of the inhibition compounds, no corrosion of the equipment, no/less chemical requirement.[120] However, this method is limited to use for softwood biomass due to lack of acetylated hemicelluloses in softwood.[121] To increase hemicelluloses recovery, decrease the production of the inhibition compounds, and extend application to softwood, acid catalyst has been introduced alternatively.[121] SO_2-steam explosion pretreatment, alternated from steam explosion pretreatment by the addition of dilute

sulfuric acid, allows shorter retention time and lower reaction temperature to maximize hemicellulose hydrolysis with reduction of the inhibition compound production compared to normal stem explosion pretreatment.[122-123] Moreover, it can be used for softwood biomass regarded as one of the most effective pretreatment method.[124] Without acid catalysis, alternative steam explosion and liquid hot water (LHW) have been also introduced by modifying pretreatment process in order to overcome their drawbacks. For example, two-step steam explosion pretreatment divides heating temperature into two phases: low temperature for hemicelluloses hydrolysis and high temperature for cellulose disruption.[124] This alternative process offers some additional advantages such as higher ethanol yields with lower enzyme dosages during subsequent enzymatic cellulose hydrolysis.[125] Typical pretreatment methods and their features reported in the literature are described in Table 10.

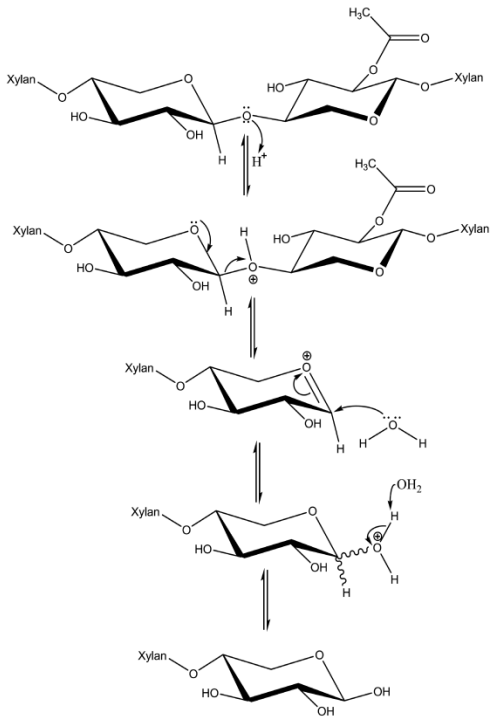

Figure 21 Acid-catalyzed hydrolysis of xylan.

2.3.2.3 Ammonia fiber explosion (AFEX) pretreatment

AFEX pretreatment uses liquid anhydrous ammonia (1-2 kg ammonia/kg biomass) exposed to biomass at mild temperature (< 100 ℃) and high pressure (1.7-2.0 MPa) for few minutes and then the pressure is explosively released similar to stem explosion pretreatment.[100,126] The rapid expansion of ammonia gas at the end of pretreatment causes the swelling and physical disruption of lignocellulosic biomass, resulting in decreasing cellulose crystallinity and disrupting lignin-carbohydrate linkage.[127] However, only a small amount of hemicelluloses and lignin is solubilized due to ammonia vaporization. The advantage of AFEX pretreatment is very low formation of inhibition compounds, full recovery of loading solid material, and lower moisture content.[126] The AFEX pretreatment is more effective on agricultural residues and herbaceous crops.[100] AFEX is limited for high lignin content material such as woody biomass.[128] Other issues include the requirement of the ammonia gas recovery system to reduce the operating cost. Typical pretreatment methods and their features reported in the literature are described in Table 10.

2.3.2.4 Organosolv pretreatment

Organosolv pretreatment uses organic or organic aqueous solvent mixtures in order to solubilize lignin and hemicelluloses in liquid phase, resulting in increasing cellulose digestibility.[129] Numerous organic solvent mixtures such as methanol, ethanol, acetone, ethylene glycol, triethylene glycol, and tetrahydrofurfuryl alcohol, have been utilized with an inorganic acid catalyst such as sulfuric or hydrochloric acid in order to obtain significant improvement of hemicellulose hydrolysis.[130] Organic solvents solely removed

lignin at high temperature (above 185 ℃), but very low yield of xylose was obtained.[131] Thus, organosolv pretreatment combined with acid hydrolysis allows the separation of hemicelluloses and lignin in a two-stage fractionation, resulting in high lignin removal (70%) and minimum cellulose loss (less than 2%).[129] The advantage of the organosolv pretreatment is the recovery of pure lignin which can be used for valuable co-products.[130] However, organic solvent has to be separated due to its inhibition role at downstream enzymatic cellulose hydrolysis. In addition, organic solvent has to be considered to be reused due to the high commercial price of solvents.[121] Typical pretreatment methods and their features reported in the literature are described in Table 10.

Table 10 Selected pretreatment methods and typical conditions.[132]

Methods	Procedures/Agents	Remarks	Examples of pretreated materials
Dilute acid pretreatment	0.75-5% H_2SO_4, HCl, or HNO_3 $p \sim 1$ MPa; continuous process for Low solid load (5-10 wt% dry substrate/mixture): T = 160-200 °C; batch process for high solids loads (10-40 wt% dry substrate/mixture): T = 160-200 °C	pH neutralization is required that generates gypsum as a residue >80% hemicellulose hydrolysis, 75-90% xylose recovery Cellulose depolymerization occurs at certain degree High temperature favors further cellulose hydrolysis, but inhibition compounds occurs	Poplar wood Bagasse, corn stover, wheat straw, rye straw, rice hulls Switchgrass, Bermudagrass
Steam explosion	Saturated steam at 160-290 °C, $p \sim 0.69$-4.851 MPa for several sec or min, then decompression until atmospheric pressure	High solids loads Size reduction with lower energy input compared to coomminution 80-100% hemicellulose hydrolysis, destruction of a portion of xylan fraction, 45-65% xylose recovery	Poplar, aspen, eucapyptus Softwood (Douglas fir) Bagasse, corn stalk, wheat straw, rice straw, barley straw, sweet sorghum bagasse, *Brassica carinata* residue, olive stones
Liquid hot water (LHW)	Pressurized hot water, p > 5 Mpa, T = 170-230 °C, 1-46 min, solid load < 20%	Addition of H_2SO_4, SO_2, or CO_2 improves efficiency of further enzymatic hydrolysis Cellulose depolymerization occurs at certain degree Lignin is not solublized, but it is redistributed 80-100% hemicellulose hydrolysis, 88-98% xylose recovery, >50% olygomers Low or no formation of inhibitiors Cellulose depolymeriation occurs at certain degree Further cellulose conversion >90% Partial soubilization of lignin (20-50%)	Timothy grass, alfalfa, reed canary grass Bagasse, corn stover, olive pulp Alfalfa fiber
Ammonia fiber explosion (AFEX)	1-2 kg ammonia/kg dry biomass, 90 °C, 30 min, p = 1.12-1.36 MPa	Ammonia recovery is required 0-60% hemicellulose hydrolysis depending on moisture, >90% olygomers No inhibitors formation Cellulose depolymerization occurs at certain degree Further cellulose conversion can be >90% for high-lignin biomass (<50%) 10–20% lignin solubilization	Aspen wood chips Bagasse, wheat straw, barley straw, rice hulls, corn stover Switchgrass, coastal Bermudagrass, alfalfa Newsprint
Organosolv	Orgnic solvents (methanol, ethanol, acetone, ethylene glycol, triethylene glycol) or their mixture with 1% of H_2SO_4 or HCl; 185 °C, 30-60 min, pH = 2.0-3.4	Solvent recovery required Almost total hydrolysis of hemicelluloses, high yield of xylose Almost total lignin solubilization and breakdown of internal lignin and hemicellulose bond	Poplar wood Mixed softwood (spruce, pine, Douglas fir)

2.4 Advanced imaging analysis for lignocellulose

To improve the detailed knowledge of plant cell wall and its change during pretreatment or deconstruction process, there is a demand for advanced analytical methods beside the conventional biomass laboratory analytical techniques. Thus, advanced imaging techniques have been recently highlighted and expended in the lignocellulosic biomass characterization. Imaging techniques visualize the chemical and physical changes on the surface of plant cell wall, resulting in an insight into the selection of more appropriate feedstock-pretreatment combinations or the optimization of processes. This section discusses the resulting spectroscopic (e.g., Raman and IR) and microscopic data (e.g., AFM, EM, and SMS). Specifically, the imaging mass spectrometry is fully described in Chapter 3.

2.4.1 Spectroscopic imaging analysis

Raman and infrared (IR) spectroscopy provide characteristic fundamental vibrations of a particular molecular structure which is obtained from the transition in vibrational and rotational energy levels of the molecule on absorption of radiations.[133] Raman spectroscopy involves inelastic scattering with a photon from a laser light source, whereas IR spectroscopy involves photon absorption with a molecule excited to a higher vibrational energy level. In addition, Raman scattering depends on the changes in the polarizability and IR absorption is based on the changes in the intrinsic dipole moments. Therefore, both provide complementary information of a sample with respect to the molecular vibration, providing both quantitative and qualitative molecular information. Both

techniques have been used for analyzing a variety of lignocelluloses with a capability of chemical mapping and imaging for the lignocelluloses.[134-135] Features of these imaging techniques are chemical specificity without tagging labels, non-invasiveness, high spatial resolution, and real-time monitoring capability. Thus, both have been developed as an important tool for biomass characterization.

In the effort of the application of Raman microscopy for lignocelluloses last decade, cellulose and lignin signals can be clearly distinguished without an interference of hemicellulose signals. In addition, a higher spatial resolution (~ 1μm) can be achieved by modifying a laser source in confocal microscopy mode which can distinguish multiple plant cell wall layers (e.g., secondary cell wall and middle lamella).[136-137] Gierlinger et al. has demonstrated spatial distribution of lignin molecules in a cross-section of poplar sample using the high resolution confocal microscopy.[135] The lignin molecules were preferentially located in the middle lamella and the cell corners in a cross-section of poplar sample. Recently, new techniques by modifying Raman microscopy have been employed to acquire the high resolution signals which are orders of magnitude stronger than spontaneous Raman scattering signals in biomass. There are two state-of-art Raman microscopies: one is coherent anti-Stokes Raman scattering (CARS) microscopy and another is stimulated Raman scattering (SRS) microscopy.[138-139] CARS has been adopted with a nonlinear optical process which is utilized with two laser beams: a pump beam and a Stokes beam.[140] Two beams interact with a sample and generate a coherent optical signal at the anti-Stokes frequency. The signal, then, is resonantly enhanced when two frequencies (anti-Stoke and Raman resonance) coincide. Ding et al. introduced CARS

microscopy to visualize spatial lignin distributions in a cell wall from both wild-type and lignin-downregulated Alfalfa.[138] CARS microscopy is also used to monitor dynamic change of lignin during microbial digestion of poplar sample. SRS microscopy is technically similar to CARS microscopy, but SRS microscopy has an advantage of detecting non-resonant electron background which allows detecting cellulose in biomass as well as lignin. In addition, characteristic signals are observed at the same frequencies of spontaneous Raman scattering, allowing spectral assignment easy by the rich spectral library.

Fourier Transform (FT) IR microscopy equipped with a focal plane array (FPA) detector allows rapid chemical mapping over large area with decreasing spectral acquisition time.[141] In FTIR microscopy, characteristic signals such as different oligosaccharides, lignin, and proteins are well-defined and a sample spectrum is readily assigned based on unique spectral bend.[142-143] However, FTIR microscopy is limited to spatial resolution due to long wavelength of infrared radiation and reduced penetration depth in high water content substrate. Yin et al. has demonstrated FTIR microscopy for investigating the effects of the chemical changes in spruce wood lumber during steam pretreatment, monitoring the secondary cell wall degradation.[144]

2.4.2 Microscopic imaging analysis

Microscopic techniques have been traditionally, commonly applied to understand morphology and ultrastructure of plant cell wall. Most common microscopic techniques are atomic force microscopy (AFM), scanning electron microscopy (SEM), transmission

electron microscopy (TEM), and light/optical/fluorescent microscopy. Each technique has been improved for better understating morphological feature of plant cell wall from micrometer to nanometer scale, resulting in providing multimodal information such as three dimensional structure or compositional properties.

AFM is a member of the scanned-proximity probe microscopy, i.e., scanning without surface contact, which represents high resolution surface topography under nanometer scale. Briefly, a microcantilever with a nanometer scale tip scans a sample surface and the deflections of the microcantilever are measured by multichannel photodiode detector. AFM has been used to measure the nanometer scale cellulose microfibrils on the surface of plant cell wall, resulting in understanding a molecular structure of plant cell wall.[145-147] For example, cellulose microfibrils at primary cell wall in native plant were observed as smaller, uniformly distributed, and highly parallel, whereas the microfibrils in dried plant cell wall were aggregated, disorganized, and twisted.[31, 148] These results suggest that the dehydration processes could alter microfibril structure and arrangement at primary cell wall. Ding et al. also proposed a new molecular model of the cellulose microfibril configuration in plant cell wall using high-resolution AFM.[149] With modifying system or alternative tip AFM can provide rich information such as porosity, granularity, elasticity, density, and morphology in plant cell wall. For example, mode-synthesizing atomic force microscopy (MSAFM), ultrasonic-based atomic force microscopy, has been employed for biomass characterization.[150-152] MSAFM allows the probe and sample to engage in nonlinear mechanical interaction, which is collected by a mode synthesizing sensor. Then, the signal provides multiple information such as subsurface mechanical

property and high resolution topography. Tetard et al. reported that oxidative delignification process caused significant change in middle lamella on a cross-section of poplar sample.[150] In addition, cell wall multilayer showed different mechanical properties (e.g., Young's modulus) in poplar samples. [152]

Electron microscopy such as SEM or TEM has been widely used for structural analysis of biomass due to a capability of the high spatial resolution imaging. Nanometer scale images allow understanding the orientation of microfibrils or the degrees of porosity of the membranes in plant cell walls.[54,153-154] In particular, environmental mode SEM (ESEM) development in recent years has enabled high resolution morphological information on fully hydrated tissues of lignocellulosic biomass. [155] ESEM allows the examination of practically any specimen under any gaseous conditions, resulting in imaging in wet and non-conductive system. Hamm et al. has demonstrated ESEM to observe an effect of thermal dehydration on wood stems.[155] Electron tomography (ET) providing a three-dimensional (3D) structure has been introduced in biomass characterization.[156-157] ET is based on the acquisition of multiple projection images (100-200) obtained from tilted angle frames by TEM. Then, these projections are aligned and combined, generating a 3D reconstruction of the original object. ET has showed the orientation of cellulose microfibrils and the arrangement of lignin and hemicelluloses in secondary cell wall of radiate pine.[157]

Light or optical microscopy is easy to access but is limited by the spatial resolution which is constrained by the diffraction limit of visible light (~200 nm).[158] Thus, several

microscopic techniques have been recently developed with increasing spatial resolution up to 50 nm: stimulated emission depletion (STED), reversible saturable optical linear fluorescence transitions (RESOLFT) microscopy, saturated structured illumination microscopy (SSIM), stochastic optical reconstruction microscopy (STORM), and total internal reflection fluorescence microscope (TIRFM).[159-160] These techniques, referred to as single molecular spectroscopy (SMS), are used to detect interaction between plant cell wall polymers, cellulolytic microbes, and enzymes in order to investigate a molecular dynamic and kinetic.[161] For example, SMS utilized with fluorescent tagging materials captures transient intermediates and provides direct information on the distribution of physical properties of a single molecule in a highly heterogeneous system. Ding et al. reported a capability of a single molecular detection and mapping at the molecular level of resolution when the tagged carbohydrate-binding modules (CBM) probed and detected a target molecule on the surface of plant cell wall by TIRF microscopy.[161] SMS images are frequently compared with other high resolution imaging techniques such as TEM or AFM.

CHAPTER 3

LITERATURE REVIEW B: IMAGING MASS SPECTROMETRY

Imaging mass spectrometry (IMS) is a powerful technique combining the chemical specificity and parallel detection of mass spectrometry with microscopic imaging capabilities.[162] The ability to simultaneously obtain chemical images from all analytes on sample surface provides spatial distribution of interesting species from atomic to macromolecules and their chemical organization. In addition, the chemical image can be correlated with physical features.[162-163] There are generally two types of imaging mass spectrometry based on the method of scanning a sample and generating a surface image: secondary ion mass spectrometry (SIMS) and matrix-assisted laser desorption/ionization (MALDI)-IMS techniques.

The first type of imaging mass spectrometry, SIMS, generates secondary ions using bombardment of an accelerated primary ion (PI) on the surface of samples.[164] On the other hand, MALDI-IMS uses pulsed laser to desorb molecules associated with a matrix from sample surface.[165] Ejected secondary ions or matrix associated fragment ions are simultaneously detected by a time-of-flight (TOF) mass spectrometry and mapped as an ion image across the sample.[162] Both MALDI and SIMS imaging provide spatial information about different classes of biomaterials on sample surface. For this reason, both imaging techniques are increasingly used to investigate a wide variety of chemicals within biological systems at tissue and single cell levels.[166] Both techniques are complementary with respect to spatial imaging resolution, mass detection range, and

degree of surface damage by ionization process.[167] In terms of the spatial resolution, SIMS can generate 2-dimensional (2D) chemical images at micron to 100 nm level while MALDI provides relatively lower spatial resolution images at ~ 10 µm.[168-170] Comparing the range of mass detection, MALDI has a capability to detect large molecules (theoretically unlimited) but SIMS can detect relatively lower mass species due to very low secondary ion efficiency above *m/z* 1000.[164,167] In terms of 3-dimensional (3D) imaging capability, SIMS equipped with dual beams (primary and sputter beams) can generate *in situ* 3D chemical image as well as depth profiling, whereas MALDI requires series of sectioned samples to generate a 3D chemical image.[171-172]

The advantage of IMS is that both techniques, in common, provide versatile information through retrospective data analysis such as four different modes of interpretation at single experiment: total ion image, total area spectrum, regions of interest (ROI) spectra, and mass-specific images (Figure 22).[167]

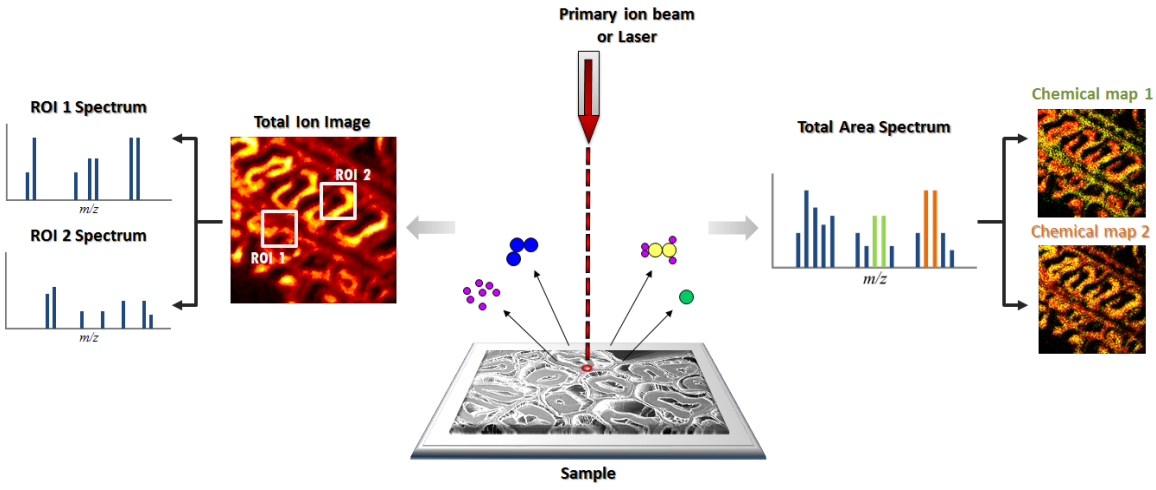

Figure 22 Overview of retrospective data process for two-dimensional image analysis.

Total ion image approximately shows how many different regions exist and where the target species are located on the analyzed area. In a total ion image, all of detected ions are visualized using pseudo-color scale at each pixel. Different level of color intensities at each pixel can be assumed as different chemical species which can be used for further MS interrogation. Total area spectrum acquired by summation of all the ions at the same mass-to-charge range gives an answer how many different chemical species exist within the analyzed area. Characteristic signals in the total area spectrum can be assigned using comparison with mass libraries or further experiment (e.g., MS/MS in MALDI-IMS). Once understanding the number of chemical species in the sample, the interesting species in ROI can be identified by summation of mass spectrum at each pixel and ROI spectra can be classified in all ROI across the surface. Finally, a mass-selected image, the chemical image of interesting species based on the identified mass signals, can represent spatial distribution on the surface of the sample. The number of mass-selected images can be generated as many as the number of interesting species on the surface of the sample. This chapter reviews imaging mass spectrometry fundamentals and their applications on lignocellulosic biomass.

3.1 TOF-SIMS: basic principle, instrumentation, and applications

3.1.1 Basic principle

Secondary ion mass spectrometry (SIMS) is a highly refined mass spectrometry (MS) technique specialized for surface analysis by detection of ionized particles (i.e., secondary ions) on the surface of the sample.[167] The basic mechanism to generate secondary ions is that a pulsed ion beam (i.e., primary ion: PI) with high energy

bombards a small spot on the surface and the PI energy is transferred to the atom which interacts with neighbor atoms, referred to as a collision cascade. [164,167] During the collision cascade, atoms or molecules receiving enough momentum return to the surface and are sequentially ejected as either neutrals or ions, referred to as sputtered particles (Figure 23). Only a small portion of positive or negative ions among the sputtered particles are considered as secondary ions and detected by mass spectrometer, e.g., time-of-flight (TOF) analyzer. Ionization probability of the species is totally based on the nature of the species, such as the chemical state of the surface or the environment of the species, referred to as matrix effect.[164,167]

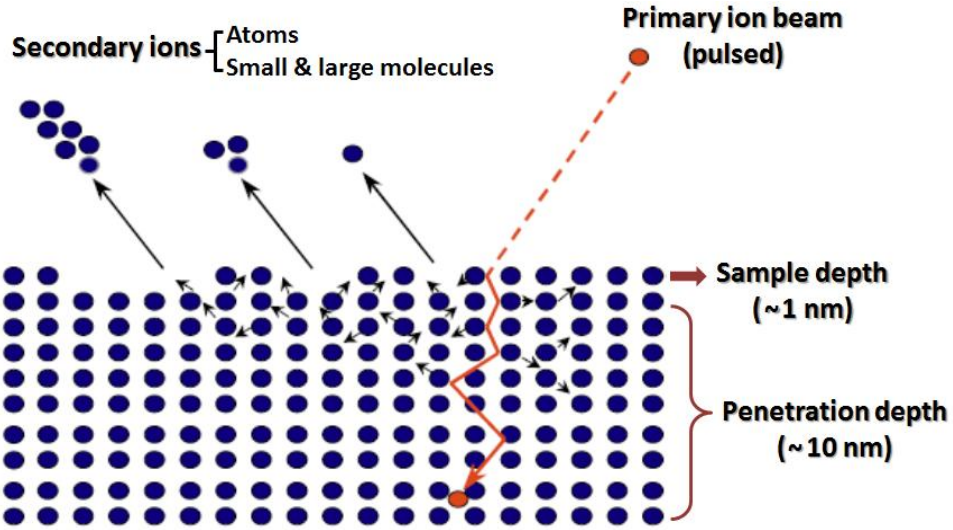

Figure 23 Schematic diagram of secondary ion emission process initiated by the impact of a primary ion on the surface of sample.[173]

3.1.2 Instrumentation

SIMS is generally equipped with liquid metal ion gun (LMIG) as a primary ion source using monatomic, polyatomic, or cluster ions. LMIG has become the standard gun because of its ability for rapid submicron imaging.[174] LMIG is the most important part that can significantly improve the sputter yields especially in organic and larger molecules. For example, static SIMS suffers from low secondary ion yields since limited PI dose less than 1.0×10^{13} ions/cm^2 is used to avoid chemical or molecular damage on the surface. In addition, ejection of large organic species or their fragments from the surface has also been limited even at dynamic SIMS mode which uses a continuous PI beam. For these reasons, recently cluster ions of gold (Au_n^+), indium (In_n^+), bismuth (Bi_n^+) and fullerene (C_{60}^+) have been developed as LMIG sources in order to improve secondary ion yields, replacing conventional monatomic ions (e.g., gallium). [164,167] The cluster ions dramatically increase sputter yields compared to conventional monatomic ions resulting in significant improvement of secondary ion yields, particularly of high mass species. For example, sputtering yields of water molecule from thin water ice film were calculated between Au^+ and cluster ions bombardment. The result showed that the cluster ions generate ~ 25 times more sputtered particles as determined by molecular dynamics computer simulation (Table 11).[164,175] Therefore, cluster ions have an advantage for analyzing and imaging biopolymer samples such as cellulose or lignins.

Table 11 Sputter yields of water molecules from ice under bombardment by 20 keV Au_n^+ ions compared with C_{60}^+.[164]

Primary ion sources	Au^+	Au_2^+	Au_3^+	C_{60}^+
Removed # of H_2O equivalents	100	575	1190	2510

To analyze insulators such as non-conducting organic or biopolymer materials, surface charging has to be considered due to increasing surface potential by cumulative positive primary ions. High potential beyond the acceptance level of analyzer leads to lose SIMS spectrum. For this reason, a flooding gun is applied to neutralize the surface (i.e., charge compensation) by irradiating with relative amount of a flux of electrons between PI intervals in duty cycle (Figure 24).[164,176]

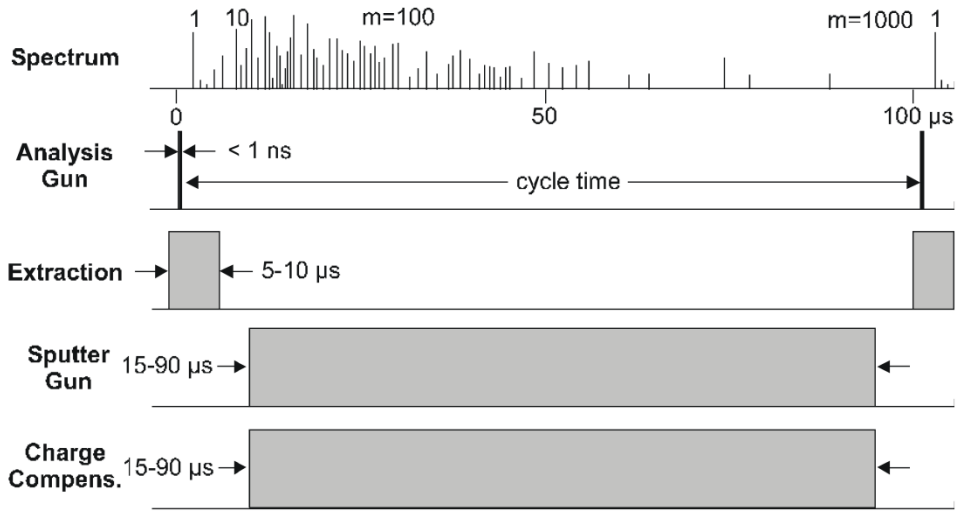

Figure 24 The duty cycle of the extractor, analysis gun, sputter gun and flood guns in TOF-SIMS.[177]

Emitted secondary ions voyage into mass analyzer by a high voltage potential to determine their mass as mass-to-charge ratio (*m/z*).[164,176] There are different types of mass analyzer: time-of-flight (TOF) mass spectrometer (MS), quadrupole mass analyzer, and magnetic sector.[164,178] Herein, TOF analyzer widely equipped with SIMS is briefly introduced. TOF-MS is based on a simple mass separation principle by time duration. Ionized secondary ions travel from the same staring position at the same time and are accelerated by means of a constant homogeneous electrostatic field. The velocity of accelerated ions is, of course, related to its mass-to-charge ratio and the time of arrival (*t*) to a detector is used to determine its mass, calculated as:

$$t = L\left(\frac{m}{2zV}\right)^{1/2} \quad \textbf{(2)}$$

where L represent length of flight path; m, mass of ion; z, charge of ion; and v, acceleration potential.[164] Hence, low mass ions will travel faster and hit the detector before heavier ions. TOF analyzer needs to be coupled with a pulsed ion beam due to separation of all the ions by mean of flight time duration. Accordingly all emitted ions can be detected over the full mass range. The advantages of TOF analyzer are great sensitivity, wide mass range detection, and high mass and spatial resolution compared to other types of mass analyzer.

The great function of TOF-SIMS is depth profiling which allows measuring vertical chemical information such as qualitative chemical composition or 3D ion image from the surface to subsurface of the sample. To erode an analyzed layer TOF-SIMS is equipped with a sputter gun using a focused DC ion beam which uses low ion energy (1keV ~

10keV).[167] In ION-TOF instrument, Dual source column (DSC) mounted with two different ion sources (commonly cesium and oxygen) is used to erode the surface. DSC is useful to switch between a thermal ionization cesium (Cs) source and an electron impact (EI) oxygen source.[167] The Cs source is used for profiling electronegative secondary ions while oxygen EI source is used for profiling electropositive ones.

3.1.3 Mode of operation for high mass resolution or high spatial resolution

In TOF-SIMS, there are the interrelationships between mass resolution, spatial resolution, and signal intensity and thereby a mode of operation has to be selected in order to obtain desired information such as high mass resolution spectra or high spatial resolution image. The mass resolution primarily depends on the duration of the PI.[162-163] It is noted that bunching a pulsed PI beam, referred to as bunched mode, can result in the highest mass resolution without concurrent loss of ion counts in TOF-SIMS (Figure 25).[174] However, the bunched mode is often a trade off in the spatial resolution which is no better than 2-5 μm. To improve the spatial resolution by submicron scale, the pulsed PI beam is operated under non-bunched mode with narrowing PI beam, referred to as burst alignment or collimated mode. However, both non-bunch modes seriously lose mass resolution so that close signals in mass spectrum can be not separated (Figure 25). The loss of the mass resolution results in a barrier for TOF-SIMS application in bio or organic materials because the number of possible interferences for molecular ions can be very high. To compromise the drawback of each mode, e.g., low mass resolution in non-bunched mode or low spatial resolution in bunched mode, a series of short PI pulses (~1.5ns) with non-bunching, referred to as burst mode, has been introduced only in ION-

TOF instrument. The burst mode, thereby, generates a series of separated signals from one species which can be summed up during mass interpretation, while the high spatial resolution is kept (Figure 25).

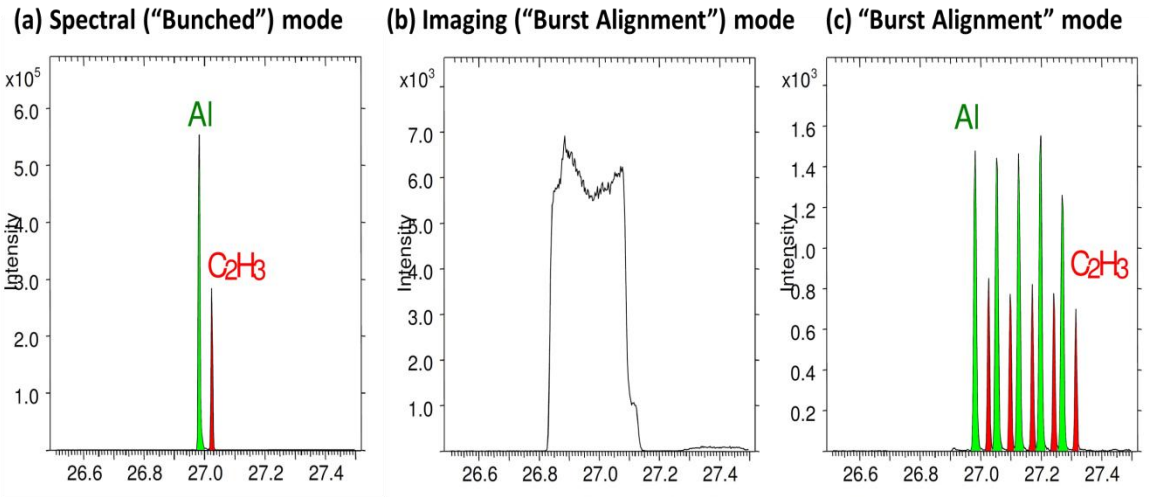

Figure 25 Examples of mass spectra based on operational modes.[179]

3.1.4 Two-dimensional (2D) image analysis

Visualizing chemical species with a spatial distribution on the surface of the sample provides valuable information in many areas, which is a crucial role of TOF-SIMS. There are two types of imaging modes: microprobe (scanning probe) and microscope modes (Figure 26).[162,178,180]

Microprobe mode is widely used due to technically simplicity and wide comparability with different type of mass analyzers. In microprobe mode, a small diameter of PI hits a spot at the whole region of interest and secondary ions are subsequently collected as a mass spectrum. Then the sample stage sequentially moves to the next spot for ionization

by the PI and the spectrum is recorded in a parallel manner.[167] These processes are repeated until the whole region of interest is scanned. All mass spectra obtained across the surface of the sample are recorded and reconstructed as the mass spectrometry image. Firstly, the intensity of each spectrum is assigned using pseudo-color scale and is displayed in a single pixel which is used to determine spatial resolution. In other words, spatial information inside a pixel governed by PI beam is lost, a major drawback of microprobe mode. However, the drawback may not be seriously affected in TOF-SIMS image since the image shows the greatest spatial resolution with sub-micron scale among the other IMS. All species detected by TOF analyzer are represented as total ion image which is summation of all of ions in mass spectrum in each pixel. Total ion image is useful to understand topographic information and to be correlated with optical/electron images. Characteristic ions assigned in total mass spectrum are also mapped and superimposed in the total ion image as many as the number of interesting species. In addition, ROI spectra where the interesting ions are localized in total ion image can be extracted for further analysis.

Microscope mode is technically complex and only comparable with TOF analyzer, but it provides superior spatial resolution which is not governed by PI beam. [162,178,180] In microscope mode, a large diameter PI beam illuminates the surface of the sample and emitted secondary ions are subsequently detected via TOF analyzer at a time. The detector records both the mass information (e.g., intensities of the interesting species) and geometrical position (e.g., x and y positions) of each ion. In microscope mode, therefore,

one image of one *m/z* can be generated at a time and then multiple shots of PI beam are repeated as many as the number of interesting species.

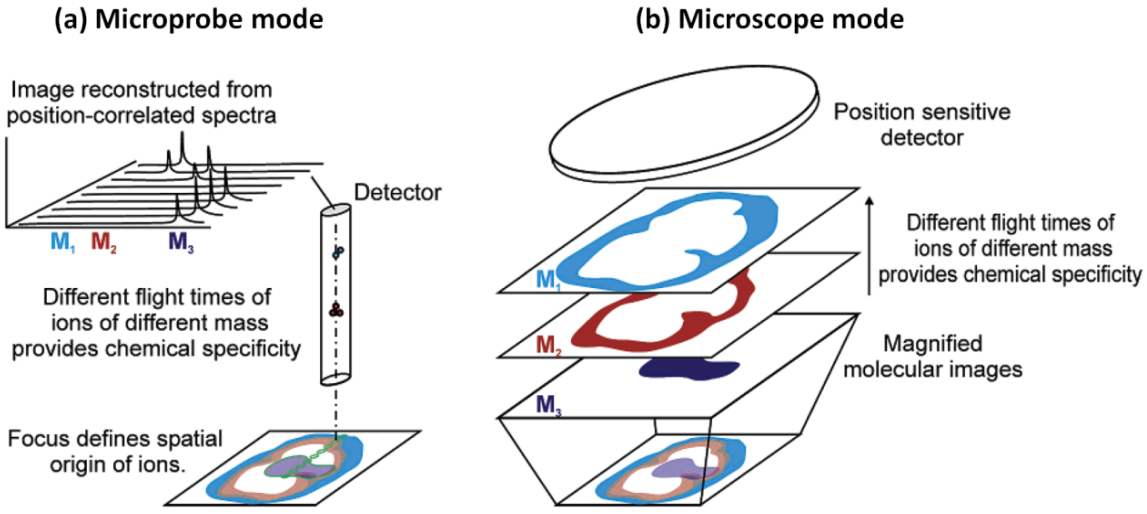

Figure 26 Schematic diagram of the two approaches for molecular imaging mass spectrometry: (a) microprobe and (b) microscope modes.[180]

3.1.5 Three-dimensional (3D) image analysis

Unique feature of TOF-SIMS is three dimensional (3D) MS imaging of the sample combined with the surface erosion using sputtering process, which provides vertical and lateral chemical information from surface to sub-surface.[169] The origin of secondary ions is the outmost one or two atomic or molecular layers although the energy of PI is distributed wider. As a result TOF-SIMS is possible to characterize ultrasurface rather than other techniques (e.g., XPS or Raman spectroscopy).[164]

A focused DC ion beam equipped in TOF-SIMS is capable of shallow surface erosion from several nm to μm so that the new surface below the analyzed surface can be

revealed.[167] Sequential TOF-SIMS analysis and surface sputtering allows monitoring of all interesting species simultaneously, referred to as depth profiling. The 2D imaging combined with the depth profiling under the optimal condition for the certain area removal can allow for 3D image reconstruction. 3D imaging by TOF-SIMS, referred to as 3D microarea analysis, is generally performed under dual beam mode (i.e., combination of DC ion beam and PI beam) in order to maintain high mass resolution and high spatial resolution during 2D TOF-SIMS imaging process. The advantage of the dual beam mode is the choice of the DC ion beam based on the composition or the desired kinetic energy so that a sputter rate and a penetration depth of the energy cascade can be controlled. For example, the lower voltage of the DC ion beam is preferred when it is desired to minimize the artifact formation and the surface disruption at the new exposed surface. In 3D microarea analysis, secondary ions are usually collected at relatively smaller area than the etch area because secondary ions from the crater edge can reduce spatial resolution by depth differences. Timing cycle of dual beams for 3D microarea analysis of insulating materials needs to be optimized due to adding a flooding gun for charge compensation. Generally the surface charge by a DC ion beam in one cycle is not fully compensated even though the flooding gun is simultaneously operating. This leads to reducing mass resolution because of an unstable sample potential and a large integral energy spread of the secondary ions. To maintain high mass resolution, single phase of charge compensation is then inserted before the analysis phase in duty cycle, referred to as non-interlaced mode.[177] Briefly in one cycle, a DC ion beam initially removes a certain amount of material for few seconds while the PI beam is blanked. Thereafter a flooding gun neutralizes the surface by irradiating with a relative amount of a flux of

electrons prior to PI beam irradiation. Subsequently, PI beam scans the surface inside the etch area and the secondary ions are analyzed while DC ion beam is blanked. In case of multiple scans between sputtering process, a flooding gun has to be applied at the end of each scan.

3.1.6 Applications of TOF-SIMS in biomass

Initially, TOF-SIMS applications were dominated by inorganic materials for semiconductor research and lately minerals processing with regards to surface chemistry, organic contaminants and adsorbates. TOF-SIMS application on the plants began with the investigation of inorganic species such as calcium, sodium, or phosphorous as well as its earlier application on pulp and paper researches. Earlier studies on pulp and paper using TOF-SIMS have provided basic knowledge such as lignin signal assignment, resulting in widening TOF-SIMS usability for cell wall characterization. Saito et al. investigated the lignin fragment ions and its structure generated by PI bombardment in TOF-SIMS. Series of prominent fragment cations were detected and characterized from the isolated hardwood or softwood lignin.[181-182] Moreover, their structures were identified using deuterium-labeled synthetic lignin: *m/z* 107 ($C_7H_7O^+$) and 121 ($C_7H_5O_2^+$) for *p*-hydroxyphenyl units (H), *m/z* 137 ($C_8H_8O_2^+$) and 151 ($C_8H_7O_3^+$) for guaiacyl units (G), and *m/z* 167 ($C_9H_{11}O_3^+$) and 181 ($C_9H_9O_4^+$) for syringyl units (S). Tokareva et al. applied TOF-SIMS to visualize lignins, carbohydrate, and metals on the sections of aspen and spruce wood and found the uneven distribution of H-lignin and G-lignin in cell wall whereas carbohydrates were uniformly distributed.[183] Interestingly TOF-SIMS was used

for historical architecture study where TOF-SIMS image discriminates the indistinguishable sapwood from the heartwood collected from an ancient construction.[184]

Recently TOF-SIMS has been applied on the field of biofuel and biomass research. Jung et al employed TOF-SIMS to characterize the surface of poplar sample after dilute acid pretreatment.[104] In dilute acid pretreated sample, xylan content on the surface relatively increased compared to the untreated sample whereas xylan content in bulk composition significantly decreased after dilute acid pretreatment. This result indicated the possibility of different chemistry between surface and bulk upon chemical treatment of woody material. Goacher et al. also employed TOF-SIMS to measure the cellulase enzyme activity on lignocellulosic biomass.[185] Principle component analysis of polysaccharide and lignin signals in TOF-SIMS spectra represented different cellulase activities in the samples, showing the possibility of TOF-SIMS as an enzyme activity measuring tool. The spatial distribution of the syringyl and guaiacyl lignin, and their ratio is considered as an important factor in biofuel research.[186] Zhou et al. determined the spatial distribution of the S and G lignins within a single cell wall of cross sectioned poplar stem where the guaiacyl lignin was predominantly located in the vessel cell wall while syringyl lignin was mainly located in the fiber cell wall.[187] Saito et al. also reported the vessel walls were G-rich and the earlywood was S-rich in maple wood.[188]

3.2 MALDI-IMS: basic principle, instrumentation, and applications

3.2.1 Basic principle

Matrix-assisted laser desorption/ionization (MALDI) uses a soft ionization technique for transferring large and/or nonvolatile molecules into the gas phase as intact ions for mass analysis (Figure 27).[189-190] MALDI is often coupled with a discontinuous mass analyzer such as a time of flight (TOF) analyzer because of a pulsed ion source in the system (see Chapter 3.1.2). The analytes are embedded in the matrix which absorbs the UV-light emitted from a laser aiding the analyte to desorb in intact form.[191]

The ionization mechanism in MALDI is not fully discovered yet, but the photochemical ionization model has been broadly accepted proposed by Ehring et al.[192-193] The photochemical ionization is a two-step process: the ionization of analyte and the proton/electron transfer to an analyte ion.[193-194] Briefly, primary matrix ions are produced by laser absorption and analyte ions are subsequently produced by the interaction between matrix ion and analyte ions. During the multi-photon ionization process all possible routes such as excited-state proton transfer, disproportionation reaction, and thermal ionization are considered to produce the matrix ions. The second step is producing the analyte ions by protonation or deprotonation from a collision process with matrix ions. An analyte ion is produced as either positive or negative form. Other ionization models such as cluster ionization have been also proposed.[191, 195]

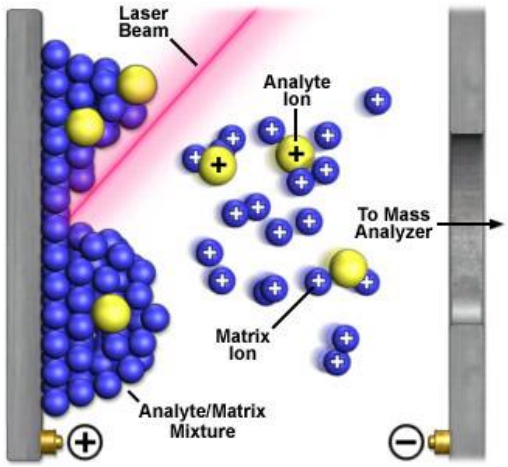

Figure 27 Schematic diagram of MALDI ionization.[196]

MALDI-based imaging mass spectrometry (IMS) was introduced by Caprioli et al. providing a capability of measuring both low and high mass species with the spatial information.[197] This MALDI-IMS leads to a significant advance in the field of MS. Once MALDI-IMS has employed TOF analyzer due to the nature of pulsed laser, the image are mostly acquired under microprobe mode (see Chapter 3.1.3). MALDI-IMS is amenable to detect low and high mass species with high sensitivity and thus this is well-suited to biological sample. It is noted that the quality and reproducibility of MALDI image such as the spatial distribution is, in some degree, governed by the matrix application and sample preparation.[162-163] For example the size of matrix crystal directly affects the spatial resolution of the MALDI image where the limitation is discussed in next part. Commercial MALDI-IMS routinely provides lower lateral resolution (around 100 ~ 25 μm) compared to TOF-SIMS imaging (~ 50 nm). Recently the lateral resolution in MALDI-IMS is improved up to ~ 0.6 μm with a specialized instrument and automated matrix application.[170]

3.2.2 Instrumentation and matrix application

MALDI-MS instrument consists of ionizer, mass analyzer, and detector as well as TOF-SIMS instrument mentioned at Chapter 3.1.2. As a source of ionizer, two types of UV lasers are typically employed: nitrogen laser (337 nm), and frequency-tripled and quadrupled Nd:YAG (355 nm or 266 nm).[163, 198] The UV laser sources are used to ionize matrix-analyte complex by the proposed mechanism (see Chapter 3.2.1). Positive or negative ions generated from the analyte are separated on the basis of mass-to-charge ratio in the mass analyzer. There are various types of analyzers such as TOF, Quadrupole, or Ion trap. TOF analyzer widely used in commercial MALDI instrument is briefly reviewed earlier (see Chapter 3.1.2). The ions accurately separated via the analyzer are detected and recorded in nanometer seconds.[198]

In MALDI-MS/IMS analysis the analyte material is mixed with a suitable matrix which is typically a low molecular weight organic acid prior to laser irradiation. This is the most crucial step, so-called as the matrix application, in order to properly ionize the analyte or improve the spatial resolution.[162, 199] First, the choice of matrix depends on the type of analyte. There are several organic matrices commercially available such as sinapinic acid (SA), α-cyano-4-hydroxy-cinnamic acid (CHCA), and 2,5-dihydroxybenzoic acid (DHB). The properties and applicability of three major matrices are summarized in Table 12.[199] The matrices are required to isolate the analyte by dilution, to make co-crystal with the analyte, to absorb laser energy, and to easily disintegrate the condensed phase of the co-crystal.

Table 12 Features of common matrices for MALDI-IMS.[199]

Matrix	SA	CHCA	DHB
Other name	• Sinapinic acid • 3,5-Dimethoxy-4-hydroxycinnamic acid	• α-Cyano-4-hydroxycinnamic acid	• 2,5-Dihydroxy benzoic acid
Structural formula	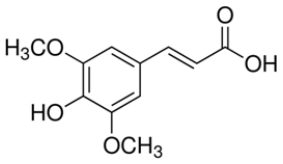	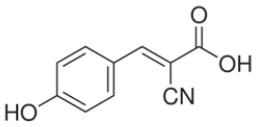	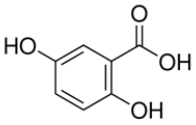
MW	224.21	189.17	154.12
Chemical formula	$C_{11}H_{12}O_5$	$C_{10}H_{12}NO_3$	$C_7H_6O_4$
Solubility	• Low solubility in H_20 • Soluble in methanol/ H_2O and poplar organic solvents	• Low solubility in H_20 • Soluble in methanol/ H_2O and poplar organic solvents	• Low solubility in H_20 • Soluble in methanol/ H_2O and poplar organic solvents
Subject	Protein (4 – 30 kDa)	Lipid and peptides (~8 kDa)	Lipid and peptides (~5 kDa)

The matrix is typically dissolved in suitable solvents such as methanol, water, acetone, acetonitrile and mixture of these. For MALDI-MS of liquid or bulk solid samples the analyte is also dissolved in appropriate solvents and then mixed with the matrix solution. For MALDI-IMS of the tissue sample containing the analytes matrix solution is applied on the surface the sample using various methods. During matrix application procedure, the matrix-analyte complex is co-crystallized on the surface. The size of co-crystal or the homogeneous coverage on the surface of the sample directly influences the quality of the MS image such as the spatial resolution. Another concern of the matrix application is that the matrix solution has to extract the analyte vertically from the sample into matrix crystals while avoiding the corresponding horizontal diffusion and analyte redistribution. For this reason several methods for matrix application have been developed such as

automatic depositing the matrix by robotic device or sublimating the matrix under reduced pressure, instead of manual dropping of the matrix.[199-200]

3.2.3 Applications of MALDI-IMS in biomass

Since Tanaka and Hillenkamp developed MALDI-MS technique, the versatility of MALDI-MS has been extended with the advent of protein profiling and imaging directly from the surface of thin biological tissue sections.[190, 197, 201-202] For example, MALDI-MS/IMS has been used to characterize a variety of microorganisms including bacteria, fungi, and viruses. Beside its clinical and biological applications, MALDI-MS/IMS has been little emphasized in plant biology, especially cell wall polymers, in part, due to the difficulty of cellulose and lignin ionization.

Metzger et al. employed MALDI-MS to determine the molecular weight (MW) of milled wood lignin (MWL) isolated from birch wood.[203] The mass spectrum of MWL showed a series of signals (i.e., different lignin oligomers) at *m/z* 2600 which was a good agreement with the average number MW (M_n) of birch MWL determined by gel permeation chromatography (GPC). Using synthetic lignin, De Angelis et al. also observed the repetitive units (mass interval: 178.6 Da) between *m/z* 500~1800 in mass spectrum. Recently, Yoshioka employed nano-assisted laser desorption/ionization (NALDI)-MS to detect synthetic lignin and observed intense of lignin signals.[204]

Cellulose is limited to ionization in MALDI-MS due to rigid and crystalline structure. Accordingly only part of cellulose has been detected by MALDI-MS up to 20

oligomers.[205-207] Sumi et al employed MALDI- to determine MW distribution of microcrystalline cellulose after hot-compressed water pretreatment.[205] The glucose oligomers in the water insoluble fraction after pretreatment were observed up to 18 glucose units containing mass interval 162Da, which was also confirmed by HPLC analysis. Jung et al. introduced MALDI-IMS to visualize cellulose oligomer distribution on the surface of poplar sample.[206] A cellulose poplar sample was prepared by removing hemicellulose and lignin and was, then, conducted to MALDI-IMS. MS images illustrated the distribution of cellulose up to 21 glucose oligomers on the surface of the poplar sample. For plant cell wall MS imaging, Lunsford et al. employed MALDI-linear ion trap (LIT)-MS in order to increase molecular specificity so that the chemical similarities of the various sugars and monolignols can be distinguished.[207] The MS images showed even distribution of both cellulose and hemicellulose ions on the surface. IMS has been also employed for the cellular distribution of metabolites in plant tissue in order to understand how the metabolism is controlled in cells.[208] For example, Burrell et al. reported that phosphorylated metabolites (e.g., glucose-6-phosphate) were unevenly distributed in wheat seeds upon different stages of development.[209]

CHAPTER 4

EXPERIMENTAL MATERIALS AND PROCEDURES

4.1 Materials

4.1.1 Chemicals and materials

All chemicals were purchases either from Sigma-Aldrich (St. Louis, MO) or VWR (West Chester, PA), and used as received. All gases were purchased from Airgas (Radnor Township, PA). Embedding material (OCT™) for cryotome sectioning was purchased from Sakura Finetek Tissue-Tek® (Alphen aan den Rijn, Netherlands). G8 glass fiber filter for carbohydrate analsys, double side adhesive carbon tape for SEM, and KBr powder (500 mg packet) for FTIR analysis were purchased from Thermo Fisher Scientific (Madison, WI). Glass slides and disposable blade were purchased from VWR (West Chester, PA). Plastic pouch for holocellulose pulping was purchased from Kapak Corporation (Minneapolis, MN).

4.1.2 Biomass substrate

Hybrid poplar clones were grown in for six months in a greenhouse at different locations. *Populus. deltoides* x nigra (DN34) clone was grown at National Renewable Energy Lab (NREL, Golden, CO) and *Populus tremula* x *alba* (PTA) clone was grown at Oak Ridge Nation Lab (ORNL, Oak Ridge, TN). The plants were grown on a flood table and watered four times a day automatically. The greenhouse maintained 16 h of light per day with 30-60% humidity. The entire poplar stems were cut and stored at -20 ℃. *Populus*

trichoparpa x deltoids (baseline poplar) was harvested between 2007 and 2008 by ORNL. Logs were debarked, split with an axe, chipped (Yard Machines 10HP, MTD Products Inc., Cleveland, OH), and knife milled (Model 4 Wiley Mill, Thomas Scientific, Swedesboro, NJ) through a 1 mm screen size; all of these operations were performed at NREL. After one month of air-drying at NREL, the chips had a moisture content of approximately 5 wt%. The material was further milled through a 20-80 mesh screen to produce particles with diameters of 0.18 mm to 0.85 mm (Thomas-Wiley Laboratory Mill Model 4, Arthur H. Thomas Company, Philadelphia, PA) before being shipped to Georgia Tech.

4.1.2.1 Milled poplar stem

Fresh poplar stem was pre-dried in vacuum oven at 40 ℃ overnight prior to milling. Dried poplar stem was milled using Thomas-Wiley Laboratory Mill machine and was simultaneously sieved through a 20-80 mesh screen. Milled sample was stored at -20 ℃ for further treatments.

4.1.2.2 Cryotome section of poplar stem

Cross-section samples of poplar were accomplished by employing a slight modification of the literature method.[210] A piece of poplar stem less than 2 cm in diameter was cross-sectioned to 50 μm thickness using a LEICA CM 3050S cryostat (Leica Biosystems, Richmond, IL) equipped with a disposable steel blade and embedding material (OCT™, Sakura Finetek). A disposable steel blade was installed and used after removing the lubricant on the blade surface using dichloromethane and ethanol. To avoid any

contamination from the embedding material, a piece of poplar stem was attached on the metal plate using a small amount of glue on the bottom edge instead of embedment (Figure 28). The chamber temperature for cryotome section was adjusted at -8 ℃ and cutting speed was manually controlled. Sectioned sample was stored at -20 ℃ for further treatments.

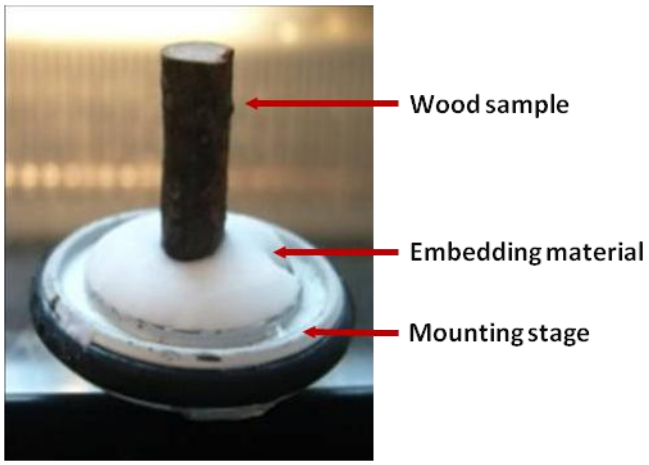

Figure 28 Non-embedding sample mount for a cryotome section.

4.2 Experimental Procedures

4.2.1 Soxhlet Extraction

Extractive-free poplar was prepared with sequential 5 h Soxhlet extractions according to TAPPI method T 204 cm-07.[211] Extractives for both the cross sectioned and milled samples were removed by placing the samples (5.00 g of dry weight) into an extraction thimble in a Soxhlet apparatus. The extraction flask was filled with CH_2Cl_2 (300 mL) and then refluxed with boiling rate of five solvent cycles per hour. The extractive-free solids were air dried overnight.

4.2.2 Holocellulose pulping

Holocellulose poplar was isolated from the extracted sample by removing lignin following well-cited procedures.[212-213] Extractive-free sample was subjected to an oxidative treatment with $NaClO_2$ (1.30 g/g sample) and acetic acid (0.14 M, 375 mL) in a sealed plastic pouch (Kapak Corporation). The pouch was then placed in a reciprocating water bath at 70 ℃ for 1 h. The oxidative treatment was repeated three more times to produce holocellulose. The holocellulose was recovered by filtration and washed thoroughly with deionized (DI) water, and air dried overnight.

4.2.3 Cellulose isolation

Cellulose poplar was isolated from the holocellulose samples by removing hemicellulose according to literature procedure.[214] Holocellulose sample was subjected to an acid hydrolysis with HCl (2.5 N 100 mL) at 100 ℃ for 4 h. The cellulose was recovered by filtration and washed thoroughly with deionized (DI) water, and air dried overnight.

4.2.4 Dilute acid pretreatment

Dilute acid pretreated samples were prepared using different sulfuric acid concentration and temperature. A sample (2.00 g dry weight) was presoaked in 1-2 vol. % H_2SO_4 (v/v, 200 mL) for 4 h with stirring at room temperature.[215-216] The presoaked sample was then filtered, washed with DI water, and then transferred to a 4560 mini-Parr reactor (300 ml) and added to 1-2 vol. % H_2SO_4 (% dry solids content). The vessel was heated to ~175 °C over ~30 min (at 5 ºC/min). The reactor was held at ~175 ± 2 °C (648 kPa) for ~10 min and then quenched in an ice bath. The pretreated samples were filtered and washed with

DI water and paramagnetic impurities were removed by washing the solids with a dilute aqueous solution of ethylenediaminetetraacetic acid (EDTA,300 mL, 0.2 N) and DI water followed by air dried overnight.

4.3 Analytical Procedures

4.3.1 Carbohydrate and acid-insoluble lignin (Klason lignin) analysis

Samples for carbohydrate constituents and acid-insoluble lignin (Klason lignin) analysis of both sectioned and milled poplar were prepared using a two-stage acid hydrolysis protocol based on TAPPI methods T-222 om-88 with a slight modification. The first stage utilizes a severe pH and a low reaction temperature (72 vol.% H_2SO_4 at 30 ℃ for 1 h). The second stage is performed at much lower acid concentration and higher temperature (3 vol. % H_2SO_4 at 121 ℃ for 1 h) in an autoclave. The resulting solution was cooled to room temperature and filtered using G8 glass fiber filter (Fisher Scientific). The remaining residue which is considered as Klason lignin was oven-dried and weighed to obtain the Klason lignin content. The filtered solution was analyzed for carbohydrate constituents of the hydrolyzed poplar sample using high-performance anion-exchange chromatography with pulsed amperometric detection (HPAEC-PAD) using Dionex ICS-3000 (Dionex, Sunnyvale, CA).[217] Error analysis was conducted by performing carbohydrate and acid-insoluble lignin analysis at least three times on milled samples. The plotted data represent the average and the error bars are one standard deviation.

4.3.2 TOF-SIMS analysis

TOF-SIMS analysis was performed using PHI TRIFT III spectrometer (Physical Electronics, Chanhassen, MN) or ION-TOF TOF·SIMS V instrument (ION-TOF, Münster, Germany). PHI TRIFT III spectrometer equipped with a ^{69}Ga liquid metal ion gun (LMIG) as a primary ion source. The instrument was operated in positive mode (22 keV) with 600pA of primary ion current. A raster size of 200 μm × 200 μm was used for all data acquisition from the samples. ION-TOF TOF·SIMS V spectrometer was equipped with a Bi liquid metal ion gun (LMIG) as a primary ion source and an O_2 sputter ion source. With a pulsed Bi_3^+ primary ion gun (25 keV) at a current of 0.18 pA positive spectra were obtained in either a high-mass resolution mode or in a high spatial resolution imaging mode. For a high-mass resolution mode, the sample (500 × 500 μm^2) was rastered by Bi_3^+ primary ion gun and charge compensation was subsequently applied using pulsing low-energy (25 eV) electrons onto the sample between successive primary ion pulses. Three data points per each sample were acquired from the three replicates, at least, to reduce site specificity and error analysis was conducted. For a high spatial resolution imaging mode, 2D SIMS image was generated by scanning the Bi_3^+ primary ion beam over the sample (50 × 50 μm^2, 256 × 256 pixels) for 100 times using a software (SurfaceLab6, ION·TOF, Münster, Germany). After 100 scans of topmost layer, surface erosion by O_2^+ sputtering source (300 × 300 μm^2, 2 keV) at a current of 0.65 pA was applied for 2s at non-interlaced mode. The imaging/sputtering cycles were repeated for 30 times and the data set was used for 3D image reconstruction. A 3D SIMS image was generated by stacking multiple 2D images using a software (ImageSurfer ver. 1.20, http://imagesurfer.cs.unc.edu/).[218]

4.3.3 Matrix application for MALDI-MS/IMS

Three matrixes were tested with cellulose to determine the best signal response: 2,5-dihydroxybenzoic acid (DHB), α-cyano-4-hydroxycinnamic acid (CHCA), and sinapinic acid (SA). Matrix solution was composed of 20 mg/ mL matrix (e.g., DHB) dissolved in acetonitrile/trifluoroacetic acid solution (TA:10% acetonitrile and 0.1% trifluoroacetic acid (v/v) in DI water). For MALDI-MS analysis, the section of each sample was milled for 10 min, while vibrating at 15 Hz using MM200 mixer mill (Retsch Inc, Haan, Germany). After 2 min of vortexing the milled sample (100 mg/ mL) with TA solution , the suspension was mixed with the matrix solution at a 1:100 (suspension: matrix solution) volume ratio. The mixture (~2 µL) was spotted onto a stainless steel MALDI plate and air dried. For preparing MALDI-IMS samples, an oscillating capillary nebulizer (OCN) matrix application system was employed.[219] Cross-section of poplar cellulose was fixed on a stainless steel MALDI plate using adhesive tape. The DHB matrix solution was delivered to OCN sprayer using a syringe pump (KD Scientific, Holliston, MA) at 60 µL/ min flow rate and uniformly dispersed through an oscillating capillary (Polymicro Technologies, Phoenix, AZ) with a nitrogen pressure of ~ 345 kPa for 20 min.

4.3.4 MALDI-MS/IMS analysis

MALDI-MS was performed using a Voyager DE STR MALDI-TOF-MS (Applied Biosystems, Framingham, MA) equipped with a 337 nm N_2 laser. The data was acquired under delayed extraction conditions in both reflectron and linear positive ion modes using an external mass calibration. Positive ion MALDI-MS data was acquired in both linear

and reflectron mode at an accelerating voltage of 12 and 20 kV, respectively, with an 85% grid ratio and a delay time of 400 ns. The laser power was set to a minimum for ionization (2900 arbitrary units (AU) for reflectron mode and 3300 AU for linear mode), and then increased by 100-200 units for medium and high laser intensity. The spectra were accumulated for 100 laser shots in a sample spot.

MALDI-IMS data were acquired at an accelerating voltage of 12 kV with optimized laser power (3100 AU) in linear positive ion mode. Raster scans were performed automatically on the sample surface with 12 shots for each spot. MALDI-IMS data was processed using the data acquisition software (MALDI MS Imaging Tool, MMSIT; Novartis Pharma AG, Basel, Switzerland, http://www.maldi-msi.org/) over the sectioned poplar cellulose. Mass spectra were processed for baseline correction and normalization using Data Explorer 4.0, which was supplied with the mass spectrometer. The MS images were reconstituted using Biomap software (Novartis Pharma AG, Basel, Switzerland).

4.3.5 Scanning Electron Microscopy

All cross-sectioned samples were mounted onto a stage and then coated with gold for 2 min by EM350 sputter. Images were acquired via a JEOL-1530 Thermally-Assisted Field Emission (TFE) Scanning Electron Microscope (SEM) (JEOL, Peabody, MA) at various resolving powers under 5 kV.

4.3.6 Fourier Transform Infrared (FTIR) Spectroscopy

FTIR spectra were measured on a Nicolet Magna 550 spectrometer (Thermo Fisher Scientific, Madison, WI) with deuterated triglycine sulfate (DTGS) detector and OMNIC 6.0 software. 64 scans at a resolution 4 cm^{-1} were averaged. Poplar sample (10mg of dry weight) was uniformly ground and well mixed with KBr powder (500 mg packet, Thermo Fisher Scientific). The samples were then transferred to a pellet making die and FTIR pellets were prepared applying ~11 Pa ram pressure (PHI Hydraulic laboratory press, City of Industry, CA) for 2 min under vacuum and FTIR spectra was acquired under N_2.

4.3.7 Solid-state NMR analysis

The NMR samples were prepared with milled wood or isolated cellulose added into 4-mm cylindrical ceramic MAS rotors. Solid state NMR measurements were carried out on a Bruker Avance-400 MHz spectrometer (Bruker, Billerica, MA) operating at frequencies of 100.55 MHz for ^{13}C in a Bruker double-resonance MAS probehead at spinning speeds of 10 kHz. CP/MAS experiments utilized a 5 μs (90°) proton pulse, 1.5 ms contact pulse, 4 s recycle delay and 4–8 K scans. All spectra were recorded on pre-wet samples (30–40% water content), and the line-fitting analysis of spectra was performed using NUTS NMR Data Processing software (Acorn NMR, Livermore, CA). Error analysis was conducted by performing three individual isolations, NMR acquisitions and line-fit data processing.

CHAPTER 5

SURFACE CHARACTERIZATION OF DILUTE ACID PRETREATED *POPULUS DELTOIDES* BY TOF-SIMS[1]

5.1 Introduction

Lignocellulosic materials are the most abundant biopolymers in nature, and have been highlighted as a potential source of biofuel production. These renewable resources will be drawn from agro-energy crops (non-food crops) and biomass residues originating from both forest and agricultural ecosystems, considered a second generation biofuel resource. These bio-resources are attractive biofuel feedstocks as they avoid "food or fuel" concerns and are generally low-cost and widely distributed.[220-221] Lignocellulosic materials are composed primarily of cellulose, hemicelluloses, lignin and pectin in plant cell wall. The very same properties that make lignocelluloses attractive as plant cell wall components contribute to its resistance to deconstruction to simple monosaccharides. This property is commonly referred to as the recalcitrance of biomass. This latter property contributes substantially to the current cost of biofuels and is the primary deterrent to the widespread commercialization of these types of alternative biofuels. To overcome recalcitrance, and increase conversion of biomass to biofuels by enzymatic

[1] This manuscript was accepted for publication in Energy and Fuels, 2010. It is entitled as — Surface Characterization of Dilute Acid Pretreated Populus deltoides by TOF-SIMS. The other authors are Marcus Foston, M. Cameron Sullards, and Art J. Ragauskas from School of Chemistry and Biochemistry at Georgia Institute of Technology.

hydrolysis and subsequent fermentation, a pretreatment process has been typically employed prior to biomass deconstruction.[22] Many studies have reported dilute acid pretreatment (DAP) significantly improved cellulose enzymatic hydrolysis rate and glucose yields as DAP alters the biomass ultrastructure and increases enzyme accessibility and activity.[21] A deeper understanding of the surface change, chemically or physically, on plant cell walls during DAP will give a better idea of how to optimize this pretreatment process.

To investigate and establish the fundamental mechanisms of plant cell wall structure, various analytical techniques have been applied including nuclear magnetic resonance (NMR), infrared spectroscopy (IR), Raman spectroscopy, X-ray diffraction (XRD), and X-ray photoelectron spectroscopy (XPS).[43,222-225] Liquid and solids NMR has been widely used to characterize the chemical structures of plant macromolecules but provide little topological information.[225] Electron microscopy (EM) techniques, such as scanning electron microscopy (SEM), transmission electron microscopy (TEM), and atomic force microscopy (AFM), have also been used to study the surface morphology, although they do not provide detailed chemical information.[226-229] Fluorescence imaging using monoclonal antibodies has been widely used to analyze the surface chemistry in plant cell walls. However, their use is limited due to the small library of antibodies for specific components within the plant cell wall.

Time-of-flight secondary ion mass spectrometry (TOF-SIMS) is a powerful method for characterizing the surface on solid samples without any special treatment with high

spatial resolution. Due to its unique capabilities of analyzing a solid surface, this technique has been used for the characterization of organic and polymeric materials in various fields.[176] Recent studies have highlighted some applications using TOF-SIMS in plant and animal tissue. For example, the cross sections of Hinoky cypress have been characterized semi-quantitatively for the distribution of plant extractives and these results were used to identify the interface between sapwood and heartwood.[184] Tokareva et al. have also employed TOF-SIMS to investigate the distribution of lignin, carbohydrates, extractives and metals across the cross sections of Norway spruce.[210] Though examples exist of using TOF-SIMS to characterize plant tissue, the application of TOF-SIMS to characterize biomass resources during their conversion to second generation biofuels has not been reported yet. This is partly due to the matrix-effect, defined as various ion yields depending on the chemical environment, and is the major barrier for quantitative measurement. It is difficult to make direct comparisons of the same analytical component or species between chemically altered samples because of this matrix-effect. To counter this effect several methods have been employed in an effort to make SIMS quantitative: (1) using a relative sensitivity factor, (2) matrix isotope species ratio, or (3) utilizing a method of standard addition.[176] In recent studies, normalization of peak intensity has been used for semi-quantitative analysis of natural polymers on wood-based fiber surfaces after refining.[230]

In this study, TOF-SIMS technique was examined to characterize cell wall component changes occurring on the surface of poplar stem after dilute acid pretreatment (DAP). Cross sections of extractive-free and holocellulose poplar stem were also analyzed and

used as a reference. The change in major cell wall components (i.e., cellulose, xylan and lignins) on the surface of dilute acid pretreated poplar was semi-quantitatively compared using both relative contents and the spatial distributions of major components visualized by TOF-SIMS. To further elucidate the spatial re-distribution of major cell wall components experienced during pretreatment, SIMS images were transformed to processed mapping images via a MATLAB platform. Finally the chemical changes in the surface components after DAP were correlated with gross topological changes using electron microscopy (EM) images.

5.2 Experimental Section

5.2.1 Materials

Samples were prepared as described in Chapter 4 (4.1.2 Biomass substrate). *Populus. deltoides* x nigra (DN34) clone was grown at NREL and six-month-old juvenile poplar stem was collected for this study. Poplar stem was sectioned or milled as described in Chapter 4 (4.1.2.1-2 Milled poplar stem and Cryotome section of poplar stem). Both sectioned and milled samples were treated under same conditions with various methods. Flow diagram for sample preparation is shown in Figure 29.

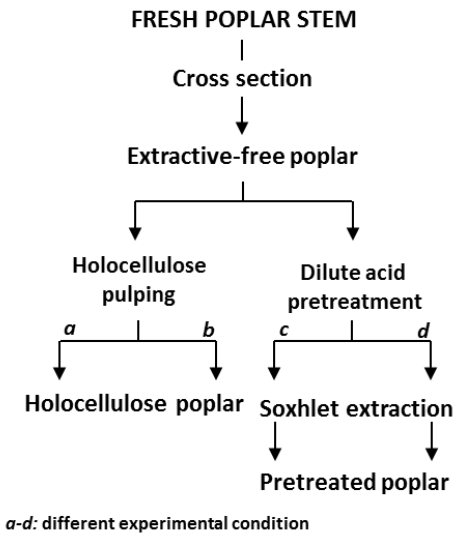

Figure 29 Flow diagram describing the sample preparation of poplar stem.

5.2.2 Extractive-free, holocellulose, and cellulose poplar preparation

Samples were prepared as described in Chapter 4 (4.2.1-4.1.3). All the results from the analyses were calculated based on the oven dry weight of biomass that was determined by measuring the moisture content using a moisture analyzer. The analyses that include standard deviations were done in three replicates.

5.2.3 Dilute acid pretreatment (DAP) and severe DAP

Dilute acid pretreatment process was performed as described in Chapter 4 (4.2.4 Dilute acid pretreatment). Two different conditions of pretreatment were applied to both sectioned and milled samples: 1 vol. % H_2SO_4 and 160 ℃ for 10 min (DAP) or 2 vol. % H_2SO_4 and 175 ℃ for 10 min (severe DAP). After post pretreatment process (e.g., DI water washing for neutralization), a sample was subsequently Soxhlet extracted with

CH_2Cl_2 in order to remove soluble residue on the surface. A sample was then air dried (between glass slides especially for a sectioned sample).

5.2.4 TOF-SIMS analysis

TOF-SIMS spectra of cross-sectioned samples were collected with a PHI TRIFT III spectrometer as described in Chapter 4 (4.3.2. TOF-SIMS analysis). The instrument was operated in positive mode (22kV) with 600pA of primary ion (^{69}Ga) current under high mass and imaging resolution mode. TOF-SIMS image of individual components was obtained by mapping selected positive ions. MATLAB platform was used for mapping process from TOF-SIMS images. Only the selected pixels over middle brightness on SIMS image were filtered and transformed by MATLAB ver.7.2.

5.2.5 Carbohydrate and acid-insoluble lignin (Klason lignin) analysis

Carbohydrate profiles and acid-insoluble lignin content in cross-sectioned and milled samples were determined as described in Chapter 4 (4.3.1 Carbohydrates and acid-insoluble lignin analysis).

5.2.6 Scanning Electron Microscopy

Surface morphology of cross-sectioned poplar before and after various treatments was observed by using JEOL-1530 TFE-SEM as described in Chapter 4 (4.3.6 Scanning Electron Microscopy). The images were taken at various resolving powers under 5 kV.

5.2.7 FTIR Spectroscopy

Transmission mode FT-IR spectra were collected with a Nicolet Magna 550 spectrometer as described in Chapter 4 (4.3.7 Fourier Transform Infrared (FTIR) Spectroscopy). Both sectioned and milled samples were finely ground to powder and dried at 105 °C for 12 h. Then, the sample (10mg of dry weight) was mixed KBr powder for making FTIR pellet.

5.3 Result and discussion

5.3.1 Effects of sample preparation

Although the pretreatment of biomass, prior to enzymatic deconstruction, is typically accomplished on sawdust or milled wood, for this study cross sections of poplar stem, e.g., extractives-free and dilute acid pretreated poplar, was elected to facilitate TOF-SIMS analysis. To ensure that the 50 µm thick cross-sectioned poplar stem was undergoing comparable pretreatment chemistry as milled wood, 20-mesh ground poplar was also dilute acid pretreated and both materials were characterized for their sugars profiles and gross chemical constituents by FTIR. The extractive-free, holocellulose, severe holocellulose, cellulose enriched, and dilute acid pretreated poplar samples were prepared. The ground and cross-sectioned poplar from samples were analyzed by FTIR in Figure 30. A major absorption band at 1740 cm^{-1} was assigned to carboxylic-ester bonding, which originates from acetyl groups of the non-cellulosic fraction in the poplar cell wall.[231] Generally, acetylated hemicellulose is contributed as a form of 4-O-methylglucuronoxylan in poplar.[232] The absorption peaks around 1595 and 1510 cm^{-1} were assigned to aromatic skeletal vibration from lignin. The absorbance at 1428 cm^{-1}

was also attributed to lignin, while other wavenumber ranges represented common absorption bands for example glycosidic linkages at 1150 cm^{-1}, β-(1→4) linkages at 890 cm^{-1}, and hydroxyl group at 3500 cm^{-1}.[233-234] In milled poplar, acetylated hemicellulose absorbance at 1740 cm^{-1} was observed in the extractive-free, holocellulose and severe holocellulose samples in Figure 30a. However, the hemicellulose absorbance peaks nearly disappeared in cellulose enriched and DAP poplar. This observation was consistent with carbohydrate composition of the ground samples, in which only trace amount of hemicellulose was detected in cellulose enriched and DAP poplar (Table 13). Two peaks corresponding lignin (1510 and 1428 cm^{-1}) were clearly observed in extractive-free and DAP poplar, while an additional lignin peak (1595 cm^{-1}) was overlapping with the adjacent broad absorption (1650 cm^{-1}) originating from water. Moreover, lignin absorption peaks were not observed in holocellulose and cellulose enriched poplar in Figure 30a. The spectra of cross-sectioned poplar presented identical spectral patterns with those of ground poplar in Figure 30b. Bulk carbohydrate analysis of both ground and sectioned poplar exhibited nearly similar carbohydrate and lignin distribution values as summarized in Table 13. The results of these analyses suggest that under the DAP conditions ground and cross-sectioned poplar are undergoing comparable chemical processes.

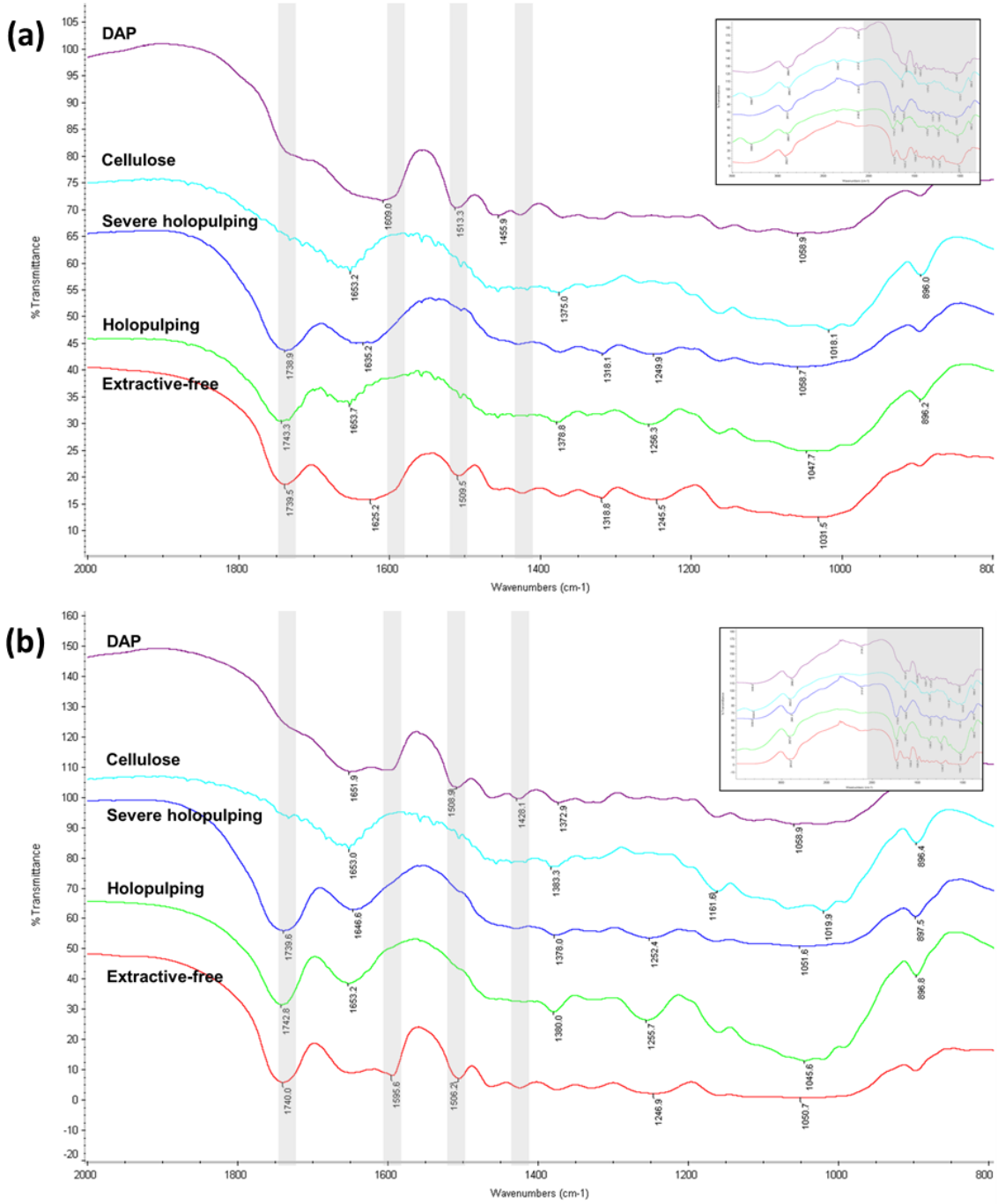

Figure 30 Part of FTIR spectra of (a) milled poplar and (b) sectioned poplar. Inner boxes represent full range spectra.

Table 13 Carbohydrate compositions of sectioned and milled poplar after treatments.

% [a] (STDEV) [b]	Extractive-free poplar		Holocellulose poplar		Cellulose poplar		DAP poplar	
	Sectioned	Milled	Sectioned	Milled	Sectioned	Milled	Sectioned	Milled
Arabinose	0.6 (1.9)	1.7 (0.1)	< 1 (1.7)	0.9 (0.1)	< 1 (0.1)	< 1 (0.1)	< 1 (0.7)	< 1 (0.1)
Galactose	2.0 (2.2)	2.3 (0.4)	1.3 (1.9)	1.6 (0.1)	< 1 (0.1)	< 1 (0.1)	< 1 (0.9)	< 1 (0.1)
Glucose	72.9 (0.9)	71.7 (0.2)	73.3 (1.1)	72.2 (0.2)	96.6 (0.3)	96.9 (0.3)	98.4 (1.5)	98.0 (1.9)
Xylose	20.2 (4.5)	21.1 (0.2)	21.5 (0.1)	22.2 (0.4)	1.4 (0.3)	1.3 (0.3)	1.0 (0.1)	0.6 (1.9)
Mannose	4.4 (0.5)	3.1 (0.2)	3.6 (1.9)	3.1 (0.1)	1.9 (0.1)	1.8 (0.1)	< 1 (0.1)	< 1 (1.9)

[a]: Average of relative carbohydrate compositions based on total sugar units, [b]: Standard deviation.

5.3.2 Carbohydrates and Klason lignin analysis

In an effort to quantitatively analyze the changes to the compositions of the structural carbohydrates and lignin, which make up the bulk of the biomass samples, monosaccharide and Klason lignin analysis were performed on cross sections of poplar stems. An extractive-free sectioned poplar was used as a baseline material for comparison. Figure 31 summarizes the variation of bulk carbohydrate and Klason lignin distribution after various treatments. The majority of the hemicelluloses seen in the extractive-free poplar, characterized by the xylose, mannose, arabinose, and galactose contents, were hydrolyzed after DAP, while the relative glucose content increased by 40% after DAP. The relative Klason lignin content detected previously in extractive-free poplar slightly increased ~ 5% as a result of DAP. After severe dilute acid pretreatment (sDAP), the relative Klason lignin content was increased significantly by ~60%, while relative glucose content increased by ~20% as compared with that of extractive-free

poplar. One possible explanation for the increment of Klason lignin content after sDAP is that cellulose is easily degraded than lignin under severe acidic pretreatment condition.

In addition, at high temperatures and long residence times during pretreatment polysaccharides have been shown to undergo acid catalyzed dehydration to yield a lignin-like structure referred to as pseudo-lignin. This material is acid insoluble and therefore could contribute to the Klason lignin content.[235] Li et al. estimated 25-40% of the residual lignin content in steam-exploded aspen wood (170 ℃ for 210 min) was actually pseudo-lignin. Holocellulose poplar was obtained from cross sections of extractive-free poplar. To further clarify the component distribution, especially for lignin at the poplar surface, an additional sample was obtained from a more severe holocellulose pulping process, which is defined here as severe holocellulose poplar. The relative Klason lignin content after holocellulose pulping process dramatically decreased over 85% as compared with that of extractive-free poplar. Interestingly, the severe holocellulose poplar still contained 1.5% Klason lignin which was approximately half that of the holocellulose poplar.

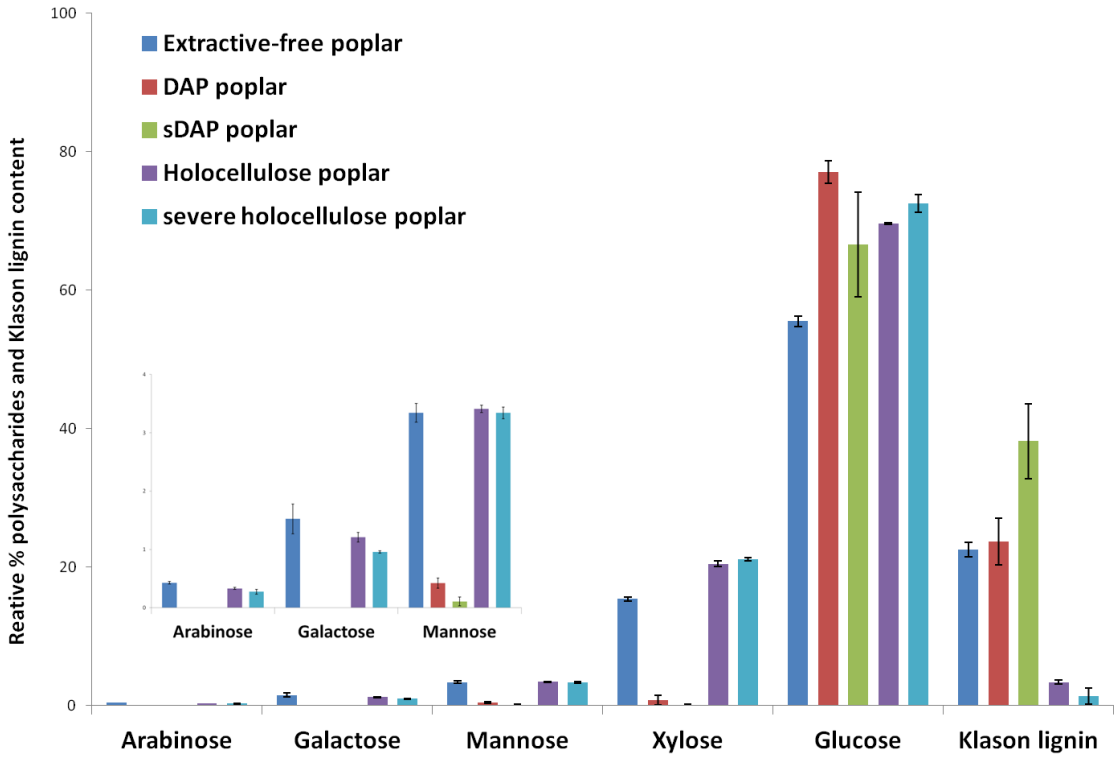

Figure 31 Carbohydrate and Klason lignin contents of cross sectioned poplar after treatment; Y scale is enlarged on inner graph to show the low contents of hemicelluloses.

5.3.3 Surface analysis of dilute acid pretreated poplar

To investigate how the chemical constituents of the cell wall change during pretreatment, the cross sections of native and DAP poplar were analyzed by TOF-SIMS. Figure 32 shows positive ion mass spectra (*m/z* 100-200) obtained from various treated poplar by TOF-SIMS. Characteristic TOF-SIMS ion fragments of the major components in poplar were identified according to published literature values.[181,229-230,236-237] Cellulose yields primary fragments of *m/z* 127 ($C_6H_7O_3^+$) and 145 ($C_6H_9O_4^+$), while xylan (major hemicellulose component) fragmented to *m/z* 115 ($C_5H_7O_3^+$) and 133 ($C_5H_9O_4^+$).[229-230] Depolymerized fragments of lignin were also assigned employing the results by Saito et al. The signals at *m/z* 167 ($C_9H_{11}O_3^+$) and 181 ($C_9H_9O_4^+$) were assigned to syringyl (S) lignin units and *m/z* 137 ($C_8H_9O_2^+$) and 151 ($C_8H_7O_3^+$) to guaiacyl (G) lignin units.[181]

All characteristic fragment ions of cellulose, hemicellulose and lignin were detected with various intensities depending on the treatment conditions as illustrated in Figure 32. Although the bulk carbohydrate and Klason lignin analysis indicated a 95% drop in the relative amount of hemicellulose sugars after DAP, TOF-SIMS analysis detected the considerable presence of xylan fragments on the surface of the dilute acid pretreated poplar as shown in Figure 32b. Also the peak intensities of xylan did not change significantly even after severe dilute acid pretreatment (sDAP) as shown in Figure 32d. Ion fragments of G-lignin units in holocellulose poplar were still observed while only trace levels of S-lignin units were detected in Figure 32c. A similar pattern of G and S-lignin units was detected even in severe holocellulose poplar (Figure 32e), which were in contrast to the results of bulk carbohydrate and Klason lignin analysis.

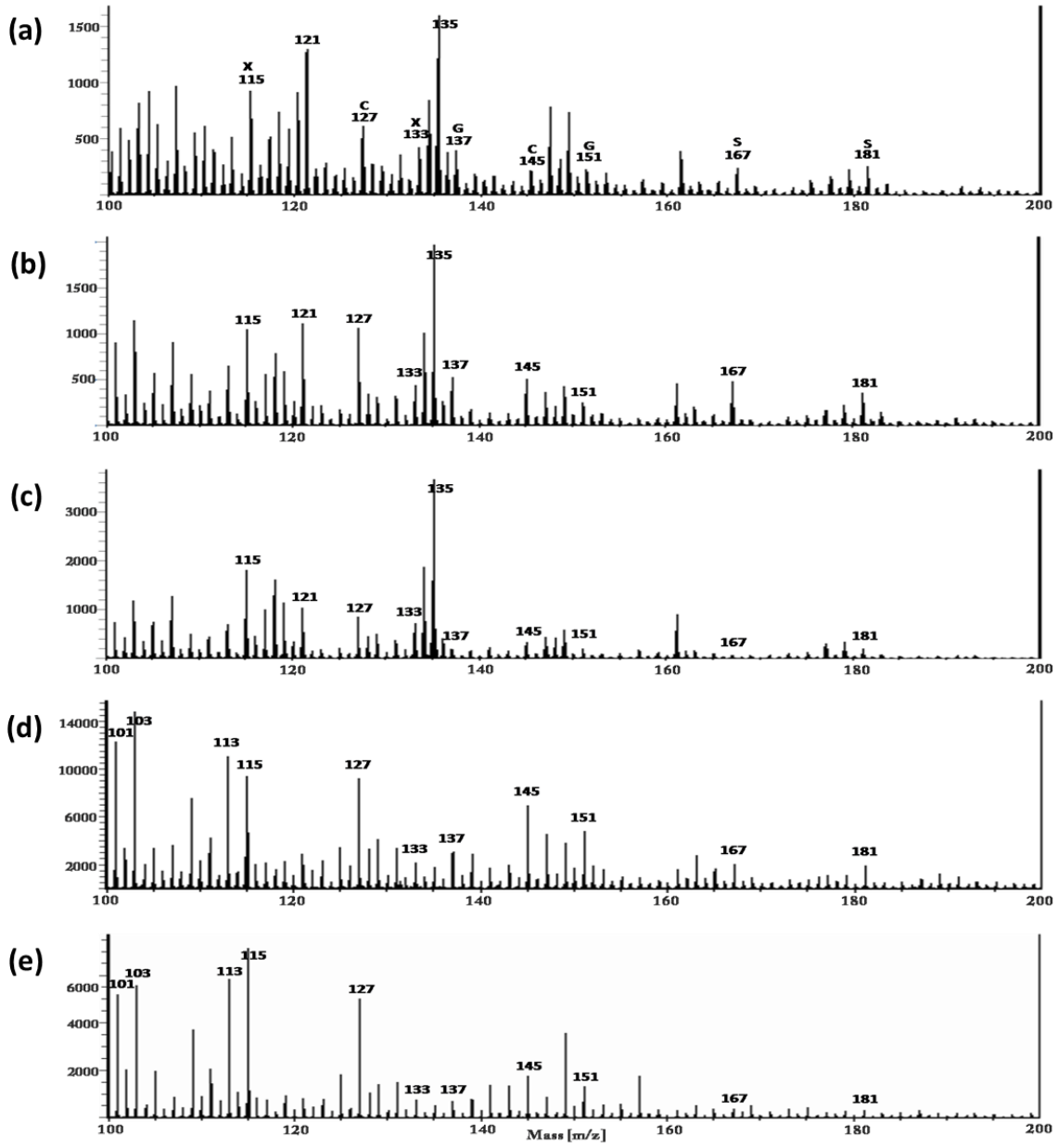

Figure 32 Part of positive TOF-SIMS spectra: (a) Extractive-free poplar, (b) DAP poplar, (c) Regular holocellulose pulping poplar, (d) sDAP poplar, (e) severe holocellulose pulping poplar. Characteristic ions are marked as C (cellulose ions), G (guaiacyl lignin ions), S (syringyl lignin ions), and X (xylan).

To observe quantitative cell wall component change on the surface of poplar, normalization of peak intensity from TOF-SIMS is required. Since secondary ion yields vary based on chemical environment, the direct comparison of the absolute ion counts cannot be employed to obtain quantitative information in SIMS.[176] Therefore ion count normalization following the procedures described by Kleen was performed prior to comparison of relative intensities.[237-238] The relative intensity of each species was calculated as the sum of its primary fragments in Figure 33.[237] The relative intensity of S-lignin units dramatically decreased on the surface of holocellulose poplar as compared with that of extractive-free poplar, but the intensity of G-lignin units only slightly decreased. However, the relative intensity of xylan increased approximately two-fold, whereas the cellulose signal did not change significantly on the surface of holopulped poplar. Interestingly, after the severe holocellulose pulping treatment, the relative intensities of the major cell wall components did not change compared with those of regular holocellulose poplar, showing almost identical normalized ion counts. This result was contrary to bulk carbohydrate and Klason lignin analysis which indicated a ~ 50% reduction of relative lignin content after severe holocellulose pulping. TOF-SIMS would suggest that only a small proportion of lignin on the surface is removed by the holopulping process. The observed increases in intensities of the characteristic cell wall components after DAP when compared with extractive-free poplar may result from two factors: matrix-effects and/or further exposure of characteristic components to the surface. Since DAP can break down the lignin-carbohydrate complex and disrupt the crystalline structure of cellulose, deformation of plant cell walls should be addressed.[239] This change in surface morphology and chemistry may permit higher yields of secondary ion

fragments from the biomass surface. The relative intensities of cellulose and G-lignin units after DAP (1% H_2SO_4 at 160 °C for 10 min) were doubled as compared to those of extractive-free poplar. This most likely suggests more cellulose was exposed to the surface, which can be partially supported by bulk carbohydrate and Klason lignin analysis. The relative glucose content in bulk carbohydrate analysis was doubled after DAP as compared to extractive-free poplar while almost all hemicelluloses were removed upon DAP. Interestingly, the relative intensity of xylan after DAP increased by 30%, while the intensity of xylan after sDAP slightly decreased as compared to extractive-free poplar. This result suggests that DAP also causes migration of xylan fragments to the surface of sectioned poplar prior to solublization of xylan due to acid hydrolysis. As additional evidence of this migration, the severe pretreatment condition (2% H_2SO_4 at 175 ºC for 10 min) seems to release xylan from the biomass which has accumulated on the surface of the poplar during the pretreatment. Brunecky et at. observed similar migration of xylan in DAP corn stover by confocal laser microscope using fluorescent labeled antibody. They detected decreasing xylan signal as a function of increased DAP severity and suggested the migration of xylan from the central cell wall to the lumen and middle lamella during DAP.[240] Notably, the intensities of S-lignin units after sDAP dramatically decreased as well as xylan, whereas the intensities of cellulose and G-lignin units remained relatively similar to those of dilute acid pretreated poplar. This may indicate that S-lignin units are more reactive than G-lignin units and therefore easily removed upon pretreatment.

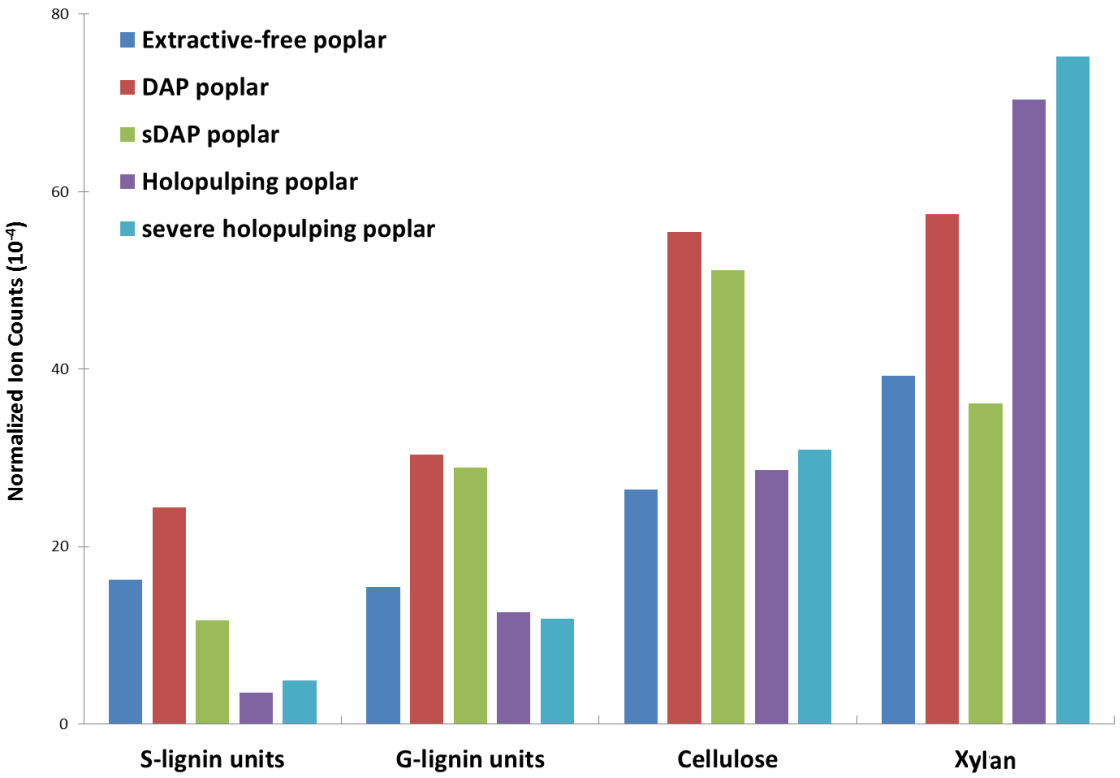

Figure 33 Relative intensities of each component in cross-sections of different treated poplar by TOF-SIMS.

TOF-SIMS images were used to determine the spatial distribution of cellulose, xylan and lignin after DAP. Figure 34 shows ion count images of characteristic cell wall species on the surface of dilute acid pretreated poplar Figure 34a represents a total ion image and the other images represent the integrated intensities of selected mass fragments as a function of pixel position (Figure 34b-e). Brighter colors on TOF-SIMS images correspond to higher intensities of the indicated species. According to Figure 34, the characteristic ions of the major components (cellulose, xylan, and G- & S-lignin units) were observed across the cell wall while the lumen were shown as black color on the surface of cross-sectioned poplar. The high number of low intensity signals often makes it difficult to identify the

spatial distribution of a particular species in areas having overlapping ion fragments for various species and to determine how they relate to each other.

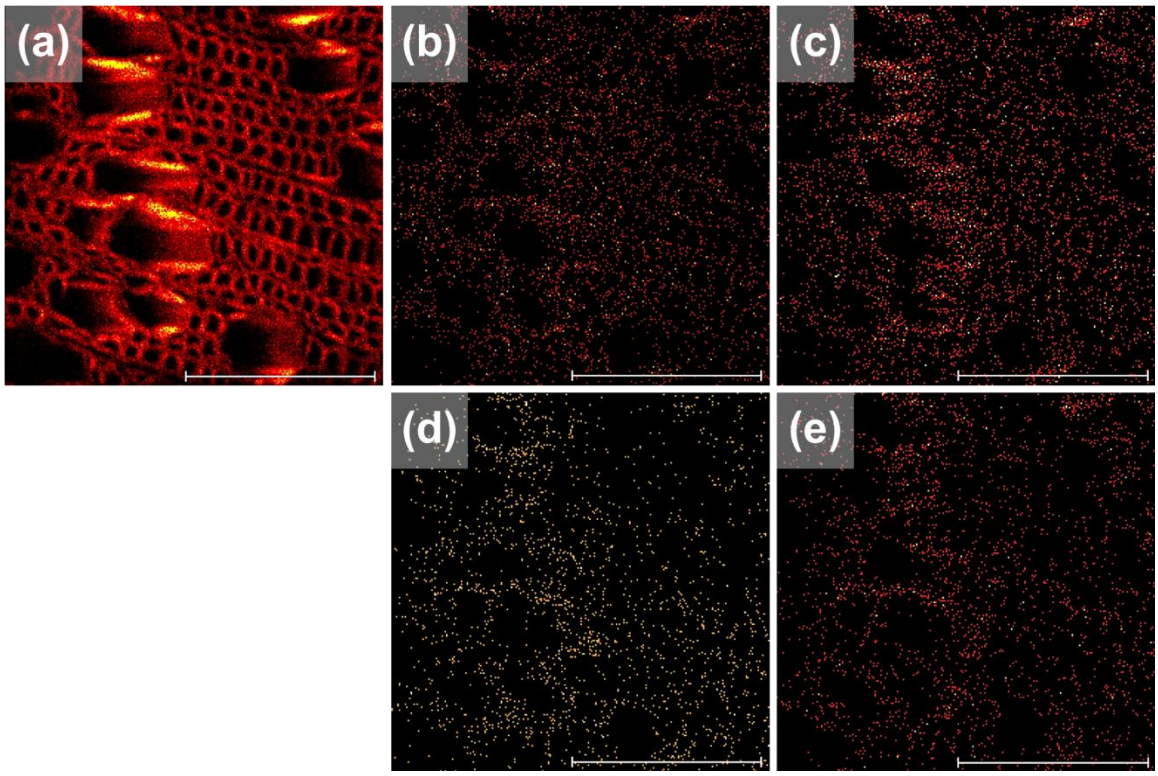

Figure 34 TOF-SIMS images of cross-sections of DAP poplar: (a) Total ion image, (b) Cellulose ion image (pooled signal for *m/z* 127, 145), (c) Xylan ion image (c, green dots, pooled signal for *m/z* 115, 133), (d) S-lignin ion image(pooled signal for *m/z* 167, 181), (e) G-lignin ion image (pooled signal for *m/z* 137, 151). Scale bar is 100µm.

To better understand where the characteristic ions are spatially located, TOF-SIMS images of dilute acid pretreated poplar were transformed by a MATLAB platform based on the pixel brightness in Figure 35. The transformed images only represent intense signals, as the MATLAB platform filters less intense spots from the original image, resulting in a visually clearer image with distinct areas of intensity. Overlaying the transformed images of individual cell wall components with one another or with the image of total ion count can permit the comparison of localized areas on cell wall surface. The image in the center area of Figure 35a can easily be cross-correlated with the TOF-SIMS image in Figure 34a. Transformed images of all characteristic components were superimposed over the total ion count image as seen in Figure 35b. Red dots represent the localized positions of intense cellulose fragments, while xylan is shown as green dots. TOF-SIMS images of G- and S-lignin units were also transformed in the same manner, and depicted as blue and pale purple dots. Notably green dots, representing xylan, appeared more frequently and more widely dispersed along the cell wall than cellulose in Figure 35b even though both species exhibited similar levels of relative intensities in Figure 33. A potential factor contributing to the random appearance of xylan fragments could be due to hemicellulose re-precipitation during DAP. Another explanation is that a part of xylan may localized in the inner cell wall layer which was exposed on the surface as the cell wall morphology was changed during DAP.[241]

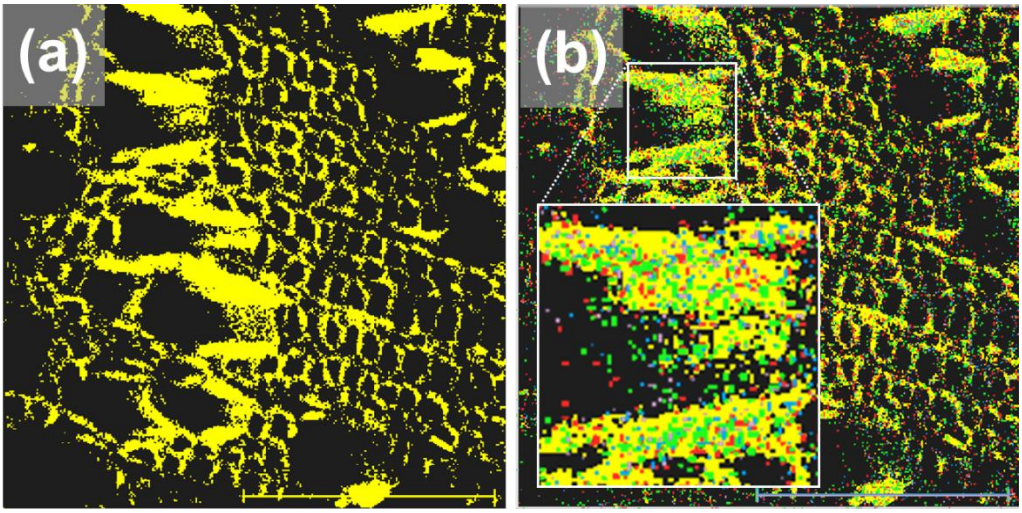

Figure 35 Images transformed by MATLAB platform using DAP TOF-SIMS images: (a) Total ion image (yellow); (b) Cellulose (red), xylan (green), G and S-lignin units (blue and pale purple) overlaid on (a). Scale bar is 100µm.

Scanning electron microcopy (SEM) images partially supported the latter as morphological changes in the cell wall before and after DAP were observed in Figure 36. The middle lamella (arrowhead) was observed in the central area of the cell wall and the thick layers adjacent to the middle lamella include multi-layer secondary cell wall as seen in Figure 36a.[242] After DAP, the inner layers of the cell wall (i.e., part of secondary cell wall) were detached from the central area (i.e., middle lamella) and the detached inner layers became widely dispersed as seen in Figure 36c. Interestingly, the detached inner layer was not observed after sDAP in Figure 36d. The thin layer in Figure 36d could be the middle lamellar and the remaining secondary cell wall because border lines were observed at both side of thin layer (arrowhead). This observation also further supports the existence of xylan located preferentially in the inner cell wall layer, as reflected in the relative intensities of xylan after DAP and sDAP in Figure 33. Essentially, the relative intensity of xylan after sDAP dramatically decreased compared to that of DAP, but the

intensity of cellulose did not change between DAP and sDAP in Figure 33. However, holocellulose pulping process did not affect the cell wall thickness much as shown in Figure 36e-f. The thickness of cell wall even after holocellulose pulping treatment was similar to that of untreated poplar and cell wall detachment was not observed.

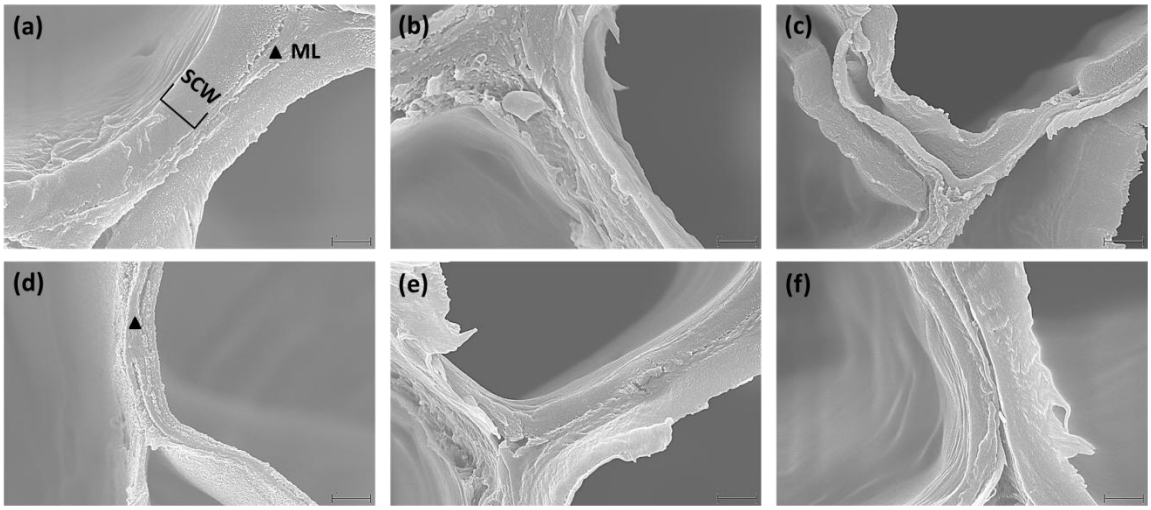

Figure 36 Electron micrograph of cross-sectioned poplar: (a) Untreated poplar, (b) Extractive-free poplar, (c) DAP poplar, (d) sDAP poplar, (e) Holocellulose poplar and (f) Severe holocellulose poplar. ML: middle lamella, SCW: secondary cell wall, Scale bar is 1μm.

5.4 Conclusion

In this chapter, a sample preparation method was introduced using non-embeded cryo-microtome technique for 50 µm thick of cross-sectioned poplar stem. The sectioned sample was suitable for surface analysis, because it was contamination-free and flat, keeping a native cell wall structure even after severe dilute acid pretreatment. Chemical comparability on both sectioned and milled samples was determined using FTIR and carbohydrate analysis prior to surface analysis since there was no study on the relationship between particle size and pretreatment effect. The sectioned sample was chemically comparable to milled sample before and after various treatments such as dilute acid pretreated or holocellulose pulping. Cross section of dilute acid pretreated poplar was then analyzed by TOF-SIMS in order to observe the changes of surface characteristics (i.e., cellulose, xylan, and lignin) and to understand different chemistry distribution between surface and bulk sample. After dilute acid pretreatment, xylan notably increased on the surface while most of hemicelluloses including xylan were removed in bulk carbohydrate analysis. In detail, TOF-SIMS image presented widely spread xylan over the surface of dilute acid pretreated poplar stem. In addition, semi-quantitative approach by TOF-SIMS showed that relative intensity of xylan in pretreated sample increased by 30% compared to untreated sample. One reasonable explanation of this result is that there was xylan re-precipitation during the low temperature quenching process. As a result there are different chemical distributions between surface and bulk sample. After severe dilute acid pretreatment, the relative intensity of xylan dramatically decreased similar to that in untreated sample on the surface, resulting from further degradation of xylan to small soluble molecules even at low temperature. Increment of

Klason lignin content after severe dilute acid pretreatment shows one of evidence of pseudo lignin formation generated from carbohydrate. Morphological changes observed by SEM also showed that cell wall thickness was decreasing with increasing pretreatment severity. These results may help explain certain aspects of the difficulty to enzymatically hydrolyze lignocellulose. Furthermore, the surface analysis of pretreated biomass by TOF-SIMS could give a clue to investigate the origin of different chemical distribution between surface and bulk biomass after a pretreatment process. Since the chemical difference could be partially resulted from re-precipitation of xylan at low temperature in batch reactor, using different type of reactor with continuous solvent flow system the mechanism can be determined. This study was performed in Chapter 6.

CHAPTER 6

EFFECT OF FLOWTHROUGH PRETREATMENT ON THE SURFACE OF POPLAR STEM: 2D CHEMICAL IMAGE ANALYSIS BY TOF-SIMS[2]

6.1 Introduction

Growing worldwide energy demands and increasing concerns of energy security and climate change have led to renewed global efforts in the development of alternative energy sources from renewable sources such as lignocellulosic biomass, to augment and replace fossil transportation fuels.[1, 3] Lignocellulosic biomass is the most abundant biopolymer in the Earth. It is considered that lignocellulosic biomass comprises about 50% of world biomass and its annual production was estimated in 10–50 billion ton.[243] The lignocellulosic complex is made up of a matrix of cellulose and lignin bound by hemicellulose chains. This structural heterogeneity and complexity of biomass contribute to natural resistance of plant cell wall. For biofuel production perspective, the inherent structural feature, however, make a big barrier for cellulose deconstruction referred to as biomass recalcitrance. Due to the inherent recalcitrance of biomass towards enzymatic deconstruction, chemical pretreatments are necessary to make the carbohydrates amenable to enzyme hydrolysis and fermentation.[3]

---

[2] Heather McKenzi, University of California Riverside, prepared water-only flowthrough pretreated poplar for this study.

Flowthrough pretreatment provides a number of advantages such as the monitoring of the evolution of pretreatment products as a function of time, the limitation of side and degradation reactions, and the removal of pretreatment products prior to quenching process thus avoiding precipitation of products. Previous study in Chapter 4, abundance of residual xylan was detected on the surface of pretreated sample. Xylan oligomers that are soluble at reaction temperatures are insoluble at lower temperatures and precipitate on the surface during the low temperature quenching process of batch reactor. A fixed bed flowthrough reactor offers the opportunity to avoid these problems. In this system, solubilized products are removed from the reactor quickly therefore hydrolysis products can be tracked as a function of time and the potential for side and degradation reactions is limited. Additionally, the evolution of hydrolysis products reflects the relative recalcitrance of the biomass fraction. Finally, few solubilized products are present in the reactor during the reaction quench thereby lowering the possibility of precipitates. Bobleter et al. pioneered the use of flowthrough reactors.[244] Flowthrough pretreatment has been shown to produce highly digestible cellulose, increase hemicellulose recovery and lignin removal. Liu et al found that flowthrough pretreatment removed more hemicellulose and lignin from corn stover than batch pretreatment.[245] A later study by Yang et al. found that flowthrough pretreated corn stover was also more digestible than the batch pretreated material.[246]

Lignin has been implicated as an inhibitor during enzymatic cellulose hydrolysis. Lignin is considered to act as both a physical barrier and an attractant to cellulases, resulting in limitation of cellulases accessibility and non-productive binding to cellulose,

respectively.[247] Therefore, many of the pretreatment methods currently being explored have tried to decrease the lignin content in biomass with minimizing the degradation of carbohydrates.[21] In addition, lignin distribution is also considered as an important factor as well as the actual lignin content because a lignin redeposition on the surface of biomass also occurs during pretreatment process.[248] Donohoe et al. found an evidence of lignin extrusion at cell wall layer, mostly at cell corner and middle lamella, and proposed a mechanism for lignin removal during thermochemical pretreatments. When thermochemical pretreatments reach a certain temperature above the range for lignin phase transition, it can cause lignins to coalesce into larger molten bodies that migrate within and out of the cell wall, and can redeposit on the surface of plant cell walls. Sannigrahi et al. also reported that pseudo-lignin can be generated from carbohydrates without significant contribution from lignin during dilute acid pretreatment, especially under high severity pretreatment conditions.[116] The pseudo-lignin also observed on the surface after pretreatment.

To delineate the spatial distribution of lignin on the surface, a series of water-only pretreatments were performed on poplar sample. Cross section of juvenile poplar stem was pretreated under mild temperature in order to avoid losing original structure of plant cell wall. Instead of temperature controls, a series of pretreatments were performed under longer reaction time (10 min ~ 150 min) than typical conditions (~ few min). Different lignin contents of pretreated sample were acquired and analyzed by time of flight secondary ion mass spectrometry (TOF-SIMS). TOF-SIMS is an emerging technique providing chemical information directly from the surface of biomass without

sample treatment such as matrix application or radioactive labeling.[164] Mass spectra obtained over the sample surface as a result of secondary ion emission can be mapped into a 2D molecular image representing the lateral distribution of characteristic species at a sub-micron scale. The spatial distribution of lignin on the surface of pretreated poplar stem was visulaized and compared to each other.

6.2 Experimental Section

6.2.1 Materials

Samples were prepared as described in Chapter 4 (4.1.2 Biomass substrate). *Populus. deltoides* x nigra (DN34) clone was grown at NREL and six-month-old juvenile poplar stem was collected for this study. Poplar stem was sectioned as described in Chapter 4 (4.1.2.2 Cryotome section of poplar stem).

6.2.2 Extractive-free poplar preparation

Samples were prepared as described in Chapter 4 (4.2.1-4.1.3). A sample was Soxhlet extracted before and after flowthrough pretreatment. All the results from the analyses were calculated based on the oven dry weight of biomass that was determined by measuring the moisture content using a moisture analyzer. The analyses that include standard deviations were done in three replicates.

6.2.3 Water-only flowthrough through pretreatment

Water-only flowthrough pretreated samples were prepared by Dr. Heather McKenzie (University of California Riverside). In brief, a sample was subjected to flowthrough pretreatment at 160 ℃ with water solvent using Custom-built reactors. The reactors were constructed from stainless steel tubing with an outer diameter of 12.7 mm and a length of 150 mm. The reactors were sealed using threaded caps (SS-810-C, Swagelok, San Diego, CA). One reactor was prepared with a thermocouple (.062-K-U-4"-T3-10 ft TF/TF-MP, Wilcon Industries, Lake Elsinore, CA) inserted along the centerline to record the reactor temperature as a function of time using a Digi-Sense DualLogR Thermocouple Meter (15-176-96, Fisher Scientific, Pittsburgh, PA). Data was transferred from the meter to a computer using an infrared adapter (EW-91100-85, Cole Parmer, Vernon Hills, IL). The reactor was loaded with 1 g moisture free biomass and then installed in the piping system. The pump was set to a flow rate of 25 mL/min and started. The back pressure valve was adjusted to 1.1 MPa. Once the system was verified to be leak free, the reactor and heating coil were lowered into the sand bath and heated. The hydrolysate produced as the reactor was heated to 160 ℃ was collected. Once this temperature was attained the reaction was said to have started. Hydrolysate was collected in three minute intervals until the desired reaction time was reached. Reactions lasted 10 to 150 minutes. The reactor and heating coil were then transferred to a water bath in order to stop the reactions. A run was also performed in which the reactor was cooled immediately after reaching 160 ℃; this was taken as "zero minutes". The residual solids were collected from the reactor by filtration, washed, and retained for analysis.

6.2.4 TOF-SIMS analysis

TOF-SIMS spectra of cross-sectioned samples were collected with a ION-TOF TOF·SIMS V spectrometer as described in Chapter 4 (4.3.2. TOF-SIMS analysis). The instrument was operated in positive mode (25kV) with 0.18 pA of primary ion (Bi_3^+) current under high mass and imaging resolution mode. For a high-mass resolution mode, the sample (500 × 500 μm^2) was rastered under bunched mode for 3 min and the spectra was collected. Three data points per each sample were acquired from the three replicates, at least, to reduce site specificity and error analysis was conducted. For a high spatial resolution imaging mode, 2D SIMS image was generated by using a software (SurfaceLab6, ION·TOF, Münster, Germany) after scanning the Bi_3^+ primary ion beam over the sample (50 × 50 μm^2, 256 × 256 pixels) for 600 time.

6.2.5 Carbohydrate and acid-insoluble lignin (Klason lignin) analysis

Carbohydrate profiles and acid-insoluble lignin content in cross-sectioned and milled samples were determined as described in Chapter 4 (4.3.1 Carbohydrates and acid-insoluble lignin analysis).

6.3 Result and discussion

6.3.1 Carbohydrates and Klason lignin analysis

Cross-section of poplar stem was water-only flowthrough pretreated under four conditions as mentioned in the Experimental Section. These conditions from mild to severe were chosen because they exhibited different cellulose/hemicelluloses recovery and delignification efficiencies. Bulk compositional changes of the structural carbohydrates and lignin on cross sectioned samples were quantitatively analyzed (Figure 37). Extractive-free poplar (i.e., control) has an initial glucose content of ~58% which is mostly originated from cellulose, and a Klason lignin content of ~27% with rest portion of xylose and minor sugars originated from hemicelluloses. After 10 min pretreatment, the relative glucose content increased by ~5% compared to that in control, while hemicelluloses and Klason lignin contents were a trade-off. For the minor sugars, only small variations were noted. Thereafter, the glucose content was proportionally increased with longer retention time in reactor. After 120 min pretreatment, the proportion of glucose significantly increased by ~50% compared to that in control, Klason lignin and xylose contents relative decreased by ~45% and 75% compared to control, respectively. However, this trend was changed after 150 min pretreatment. It was observed that, after most severe pretreatment (150 min), the glucose content decreased and the Klason lignin and xylose contents increased compared to 120 min pretreated sample.

This result should indicate that there is a turning point of cellulose degradation under severe pretreatment condition. Notably, a part of Klason lignin increment after 150 min pretreatment should be contributed by pseudo-lignin formation. Recently, Sannigrahi et

at. proposed that the formation of pseudo-lignin by the combination of carbohydrate and lignin degradation products is responsible for the increased Klason lignin content in pretreated biomass under severe conditions.[116] This pseudo-lignin negatively influences enzymatic cellulose hydrolysis.[115]

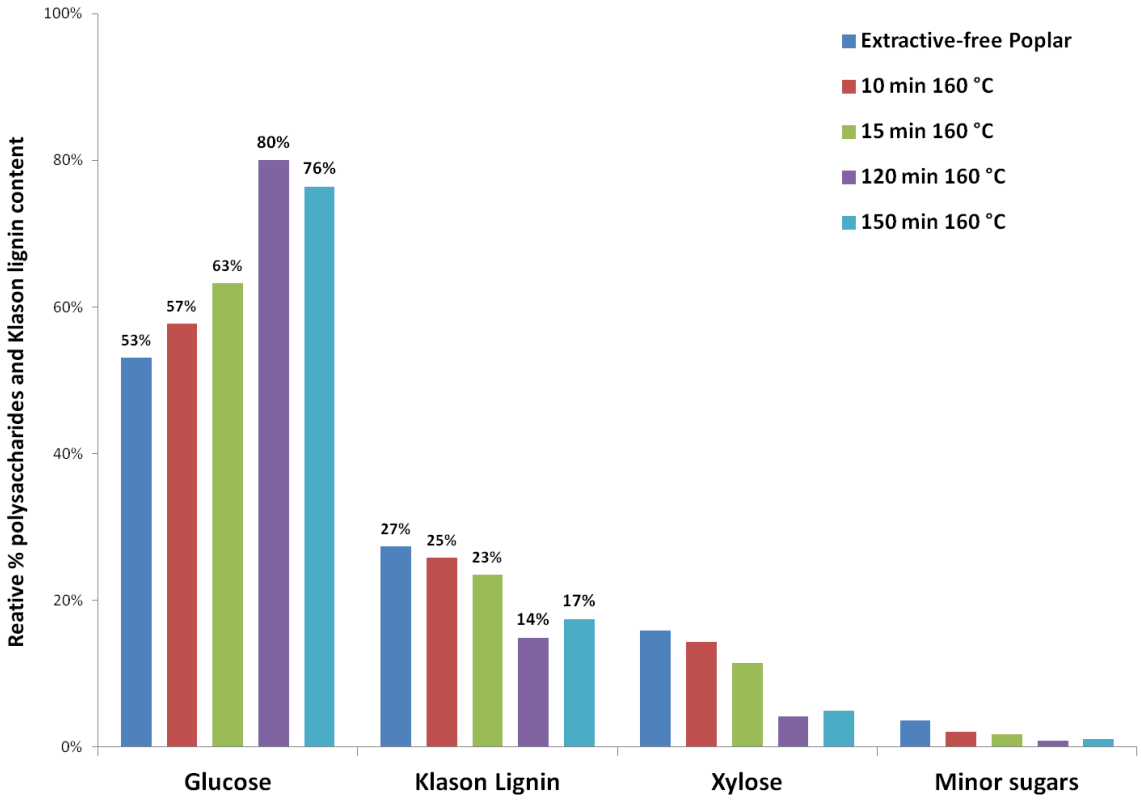

Figure 37 Carbohydrate and Klason lignin contents of cross sectioned poplar after water-only flowthrough treatments; Y scale is enlarged on inner graph to show the low contents of hemicelluloses.

6.3.2 Surface analysis of dilute acid pretreated poplar

The positive spectra of the pretreated samples were obtained from the surface of each sample. Then, the characteristic monomeric ions of lignin were assigned at *m/z* 137 and 151 for guaiacyl (G) and at *m/z* 167 and 181 for syringyl (S) lignin unit. Cellulose ions were at *m/z* 127 and 145 as assigned in the literature.[182,229-230] For semi-quantitative approach, the changes in the relative intensities of characteristic ions were compared after normalization. Normalized ion intensity of lignin or cellulose was obtained from the summation the characteristic ions and compared in Figure 38. Cellulose ions showed an increasing trend with increasing pretreatment duration till 120 min pretreatment as well as bulk carbohydrate data. Notably, after 10 min pretreatment cellulose ions were almost doubled as compared with that of control, while bulk cellulose composition represented only 5% differences in Figure 37. More cellulose observation on the surface was due to the disruption of cell wall structure such as hemicellulose hydrolysis, resulting in more cellulose exposure to surface.

This result reasonably accounts for why the pretreatment process is a demand for higher yield of sugar release for enzymatic cellulose hydrolysis. Interestingly, the level of lignin ions on the surface did not change after 10 min pretreatment, which was very similar to bulk Klason lignin data in Figure 37. These results should indicate there is a chemical difference between surface and bulk before and after pretreatment. This is consistent with the finding in Chapter 4 that xylan content was different between surface and bulk after dilute acid pretreatment. After 120 min pretreatment, cellulose ions were relatively increasing by three times while the lowest lignin ions were observed. This significant

increase of relative cellulose ion intensity could most likely be interpreted as the result of a degradation and loss of lignin and hemicelluloses, respectively, from the cell wall structure. Further pretreatment for 150 min resulted in decreasing cellulose ions and increasing lignin ions on the surface as well as bulk composition data. These results indicate the point of maximum cellulose and minimum lignin presence on the surface of pretreated sample.

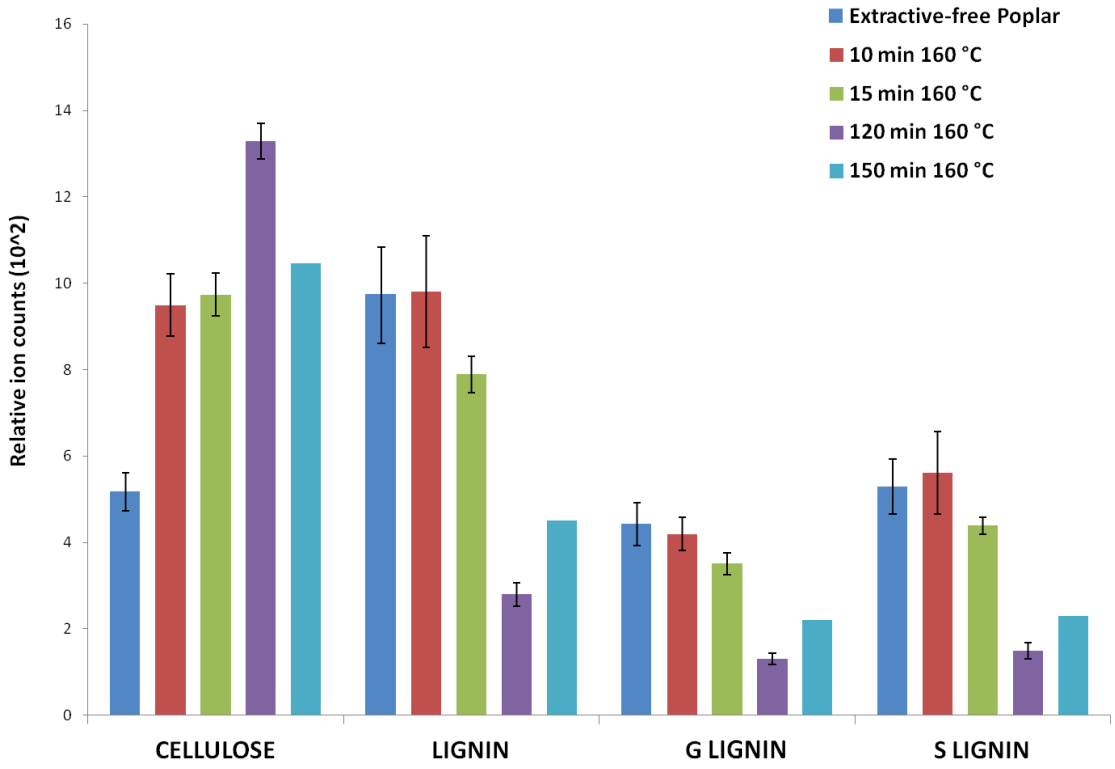

Figure 38 Relative intensities of each component in cross-sections of different pretreated poplar by TOF-SIMS.

Molecular ion images of pretreated samples represent the chemical characteristic features of lignin (Figure 39). Firstly, a total ion image was generated from each spectrum, representing the population of all released ions up to m/z 800 mass range. Thereafter, lignin ions pooled signal for m/z 137, 151, 167, 181 was overlaid on the total ion image using green dots. The spatial distribution of lignin on the cross-sectioned surface can be readily observed in Figure 39. Extractive-free poplar image clearly showed that lignin ions (green dots) were evenly distributed across cell walls on the surface (Figure 39a). After 10 min pretreatment, more lignin ions were observed at cell corners (arrows) in Figure 39b. Higher intense of lignin at cell corners can be explained that lignin migration occurs during pretreatment process. Donohoe et al. observed lignin extrusion through pits, cell corners, delamination zones, and the middle lamella after a thermochemical pretreatment and suggested thermochemical pretreatment leads to lignin coalescence and migration inside cell wall matrix.[248] In addition, there is a striking pattern of lignin re-localization within the pretreated cell wall. As one evidence, lignin ion intensity after 15 min pretreatment (Figure 39c) decreased at cell corners (arrow) compared to Figure 39b, but there are still abundance of lignin ions compared to control (Figure 39a). It seems that some lignin migrated from inside cell wall matrix start to extrusion. At this point bulk lignin composition was little dropped from ~27% (extractive-free) to 25% (10 min pretreatment) to 23% (15 min pretreatment). After long time pretreatment for 120 min, most lignin ions eventually disappeared from the surface in Figure 39d. Interestingly, little lignin ions reappeared after further pretreatment (150 min) mostly at cell corners (arrow) in Figure 39e. Lignin reappearance should result from the formation of pseudo-lignin as explained early.

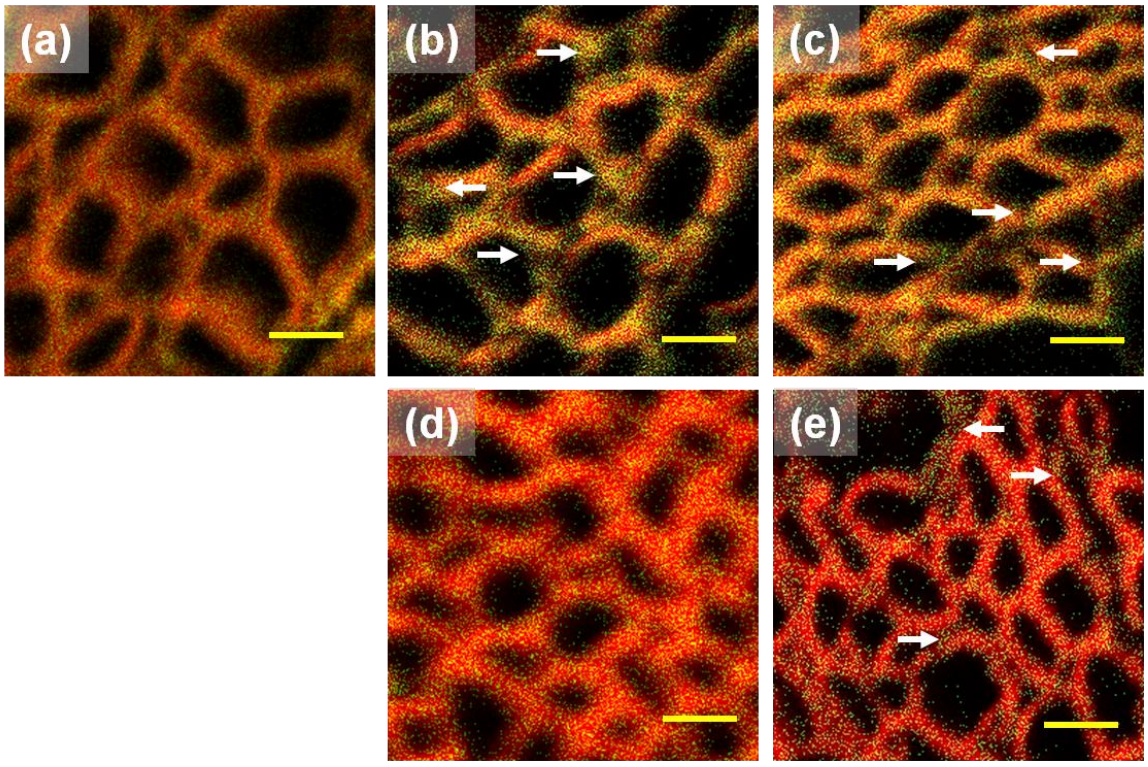

Figure 39 TOF-SIMS images of the cross sectioned poplar before and after flowthrough pretreatment. Lignin ions (green dots, pooled signal for m/z 137, 151, 167, 181) were overlaid on total ion image. (a) Extractive-free poplar, (b) 10 min, (c) 15 min, (d) 120 min, and (e) 150 min pretreated poplars. Scale bar is 10 µm.

6.4 Conclusion

In this chapter, TOF-SIMS was successfully applied for tracking lignin variation depending on pretreatment conditions. To avoid re-precipitation component during low temperature quenching process, a continuous flow reactor was employed for a pretreatment process instead of batch reactor used in Chapter 5. Therefore, cross section of flowthrough pretreated poplar stem can provide more precise surface information without external effect like re-precipitation. The spatial distribution of lignin subject to different severities of water-only flowthrough pretreatment were investigated in order to gain further insights to explain different chemical features between surface and bulk. Multiple lines of evidence have been presented that cellulose and lignin contents in bulk composition did not always correspond with those in surface composition. First of all, it was found that relative intensity of cellulose after 10 min pretreatment increased by double compared to untreated sample on the surface compared. On the contrary, there was only 5% increment in bulk cellulose content after the same pretreatment. This result can be concluded that there are chemical differences between surface and bulk composition after pretreatment as well as we found in Chapter 5. In addition, a striking pattern of lignin migration and re-localization to cell corner was observed after flowthrough pretreatments. In TOF-SIMS image, more lignin was observed at cell corner after 10 min pretreatment, resulting from the lignin coalescence and migration from inside cell wall matrix. Lignin reappearance at cell corner was observed after long time (150 min) pretreatment, which could explain part of pseudo-lignin formation. Lastly, maximum cellulose content with minimum lignin contents was found after 120 min pretreatment in both surface and bulk composition, which can be used to, at least,

optimize pretreatment condition. Surface analysis by TOF-SIMS provides an insight into understanding the effect of pretreatment. Further study combined with enzymatic cellulose hydrolysis could show the detail relationship between pretreatment and recalcitrance.

CHAPTER 7

3D CHEMICAL IMAGE USING TOF-SIMS REVEALING THE BIOPOLYMER COMPONENT SPATIAL AND LATERAL DISTRIBUTION IN BIOMASS[3]

7.1 Introduction

Many researchers consider biofuels, including bioethanol and biodiesel, as a resource to supplement or replace large portions of future transportation fuel requirements. This shift in research focus is due in part to limitations in fossil resources and recent concerns about the environment.[28,249] Lignocellulosic biomass (e.g., agricultural resides, forestry wastes, and energy crops) has been highlighted as a potential resource for biofuel production.[1-2] Lignocellulosic biomass is mainly composed of polysaccharides (i.e., cellulose and hemicelluloses) and lignin (i.e., polyphenolic macromolecules).[250] Cellulose, a major source of fermentable sugar used to produce ethanol, is known to be densely packed and embedded in a lignin-hemicellulose matrix. This intricate layering of lignin, cellulose, and hemicelluloses comprises the microstructure of biomass, and to date not fully identified. The structural complexity exhibited in lignocellulose originates from innate structural heterogeneity and has been suggested as a contributing factor in the its ability

[3] This manuscript was accepted for publication in Angewandte Chemie, 2012. It is entitled as 3D Chemical Image using TOF-SIMS Revealing the Biopolymer Component Spatial and Lateral Distributions in Biomass. The other authors are Marcus Foston, and Art J. Ragauskas from School of Chemistry and Biochemistry at Georgia Institute of Technology and Udaya Kalluri, Gerald A. Tuskan from BioEnergy Science Center at Oak Ridge National Lab.

to resist enzymatic hydrolysis, referred to as biomass recalcitrance.[3] Biomass recalcitrance has been cited as the major barrier to large-scale utilization of lignocellulosic biomass for biofuel production. Therefore, the major challenge facing future lignocellulosic biofuel research is reducing the recalcitrance of biomass through biological and chemical manipulation. For example, transgenic alfalfa down-regulated in lignin biosynthesis was shown to release more sugar by enzymatic hydrolysis.[19] Thermochemical pretreatment using oxidizing, acidic, or basic condition under high temperature and/or pressure results in structural cell wall breakdown along with changes in lignin and/or hemicelluloses, ultimately correlating with higher sugar release upon enzymatic hydrolysis.[22,239,251]

Analytical tools therefore play an important role in determining and understanding changes which occur in biomass during biological and chemical processes designed to reduce biomass recalcitrance. Typically this is done with conventional bulk analysis such as high performance liquid chromatography (HPLC), gas chromatography–mass spectrometry (GC-MS), nuclear magnetic resonance (NMR), and electron microscope (EM). However, these techniques average over a large spatial dimension, losing critical information about differences in chemical heterogeneity as a function of spatial and lateral position in the cell wall. Therefore, we have investigated chemical imaging techniques, which are well-suited to understand detailed spatial and lateral changes for major components in biomass.

In this chapter, the first 3-dimensional (3D) analysis of biomass using time of flight secondary ion mass spectrometry (TOF-SIMS) has been introduced in the specific application of understanding recalcitrance. TOF-SIMS is an emerging technique providing chemical information directly from the surface of biomass without sample treatment such as matrix application or radioactive labeling.[164] Mass spectra obtained over the sample surface as a result of secondary ion emission can be mapped into a 2D molecular image representing the lateral distribution of characteristic species at a sub-micron scale. Extending the usefulness of TOF-SIMS, a 3D molecular image can be generated by acquiring multiple 2D images in a stack. This is accomplished by reconstruction, stacking the 2D molecular images layer by layer. Each layer is produced in a dual-beam mode which uses a ion beam for surface analysis and sputtering beam for surface layer ablation, also referred to as 3D microarea analysis.[252] As a result, 3D molecular imagings allow one to semi-quantitively track and understand both vertical and lateral distributions of targeted or interesting species from surface to sub-surface layers. The ability to capture 3D data seems even more crucial to understanding bioconversion because the interfacial layer between the biomass and cellulolytic enzyme/microbe has been shown to significantly affect hydrolysis.[253]

7.2 Experimental Section

7.2.1 Materials

Samples were prepared as described in Chapter 4 (4.1.2 Biomass substrate). *Populus tremula* x *alba* (PTA) clone was grown at ORNL under tension and pooled stem segments collected from normal unstressed stems (NW), stems under tension on the

elongated side (TW) or stems under tension on the compressed side (OW). TW specifically refers to the wood containing a G-layer, while the wood between TW and OW (pith) is excluded from ground samples in an effort not to obscure further analysis. Tension was applied by fixing each stem at a 45° angle for ~60 days prior to removing stem segments. All stem material was debarked and elongated/compressed side longitudinal sections were cut manually along the entire length of the stem avoiding the pith. Each stem was sectioned or milled as described in Chapter 4 (4.1.2.1-2 Milled poplar stem and Cryotome section of poplar stem).

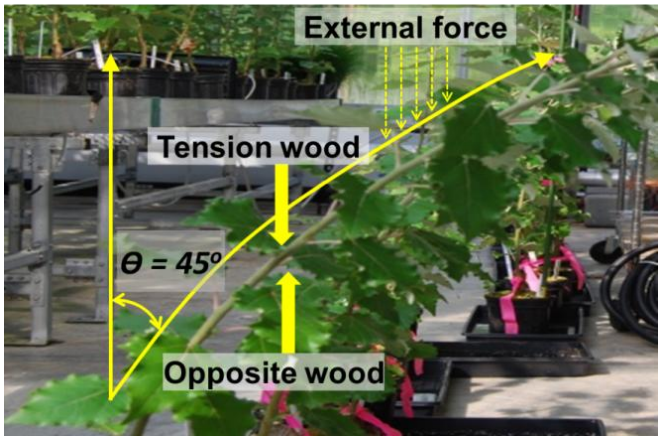

Figure 40 Greenhouse-grown *Populus tremula x alba* (PTA) plants under tension stress. Tension wood is marked as bold line yellow arrow.

7.2.2 Extractive-free poplar preparation

Samples were prepared as described in Chapter 4 (4.2.1-4.1.3). All the results from the analyses were calculated based on the oven dry weight of biomass that was determined by measuring the moisture content using a moisture analyzer. The analyses that include standard deviations were done in three replicates.

7.2.3 TOF-SIMS analysis

TOF-SIMS spectra of cross-sectioned samples were collected with a ION-TOF TOF·SIMS V spectrometer as described in Chapter 4 (4.3.2. TOF-SIMS analysis). The instrument was operated in positive mode (25kV) with 0.18 pA of primary ion (Bi_3^+) current under high mass and imaging resolution mode. For a high-mass resolution mode, the sample (500 × 500 μm^2) was rastered under bunched mode for 3 min and the spectra was collected. Three data points per each sample were acquired from the three replicates, at least, to reduce site specificity and error analysis was conducted. For a high spatial resolution imaging mode, 2D SIMS image was generated by using a software (SurfaceLab6, ION·TOF, Münster, Germany) after scanning the Bi_3^+ primary ion beam over the sample (50 × 50 μm^2, 256 × 256 pixels) for 100 times. After 100 scans of topmost layer, surface erosion by O_2^+ sputtering source (300 × 300 μm^2, 2 keV) at a current of 0.65 pA was applied for 2s at non-interlaced mode. The imaging/sputtering cycles were repeated for 30 times and the data set was used for 3D image reconstruction (Figure 41). A 3D SIMS image was generated by stacking multiple 2D images using a software (ImageSurfer ver. 1.20, http://imagesurfer.cs.unc.edu/).[218]

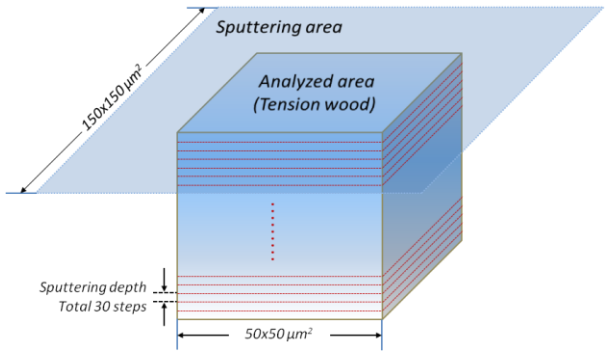

Figure 41 Schematic diagram of 3D microarea analysis.

7.2.4 Scanning Electron Microscopy

Surface morphology of cross-sectioned poplar before and after various treatments was observed by using JEOL-1530 TFE-SEM as described in Chapter 4 (4.3.6 Scanning Electron Microscopy). The images were taken at various resolving powers under 5 kV.

Enzymatic hydrolysis

7.2.5 Carbohydrate and acid-insoluble lignin (Klason lignin) analysis

Dr. Marcus Foston determined carbohydrate profiles and acid-insoluble lignin content in cross-sectioned and milled samples described in Chapter 4 (4.3.1 Carbohydrates and acid-insoluble lignin analysis).

7.2.6 Enzymatic cellulose hydrolysis

Dr. Marcus Foston measured yields of enzymatic cellulose hydrolysis. Cellulase (4-glucano-hydrolase) from Trichoderma reesei ATCC 26921 and Novozyme 188 (cellobiase) from Aspergillus niger were purchased from Aldrich–Sigma and used as received. The activities of cellulase and cellobiase were determined to be 91.03 FPU/ml and 387.70 CBU/ml respectively according to the literature procedures.38 The pulp (0.200 g) was suspended in 50.00 mM citrate buffer adjusted to pH 4.8 by sodium hydroxide at a consistency of 1% (w/v). These two enzymes were added into the suspension at enzyme loading of 20 FPU/g and 40 CBU/g respectively. The mixture was incubated at 50 ℃ under continuous agitation at 150 rpm. 0.10 mL liquid hydrolysis samples at time intervals of 4, 7, 9, 24 and 48 h were withdrawn and the hydrolysis was quenched by submersion for 5 min in a vigorously boiling water bath. The liquid samples

were then diluted to 1.00 mL and were stored at 20 ℃ until analysis on an Agilent GPC SECurity 1200 system equipped with an acidic ion-exchange column (Bio-Rad HPX-871) and Agilent refractive index (RI) detector using a 10 mM nitric acid solution as the mobile phase (1.0 mL/min) with injection volumes of 20 mL, performed similar to literature procedures.39

7.3 Result and discussion

7.3.1 Carbohydrates and Klason lignin analysis and enzymatic cellulose hydrolysis

Stress-induced tension wood was generated on poplar stems as a model substrate to investigate the application of TOF-SIMS on biomass (Figure 42). Tension wood generally appears on the elongated stem side as a result of mechanical bending. Under such conditions, angiosperms form reaction or tension wood on the elongated stem side in an effort to maintain an upright growth position.[254-256]

As a preliminary study for TOF-SIMS analysis, carbohydrate and Klason lignin content were measured in segment samples from *Populus tremula* x *alba* (PTA) grown under normal and tension conditions (Figure 42a). Based on the age of the PTA cutting, assuming consistent longitudinal sectioning with respect to the ratio of sampled normal and reaction wood cells and the amount of time the stem was grown under tension, a rough estimate indicates that the tension wood and opposite wood samples have a maximum of ~33% reaction wood. Utilizing this estimate for the percentage of reaction wood and the above carbohydrate distribution in the tension wood sample, one may expect the lignin and xylan contents within the reaction wood cell to be as low as ~7%

and 5%, respectively. The most significant finding seems to be that the ~25% increase in the amount of available glucose in the tension wood sample resulted in a ~300% increase in cellulase sugar release in comparison to the normal wood or opposite wood enzymatic hydrolysis experiments (Figure 42b). This increase in sugar yield becomes even more impressive taking into consideration all samples contained less than 2% starch by dry weight of biomass determined by a published HPLC procedure utilizing an amylase treatment.[257] Considering the differences in the magnitude of increase, this change in digestibility profile cannot be simply related to the increase of glucan content, but instead is more than likely attributed, in part, to some other combination of differences within the cell wall structure of tension wood.

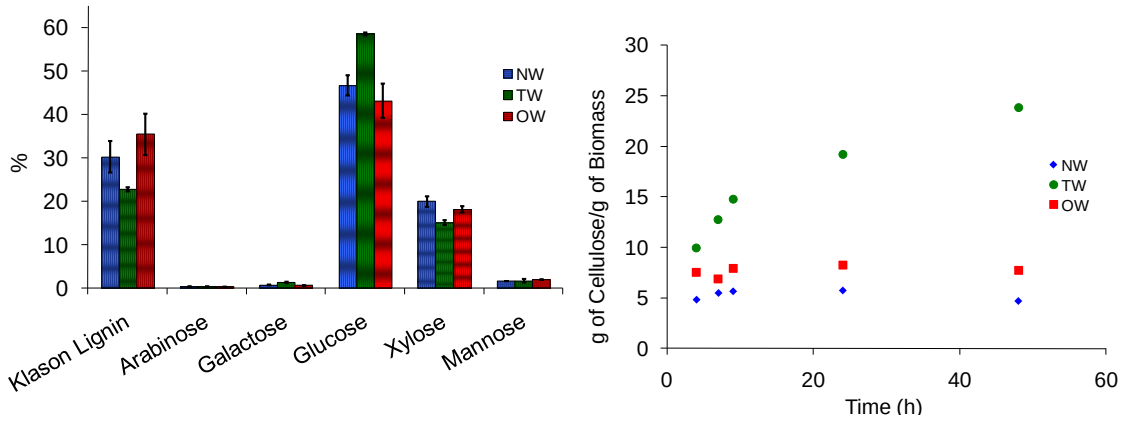

Figure 42 (a) Carbohydrate and Klason lignin content of PTA samples grown under bending or normal (erect) conditions, as determined by HPLC and normalized by the sum of all the measured components. (b) Enzymatic sugar release *Populus tremula* x *alba* (PTA) samples.

7.3.2 SEM image analysis

Tension wood sample has an additional thick cell wall layer, referred to as the gelatinous layer (G-layer). This G-layer occurs inside the secondary cell wall layer (Figure 43) and is mainly composed of crystalline cellulose whereas normal secondary cell wall layers are more of a mixture of cellulose, hemicellulose, and lignin components.[135, 258] Tension wood is therefore not only defined by the presence of this G-layer but also is ideal for demonstrations of chemical imaging because this cellulose rich area can be readily distinguished from the more chemically complex surroundings.

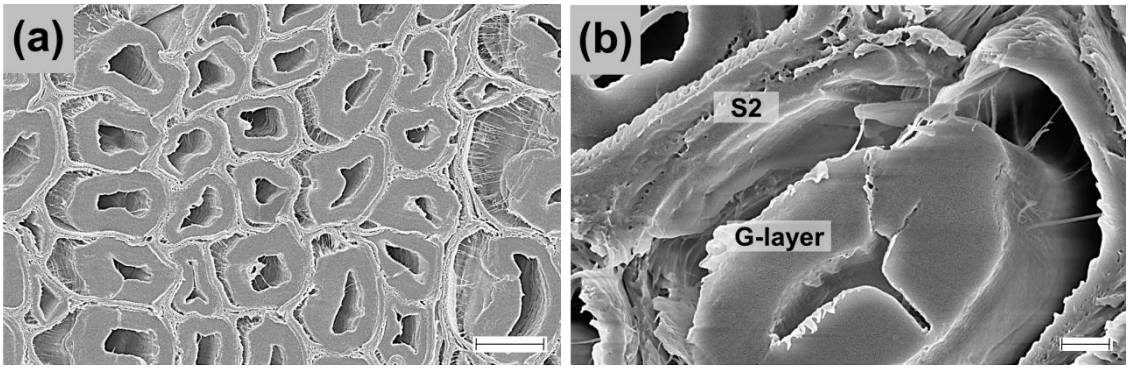

Figure 43 Electron micrograph of cross-sectioned tension wood of PTA stem. S2 is secondary cell wall and G-layer is gelatinious layer. Scale bars are (a) 10µm and (b) 1µm.

7.3.3 TOF-SIMS analysis

Tension wood surface was rastered using a Bi^{3+} primary ion beam while secondary ion images were acquired via surface ejected ions collected by a TOF analyzer. The TOF analyzer effectively determines the mass to charge ratio of released fragments/ions and produces a mass spectrum at each pixel. An entire data set can be collected by rastering an area of interest, generating characteristic ion images with sub-micron lateral resolution

(~400 nm). Major characteristic ions, clearly identified in the resulting mass spectra (Figure 44), display peaks corresponding to species such as ions originating from cellulose (*m/z* 127 and 145) and lignin ions (*m/z*137 and 151 for G-type and *m/z* 167 and 181 for S-type), as assigned in the literature.[182,229-230]

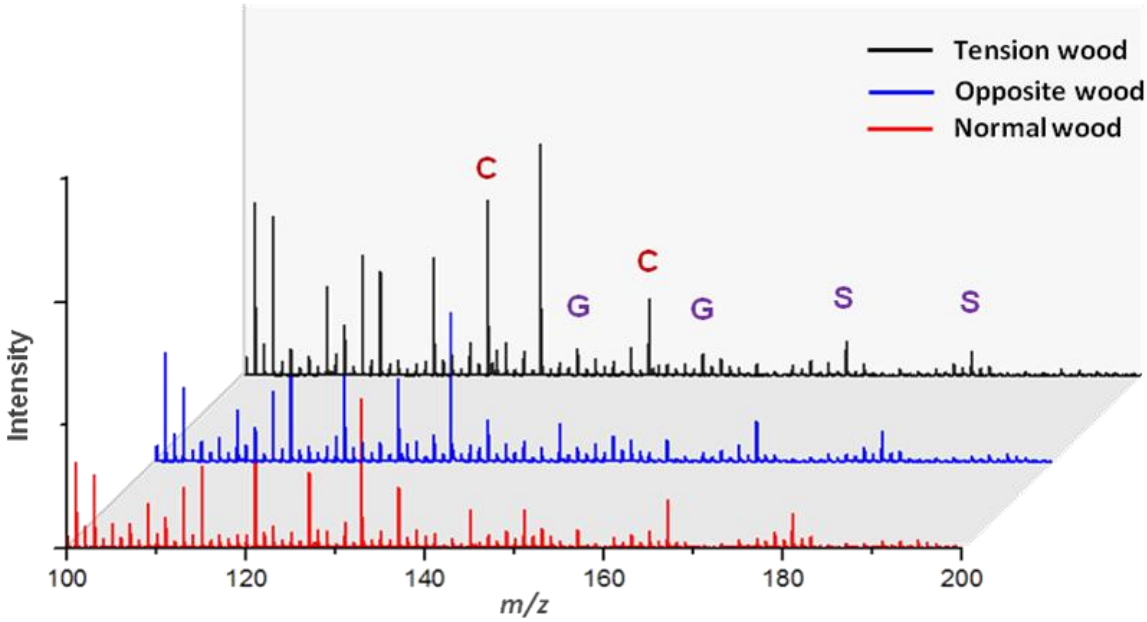

Figure 44 Part of positive TOF-SIMS spectra: tension wood (black), opposite wood (blue) and normal wood (control, red). Characteristic ions are marked as C (cellulose ions), G (guaiacyl lignin ions), and S (syringyl lignin ions).

Normalized ion intensities of cellulose (sum of two characteristic ions) in tension wood increased ~25% relative to that of normal wood (control) seen Figure 45. This result is very similar to bulk monosaccharide data determined by HPLC in Figure 42a. In contrast, normalized lignin related ion intensities in tension wood (sum of S- and G-type characteristic ions) were ~25% lower than the control. Interestingly, opposite wood (found on the compression side of the tension wood stem) displayed ~25% higher lignin content as compared to the control.

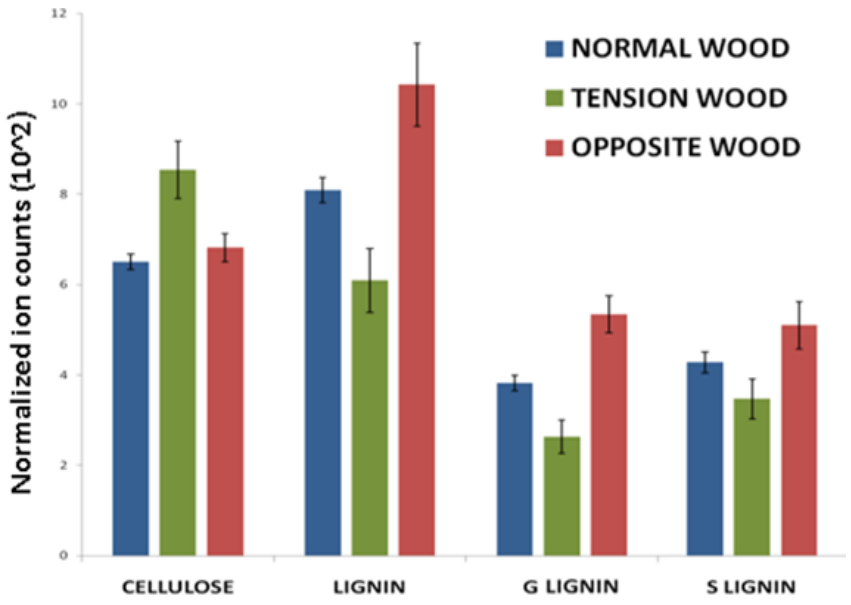

Figure 45 A comparisons of relative ion intensities of cellulose, G-, and S-lignin between tension, normal and opposite wood.

Molecular ion images of tension wood well represent the chemical characteristic features of tension wood (Figure 46). Total ion images represent the population of all released ions up to *m/z* 800 mass range, and clearly indicates the position of G-layer, secondary cell wall (S2), and cell corner (CC) regions (Figure 46a). These images are well

correlated to the electron micrograph in Figure 43. Lignin related ions (green dots in Figure 46b) overlaid on total ion image represent the spatial distribution of lignin on the cross-sectioned surface. Lignin ions are intensely located in S2 and CC but display a relatively low intensity in G-layer. On the contrary, cellulose ions (green dots in Figure 46c) evenly present over the surface of tension wood, displaying slightly more intensity in the G-layer.

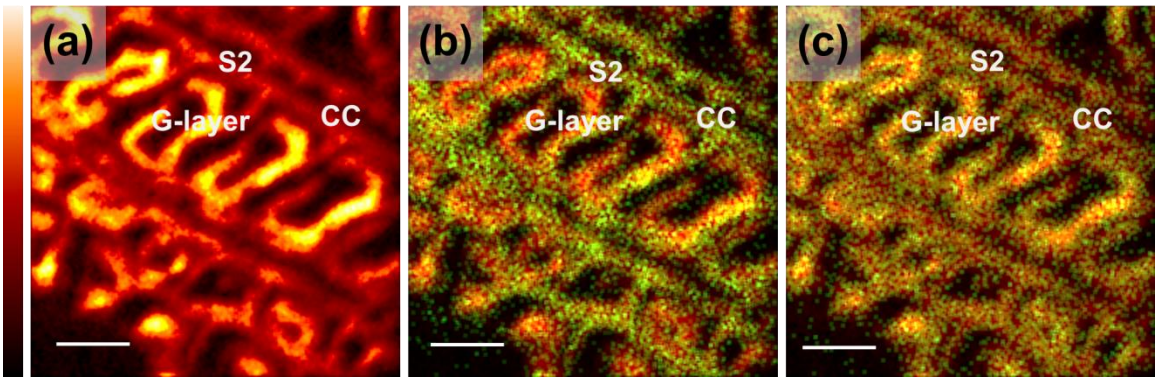

Figure 46 TOF-SIMS images of the tension wood before any sputter cycle had been applied: total ion image (a), lignin ion (b, green dots, pooled signal for *m/z* 137, 151, 167, 181) image and cellulose ion (c, green dots, pooled signal for *m/z* 127, 145) image. Scale bar is 10 µm.

To acquire vertical distributions of characteristic ions as well as lateral distributions, surface erosion by O_2^+ sputtering (2kev for 2s) was employed utilizing alternating cycles of Bi_3^+ rastering and O_2^+ sputtering in the same analysis area. The tension wood cross-sectional surface after 30 sputtering cycles appears as nano-porous. Though the surface texture changed, appearing almost sponge-like, the gross surface cell wall structure seems to be relative unaltered (Figure 47a). This is evident compared to the non-sputtered surface in Figure 43. The textural difference due to surface erosion is also represented in

Figure 47b, where the right-hand side of the image depicts the porous analysis area. This area then transitions to a smooth appearing surface on left-hand side of the image where no sputtering occurred.

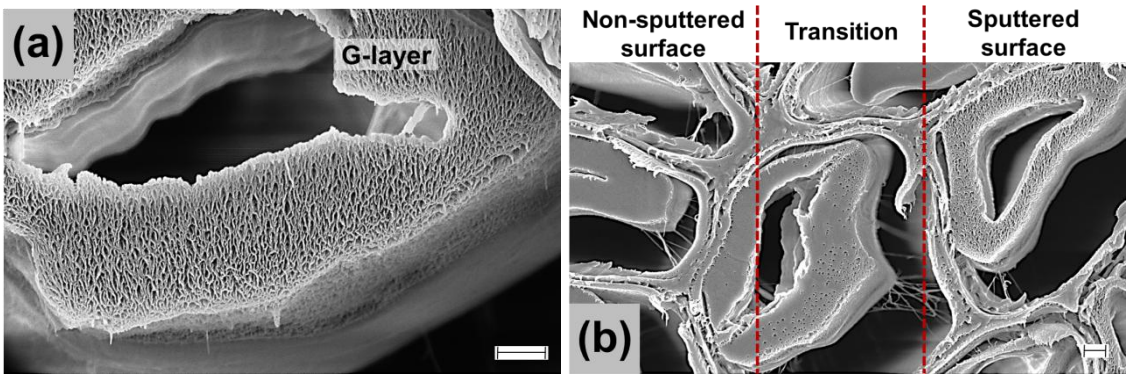

Figure 47 Electron micrograph of cross-sectioned tension wood of PTA stem after O_2^+ sputtering process. (a) Sputtered surface after 30 cycles of sequential sputtering. (b) Boundary area between the sputtered and the non-sputtered surface. Scale bar = 1 μm

Cellulose and lignin molecular ion images from each layer were combined to reconstruct a 3D molecular ion image. This image displays the spatial distribution of major cell wall components, from the topmost surface into the sub-surface of the tension wood cross-section. Cellulose related ions (green dots) in Figure 48 were also localized in the G-layer, correspond well to 2D molecular ion image, whereas lignin ions (red dots) were preferentially located at S2 and CC. A multi-angle rotation of 3D rendering can show spatial distribution from a top and side view.

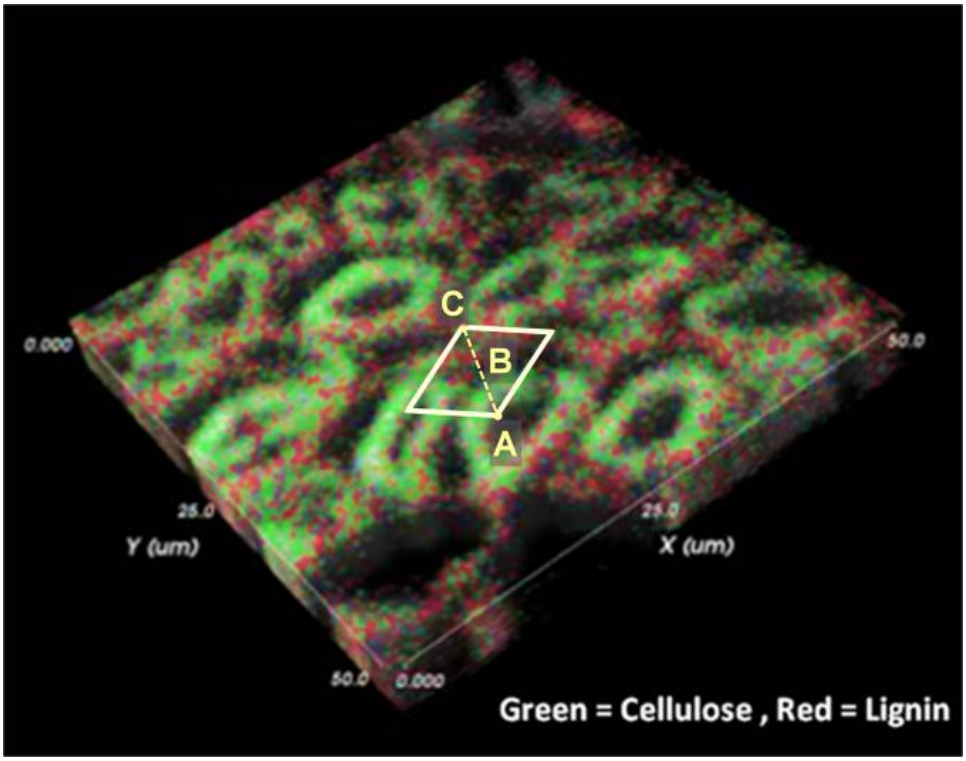

Figure 48 The spatial distribution of cellulose (green dots) and lignin (red dots) ions in 3D volume rendering of total ion image.

3D microarea analysis also provides an alternative method to visualize the data set (e.g., line scan and semi-quantitative profile) and is easily generated via retrospective analysis. For example, a region of interest (ROI, yellow box in Figure 48) was selected, covering a single cell. Mass spectral data from the topmost five layers were reconstructed applying a line scan (Figure 49a). The surface topography of the ROI can be used to determine the location of G-layer and S2 as marked in Figure 49a. The semi-quantitative profiling of major cell wall components was then obtained over the line scan (yellow dotted line in Figure 49a). Individual spatial distributions of cellulose and lignin ions were semi-quantitative determined (Figure 49b-c). An intense signal of cellulose related ions was again observed at the G-layer and a relatively low cellulose signal was shown in the S2

and CC. However, relatively higher intensity of lignin signal was observed in S2 and CC. These results, corresponding to well-known structural characteristics of tension wood, begin to indicate how the reduced chemical heterogeneity observed in the wood samples could affect enzymatic digestibility as reported by Foston et al.[259]

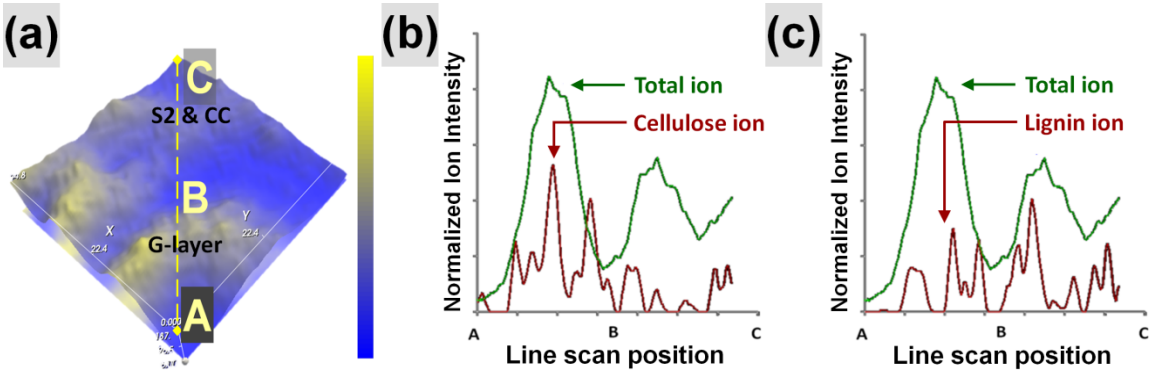

Figure 49 (a) The surface topography of a single cell reconstructed from the topmost five layers. (b-c) Semi-quantitative lateral distributions of cellulose and lignin across a single cell.

7.4 Conclusion

The reduced lignin content levels, altered carbohydrate and lignin structures, and different cell wall layer organization in poplar tension wood provided a reactive substrate for enzymatic deconstruction. Preliminary study using poplar tension wood showed that it released about 3-fold more monosaccharides than that of normal wood during enzymatic cellulose hydrolysis while it contained only 25% more bulk glucan than the normal wood. This disproportional increase in sugar release observed is in part due to tension induced changes in cell wall morphology, specifically spatial localization of cellulose.

To demonstrate chemical and ultrastructural feature of tension wood, 3D microarea analysis by TOF-SIMS was successfully employed. Surface rastering by Bi_3^+ gun in burst mode allowed to obtain a lateral resolution image up to 500 μm with reasonable mass resolution. 2D TOF-SIMS image showed uneven distribution of cellulose and lignin on the surface of tension wood. Lignin was mostly detected at the secondary cell wall and cell corner while slightly more cellulose was detected at the G-layer.

3D TOF-SIMS image of tension wood was obtained using the dual beam (imaging and sputtering) approach in order to maintain high sensitivity of analysis gun. 3D molecular image of tension wood showed both later and vertical distirbituion of cellulose and lignin from surface to sub-surface. The spatial distributions of lignin and cellulose were exactly the same as the 2D TOF-SIMS image, which demonstrate 3D microarea analysis by TOF-SIMS is properly working with biomass. The combination of biomass deconstruction and 3D microarea analysis by TOF-SIMS exploited in this work has demonstrated an ability to understand the intimate relationship between the cellular structure and its spatial component distribution of biomass, critical to bioconversion.

CHAPTER 8

DIRECT ANALYSIS OF CELLULOSE IN POPLAR STEM BY MALID-IMAGING MASS SPECTROMETRY (MALDI-IMS)[4]

8.1 Introduction

Cellulose is the most abundant biopolymer in nature and has been widely used due to its versatile application in many areas including the food, paper, and pharmaceutical industries. Recently cellulose, one of the major components in lignocellulosic bioresources, has been further highlighted as a renewable energy resource since these materials can avoid the conflict over biofuel resources competing with food resources such as corn.[1] These renewable resources can be drawn from dedicated agro-energy crops and from biomass residues originating from both forest and agricultural ecosystems.[260-261] Natural cellulose consists of glucose units linked by a β-(1→4)-glycosidic bond and exist as a linear polysaccharide embedded in hemicelluloses and lignin within the plant cell wall.

Various analytical techniques have been used to characterize cellulose to overcome biomass recalcitrance, and therefore increase the overall efficiency of converting

[4] This manuscript was accepted for publication in Rapid Communications in Mass Spectrometry, 2010. It is entitled as Direct analysis of cellulose in poplar stem by matrix-assisted laser desorption/ionization imaging mass spectrometry. The other authors are Yanfeng Chen, M. Cameron Sullards, and Art J. Ragauskas from School of Chemistry and Biochemistry at Georgia Institute of Technology.

cellulose to bioethanol. Fourier Transform (FT) Raman and infrared (IR) spectroscopy, nuclear magnetic resonance (NMR), and high-performance anion-exchange chromatography (HPAEC) have been widely used for cellulose characterization.[134,217,225] However, direct analysis of native biomass still remains a considerable challenge to the understanding of both the spatial and temporal distribution of cellulose in plant cell walls during the ethanol conversion processes.

Matrix-assisted laser desorption/ionization mass spectrometry (MALDI-MS) is a powerful tool used to analyze large molecules with high speed and sensitivity. Since MALDI-MS was successfully applied to the structural analysis of native carbohydrates by Harvey *et al*. and Stahl *et al*., it has been frequently used to analyze carbohydrates due to its analytical versatility.[262-263] To increase ionization efficiency of the carbohydrate moiety, many methodologies such as terminal derivatives and metal-cationization can be applied.[264] The versatility of MALDI-MS was extended by Caprioli *et al.* in 1997 to direct image profiling of the surface of biological tissues.[197] MALDI-imaging mass spectrometry (MALDI-IMS) can be used to determine the spatial distribution and relative abundance of specific molecules on many sample surfaces. As such, MALDI-IMS has been successfully used to investigate sectioned tissues such as human brain and rat organs.[202,265] Recent studies have reported the application of IMS in native plants as well. For example, Ng *et al*. demonstrated the spatial profiling of phytochemicals using direct analysis by MALDI-IMS in herbal tissue.[266] MALDI-IMS has also been used to determine the distribution of agrochemicals in plants.[267-268] Finally, the distribution of

water-soluble carbohydrates and metabolites has been investigated in wheat plants by MALDI-IMS.[209, 269]

In this study, we utilized the MALDI-IMS technique to obtain ion images of native cellulose directly from a sectioned poplar stem. Microcrystalline cellulose (MCC) was used as a reference compound to optimize MALDI-IMS parameters such as matrix application, laser intensity, delay time, and accelerating voltage. The resulting analysis yields a series of intense signals having an inter-peak difference of 162 *m/z* intervals for the solid phase MCC in both reflectron and linear positive ion modes. A cross section of poplar cellulose obtained by acid hydrolysis of poplar holocellulose was examined by bulk carbohydrate and Klason lignin analysis to determine the constituent monosaccharide contents. Subsequently, the poplar cellulose sample was examined using the optimized conditions in MALDI-MS, and direct ion images of cellulose on the surface of the poplar sample were acquired.

8.2 Experimental Section

8.2.1 Materials

Samples were prepared as described in Chapter 4 (4.1.2 Biomass substrate). *Populus. deltoides* x nigra (DN34) clone was grown at NREL and six-month-old juvenile poplar stem was collected for this study. Poplar stem was sectioned or milled as described in Chapter 4 (4.1.2.1-2 Milled poplar stem and Cryotome section of poplar stem). Both sectioned and milled samples were treated under same conditions with various methods.

8.2.2 Preparation of poplar cellulose

Both sectioned and milled samples were prepared as described in Chapter 4 (4.2.1-4.1.3). Sectioned poplar cellulose was stored between glass slides for MALDI-MS/IMS analysis. All the results from the analyses were calculated based on the oven dry weight of biomass that was determined by measuring the moisture content using a moisture analyzer. The analyses that include standard deviations were done in three replicates.

8.2.3 Matrix application

Matrix solutions were prepared as described in Chapter 4 (4.3.3 Matrix application for MALDI-MS/IMS). Three matrixes were tested with cellulose to determine the best signal response: 2,5-dihydroxybenzoic acid (DHB), α-cyano-4-hydroxycinnamic acid (CHCA), and sinapinic acid (SA). Matrix solution was composed of 20 mg/ mL matrix (e.g., DHB) dissolved in TA solution (10% acetonitrile and 0.1% trifluoroacetic acid (v/v) in DI water). For MALDI-MS analysis, a sample in with TA solution was mixed with the matrix solution at a 1:100 (suspension: matrix solution) volume ratio. For preparing MALDI-IMS samples, matrix solution was coated on the surface of sectioned sample using an oscillating capillary nebulizer (OCN) system.[219]

8.2.4 MALDI-MS and -IMS analysis

MALDI-MS spectra of cellulose samples were collected with a Voyager DE STR MALDI-TOF-MS spectrometer as described in Chapter 4 (4.3.4. MALDI-MS/IMS analysis). Positive ion MALDI-MS data was acquired in both linear and reflectron mode

at an accelerating voltage of 12 and 20 kV, respectively, with an 85% grid ratio and a delay time of 400 ns. The spectra were accumulated for 100 laser shots in a sample spot. MALDI-IMS data were acquired at an accelerating voltage of 12 kV with optimized laser power (3100 AU) in linear positive ion mode. Raster scans were performed automatically on the sample surface with 12 shots for each spot. MALDI-IMS data was processed

8.2.5 Carbohydrate and acid-insoluble lignin (Klason lignin) analysis

Carbohydrate profiles and acid-insoluble lignin content in cross-sectioned and milled samples were determined as described in Chapter 4 (4.3.1 Carbohydrates and acid-insoluble lignin analysis).

8.3 Result and Discussion

8.3.1 Carbohydrates and Klason lignin analysis

Prior to MALDI-MS analysis carbohydrate and Klason lignin analysis were performed on the sectioned samples; extractive-free poplar, poplar holocellulose, and poplar cellulose. Bulk chemical composition of each sample was determined using relative monosaccharide and Klason lignin contents as summarized in Figure 50. Most of the Klason lignin in the section of the extractive-free poplar was removed by the holocellulose pulping treatment, whereas the relative monosaccharide content of glucose and xylose in the section of poplar holocellulose was increased by 71% and 21%, respectively. The section of poplar cellulose obtained by removing most of

hemicellulose from poplar holocellulose was composed of ~ 95% glucose and ~ 5% residual hemicelluloses and Klason lignin.

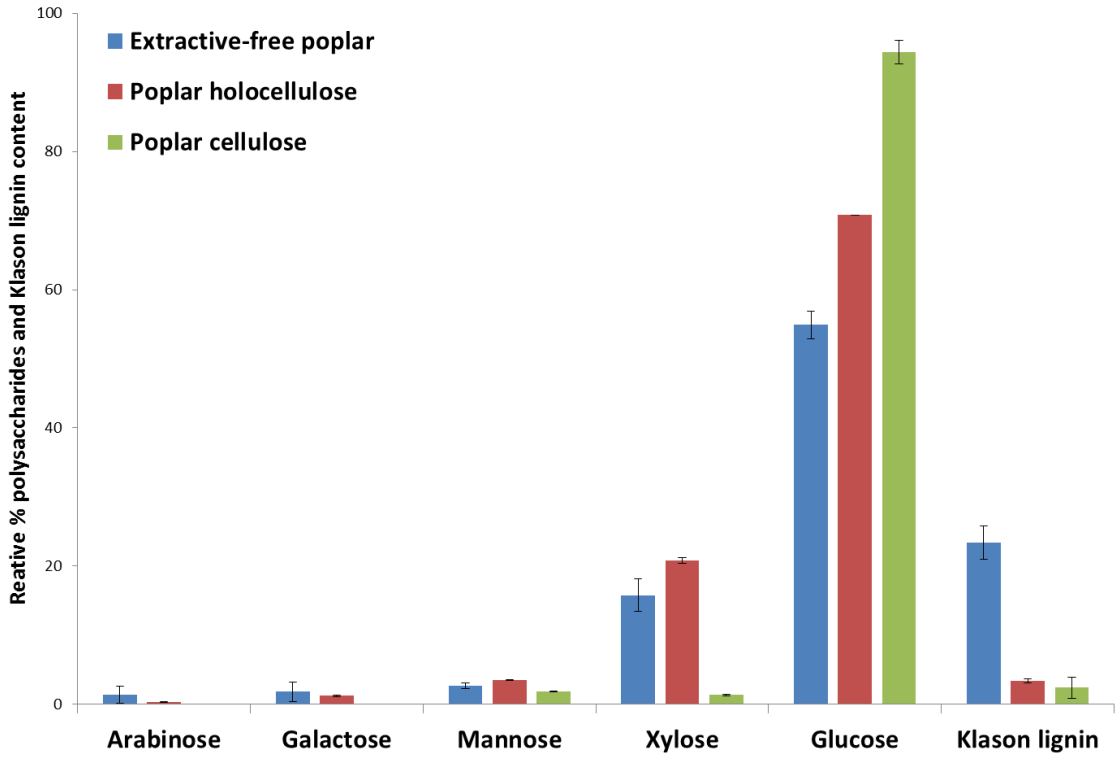

Figure 50 Monosaccharides and Klason lignin content in the treated sectioned poplar stems: extractive-free poplar, poplar holocellulose, and poplar cellulose.

8.3.2 MALDI-MS analysis of cellulose

The ionization efficiency of insoluble polysaccharide (e.g. cellulose) in MALDI-MS is relatively low because of a lack of readily ionizable functional groups in the polysaccharide and the structural rigidity of cellulose.[270] The experimental parameters such as matrix application, laser intensity, delay time, and accelerating voltage for MALDI-MS must therefore be optimized in order to detect these insoluble

polysaccharides. Microcrystalline cellulose (MCC) known as Avicel® was used as a model compound to evaluate the MALDI-MS conditions due to its structural similarity with natural cellulose. MCC is composed of glucose units connected by a β-(1→4)-glycosidic bond with a high degree of crystallinity like natural cellulose. As a result, MCC and natural cellulose are linear chain polymers containing large numbers of hydroxyl groups which make an internal hydrogen bonding network. The molecular size, in terms of degree of polymerization (DP) defined as the number of anhydroglucose units present in a single chain, is one difference between MCC and natural cellulose. The DP value of the MCC (150 – 300) is lower than that of wood plant fibers and other plant sources (800 – 10,000).[271]

The resulting mass spectrum from solid phase MCC with DHB matrix under reflectron positive ion mode conditions reveals a series of intense ions (Figure 51). Intervals of mass differences between adjacent signals were 162 *m/z*, which were derived from one glycosyl unit ($C_6H_{10}O_5$, 162.058 Da). The intense ions only appeared under certain instrument parameters such as an accelerating voltage of 25 kV with an 85% grid ratio and laser power of 2900 AU when DHB matrix was used. In the evaluation of other common MALDI matrixes (e.g. CHCA and SA) these ions were barely observed. The series of oligo- and poly-glucose ions in MCC were observed up to *m/z* 4000 while the intensities of the ions dropped off with increasing *m/z* (Figure 51a). MCC produced the highest intensity of the oligo-glucose ion at *m/z* 1338 which corresponds to 8 glucose units (DP 8) with sodium ion adducts in reflectron mode. The series of the intense ions (e.g. *m/z* 1338) under *m/z* 2000 were accompanied by minor ions (e.g. *m/z* 1320) having

the mass difference of 18 *m/z* which likely corresponds to dehydration. This is consistent with MALDI-MS results from potato and wheat starch debranched by isoamylase, which exhibited the intense ions having intervals of 162 *m/z* with sodium ion adducts and/or the loss of water.[272]

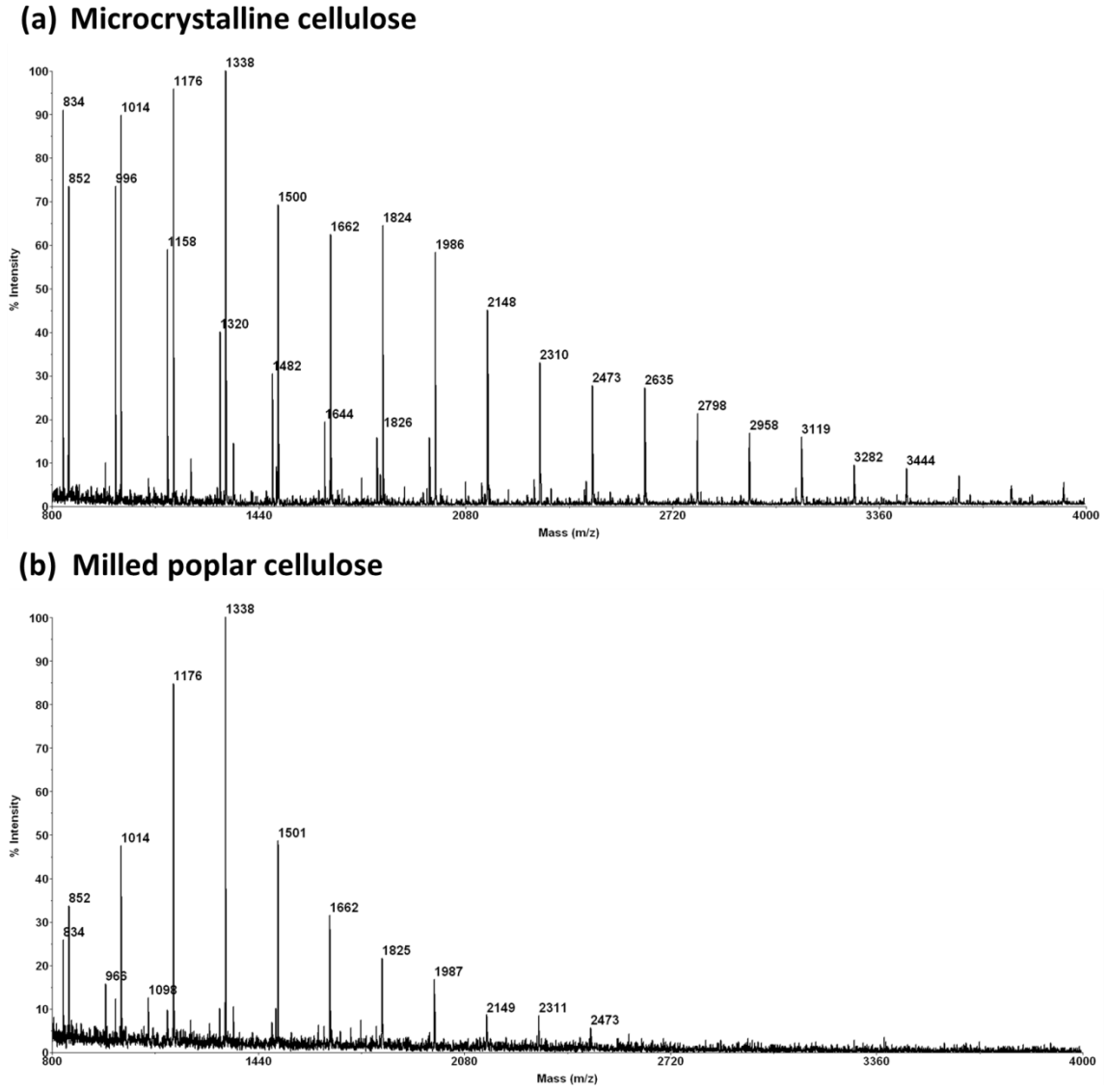

Figure 51 Positive reflectron mode MALDI mass spectra of (a) microcrystalline cellulose and (b) milled poplar obtained from a sectioned poplar stem.

The optimized MALDI conditions were also applied to the sectioned samples: extractive-free poplar, poplar holocellulose, and poplar cellulose. Prior to MALDI-MS analysis each sectioned sample was finely milled as small as the particle size of MCC in order to maintain the same level of experimental environment of MCC. The mass spectrum of the milled poplar cellulose showed intense ions derived from oligo- and poly-glucoses up to *m/z* 2500 (Figure 51b). In terms of DP, intense ions up to DP 15 were detected in the milled poplar cellulose, whereas MCC exhibited ions up to DP 25 (Figure 51). It was also observed that the intensities of ion in the milled poplar cellulose rapidly decreased after *m/z* 1338 (DP 8), whereas the intensities of ion signals in MCC decreased more slowly up to *m/z* 4000. One possible explanation is that the small molecular size (~ DP 300) of the cellulose in MCC may affect detection of the intense ions relative to the large molecular size (~ DP 10,000) of the cellulose in milled poplar cellulose. The mass spectra of the other milled samples (extractive-free poplar and poplar holocellulose) produced only very weak ion signals. It was assumed that the matrix structure of the biopolymers (e.g. cellulose/hemicellulose/lignins or cellulose/hemicellulose) in the cell wall may cause the low ionization efficiency observed in these MALDI-MS analyses. The linear positive ion mode with the same matrix system (2,5-DHB) was also evaluated for MCC and milled poplar cellulose. Here a lower accelerating voltage (12 kV), and higher laser power (3500 AU) proved optimal, resulting in higher intensity signals versus reflectron mode. Additionally, intense ions corresponding to dehydration in MCC and milled poplar cellulose were also detected in linear mode (Figure 52).[273]

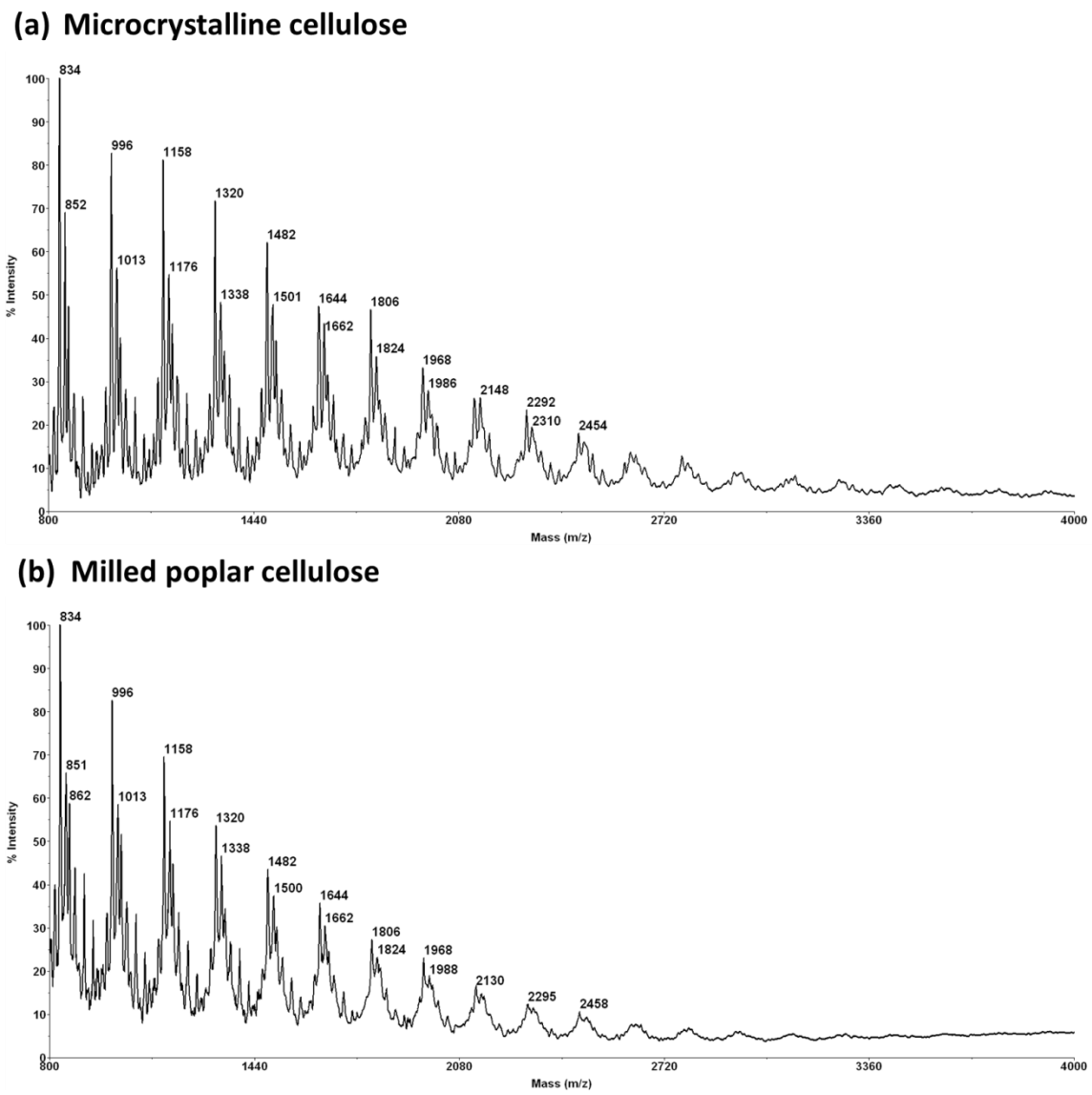

Figure 52 Positive linear mode MALDI mass spectra of (a) microcrystalline cellulose and (b) milled poplar obtained from a sectioned poplar stem.

8.3.3 Imaging MALDI-MS (IMS)

A section of poplar cellulose was coated with matrix using an oscillating capillary nebulizer (OCN) system, which can generate good matrix homogeneity on the sample surface.[219] The sample was evaluated in both linear and reflectron positive ion modes in order to find the best parameters for MALDI-IMS (Figure 53). The resulting mass spectra provided high resolution data from the surface of the poplar cellulose. However, signals were only detected on few spots across the sample surface due to low cellulose ionization yield (Figure 53a). Interestingly, the sectioned poplar cellulose produced the highest intensity ion at *m/z* 1824, which was higher in mass compared to the milled poplar cellulose at *m/z* 1338. This observation could result from a change of the cellulose structure by the mechanical milling process (e.g., milled poplar cellulose). The effect of mechanical milling in cellulose structure was the reduction of the crystalline index along with thermal stability, indicating a disruption of inter/intra hydrogen bonding in cellulose reported by Zhang et al.[274] Compared to reflectron mode, linear positive mode provided higher intensity ions over the sample surface although the resolution was lower (Figure 53b). In order to generate better molecular ion images of the spatial distribution of cellulose compounds, we chose the linear positive ion mode. A low number of laser shots were employed to maintain the intense signals since higher laser power readily depleted analyte and matrix at a given spot. Consequently, a number of oligo- and poly-glucose ions were detected up to *m/z* 4000 over the sample surface (Figure 53b).

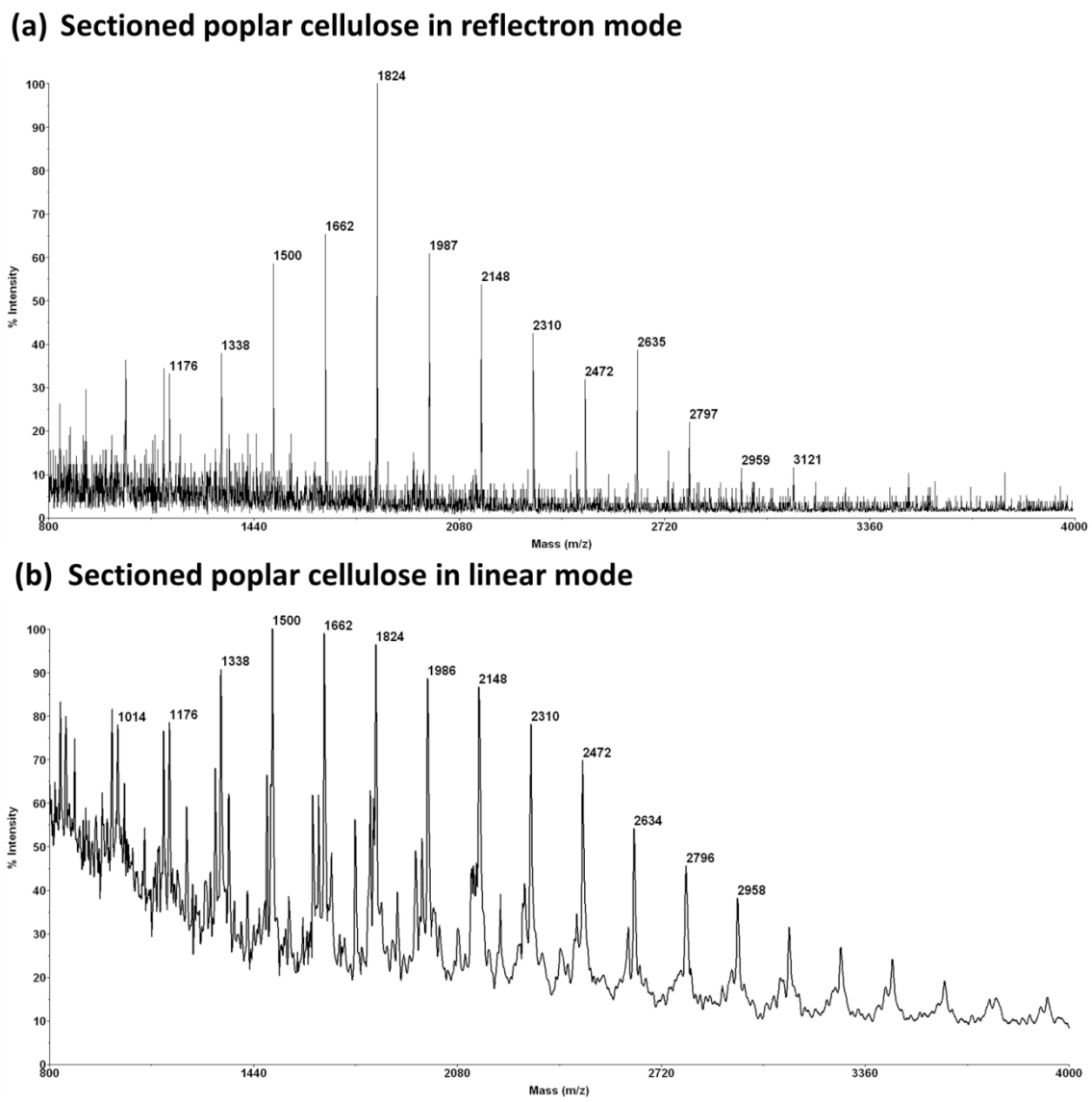

Figure 53 Positive ion MALDI mass spectra from the surface of sectioned poplar cellulose in: (a) reflectron mode and (b) linear mode.

The optical image of the sectioned poplar cellulose is shown in Figure 54(a) for a cross-comparison to MALDI-MS images. Numerous cell walls on the sectioned poplar cellulose exhibited inner cracks (arrowhead) generated during the drying process after acid hydrolysis. The positions of the inner cracks were used as standard points of alignment for spatial correlation between the optical image and MALDI-MS images

because the blanks could appear dark color in MALDI-IMS. MALDI-MS images were generated from selected ions (*m/z* 1500, 2472, and 3120) corresponding to DP 9, 15, and 19 of oligo- and poly-glucose ions, respectively (Figure 4b-d). MALDI-MS images of the sectioned sample clearly showed the spatial distribution of cellulose compounds across the cell-wall surface while inner cracks were observed to be dark in color because of the lack of cellulose (arrowhead). The image generated from *m/z* 1500 (Figure 54b) showed considerably brighter color (higher intensity) along the cell walls. The border areas between cell wall and empty space were shown as less intense color than the middle of cell-wall areas. Decreasing brightness at *m/z* 2472 and 3120 in the MS images (Figure 54c-d) clearly illustrate the reduction in the relative intensities up to 30% and 70%, respectively, compared with that at *m/z* 1500 (Figure 54b). Interestingly, the MS image of cell walls at a particular *m/z* value represented different signal intensities over the surface. For example, more intense areas (brighter color) in the MS image at *m/z* 2472 were localized in middle of cell wall area (arrows) compared to other cell wall areas. This same pattern was also observed in the MS image of *m/z* 3120. One possible explanation for this is that different MW of cellulose is distributed on the surface of cell walls and the relative DP of the cellulose affects its ionization efficiency in MALDI-MS as observed in the MCC spectrum relative to the spectrum of the milled poplar cellulose (Figure 51).

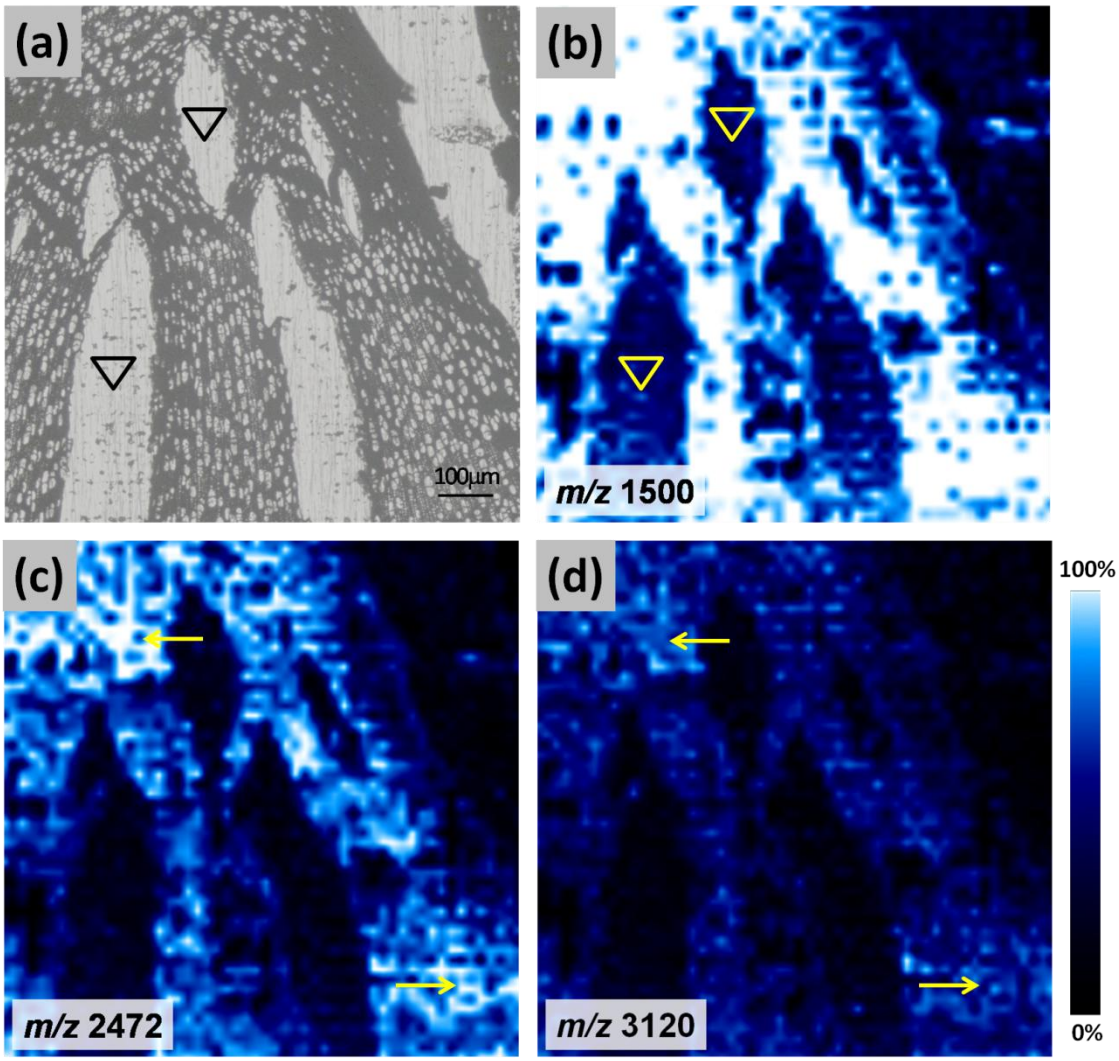

Figure 54 Images of the sectioned poplar cellulose: (a) optical image of sectioned sample coated with 2,5-DHB, (b) MS image of *m/z* 1500, (c) *m/z* 2472, and (d) *m/z* 3120. Scale bar = 100 μm. Color bar indicates the intensity levels. Typical metal surface is marked as an arrowhead; high signal intensity area is marked with an arrow.

8.4 Conclusion

MALDI-MS/IMS was successfully employed to detect insoluble cellulose directly from cross-sectioned poplar stem. To detect cellulose oligomer signals in MALDI-MS, matrix and instrument parameters were optimized prior to perform imaging mass spectrometry in cross-sectioned poplar stem. Among many choices of commercial matrixes, 2,5-dihydroxy benzoic acid matrix solution provided series of intense signals from microcrystalline cellulose in both reflectron and linear modes. A series of signals had exactly 162u of mass differences originated from one glycosyl unit ($C_6H_{10}O_5$, 162.058 Da). Under same condition, cellulose oligomer signals were detected in poplar sample, but the signal intensity was significantly lower than microcrystalline cellulose. It could be due to the interference by lignin and hemicelluloses which are non-covalently linked with cellulose. For this reason, isolated poplar cellulose composed of over 95% cellulose was used for surface analysis. Both sectioned and milled poplar cellulose were observed with a series of intense signals as high as microcrystalline cellulose. Cellulose oligomer signals were detected from DP 5 to DP 24 units on the surface of poplar stem. The cellulose oligomer images were also generated .and showed the lateral distribution of each oligomer across the surface of poplar stem.

CHAPTER 9

CONCLUSION

Lignocellulosic biomass as a source of bioethanol has been promoted instead of food-based materials for biofuel production. The major challenge facing future lignocellulosic biofuel research is reducing the biomass recalcitrance through chemical and/or biological processes. Analytical tools therefore play an important role in determining and understanding the factors related to biomass recalcitrance during the processes. In addition, the visualized surface chemistry is important to elucidate the spatial distribution of major components and their changes upon the processes. In this thesis, TOF-SIMS and MALDI-MS/IMS were employed to develop analytical methodology for biomass in order to contribute biomass recalcitrance.

The primary goal of this thesis was to demonstrate different chemistry between surface and bulk biomass after pretreatment processes. To do this, analytical methodologies using imaging mass spectrometry (i.e., TOF-SIMS and MALDI-IMS) was developed for investigating the surface chemistry of biomass was developed. As a preliminary study, a protocol for preparing frozen sections of poplar stem without embedment was developed for TOF-SIMS and MALDI-IMS analysis. First, TOF-SIMS was employed to investigate surface chemistry of dilute acid pretreated sample using batch reactor. Two-dimensional (2D) molecular image of pretreated sample showed the considerable presence of xylan over the surface. In addition, the relative intensity of xylan after pretreatment increased by 30% compared to untreated sample. On the country, bulk

sugar profile data represented most xylan over 90% was removed after dilute acid pretreatment. The conflicting result of xylan contents between surface and bulk could be due to due to hemicellulose re-precipitation during rapid quenching process at low temperature. This finding provided a clue that there are chemical differences between surface and bulk biomass after pretreatment process.

Second, lignin variation on the surface of poplar stem was also evaluated by TOF-SIMS. For tracking the lateral lignin distribution on the surface, water-only flowthrough pretreatment was employed in order to remove solubilized products continuously prior to re-precipitation on the surface. After 10 min flowthrough pretreatment, it was found that the relative intensity of cellulose on the surface significantly increased by double compared to untreated sample. However, bulk cellulose contents changed only 5% after 10 min flowthrough pretreatment. This is another evidence of chemical differences between surface and bulk biomass after pretreatment processes. In addition, a striking pattern of lignin migration to cell corner was observed after 10 min flowthrough pretreatment by TOF-SIMS images. Lignin reappearance at cell corner was observed after long time (150 min) pretreatment, which could explain part of pseudo-lignin formation.

Third, last part for TOF-SIMS study was the development of 3D imaging method as referred to 3D microarea analysis for biomass. Extending the usefulness of TOF-SIMS for biomass recalcitrance, a 3D molecular imaging was firsly introduced to biomass by acquiring multiple 2D images in a stack. For surface imaging and sputtering in biomass,

the dual beam approach was employed in order to decouple the secondary ion generation and the sample erosion, allwoing high sensitivity of analysis gun. Stress-induced tension wood in poplar stem was used as a model substrate which has a potential for investigating biomass recalcitrance. 3D molecular image of tension wood showed both later and vertical distirbituion of cellulose and lignin from surface to sub-surface. Lignin was intensely observed in secondary cell wall and cell corner but a relatively low intensity was shown in gelatinous (G) layer. On the contrary, cellulose was evenly detected over the surface of tension wood, displaying slightly more intensity in the G-layer. These patterns of lateral distribution continued from top to sub-surface.

In the last chapter in the thesis, MALDI-MS/IMS was employed to detect insoluble cellulose directly from cross-sectioned poplar stem. A capability of large molecular detection in MALDI-MS/IMS allows detecting and visualizing different DPs of cellulose oligomers on the surface of poplar stem. To optimize cellulose detection method in MALDI-MS, Microcrystalline cellulose (MCC) was used as a reference. A series of cellulose oligomer signals with an inter-peak difference of 162 *m/z* intervals were observed from the solid phase MCC. Under the optimum condition, a cross section of poplar cellulose was rastered and cellulose olgomers were detected from DP 5 to DP 24 units. The lateral distribution of different DP of cellulose was observed on the surface of poplar stem.

CHAPTER 10

RECOMMENDATIONS FOR FUTURE WORK

The analytical methodologies in this dissertation have provided a step toward in a comprehensive understand of biomass recalcitrance. The spatial distribution of cell wall characteristics and their quantitative information can provide insight into the effect of pretreatment, bioconversion, and genetic manipulation. In order to gain an even deeper insight into elucidating these relationships, several projects are worthy of further investigations

10.1 Application of 3D microarea analysis

3D microarea analysis for tension wood in poplar stem was successfully applied, presenting the capability of surface analysis from top to subsurface in Chapter 7. Application of 3D microarea analysis to pretreatment or saccharification processes should provide insight into aspects related to biomass recalcitrance. For example, 3D microarea analysis of biomass treated with cellulolytic enzyme/microbe could provide not only an enzyme/microbe binding area but also its penetration depth into biomass. From the enzyme binding area, the pore size on the surface of biomass could be estimated upon different pretreatment processes. From the penetration depth of enzyme/microbe could be used for various fields: a) pretreatment condition optimization, b) particle size determination, and c) enzyme/microbe kinetic measurement.

10.2 Topochemical investigation of transgenic plant by TOF-SIMS

Recently, transgenic poplar has been investigated in order to reduce biomass recalcitrance. For example, down-regulation of cinnamoyl-CoA reductase (CCR) in transgenic poplar showed the reduced lignin and hemicellulose with an increased proportion of cellulose.[275] To examine the effects of CCR down-regulation on lignin structure, antibodies used for topochemical visualization of lignin as well as histochemical and ultrastructural analysis (Figure 55). These conventional methods generally require a labeling or staining process, presenting single component information. IMS analysis by TOF-SIMS for transgenic poplar can provide 2D multi-component topochemical information, visualizing cellulose and lignin. In addition, the lateral distribution of different monolignols such as S- or G-type lignin can be distinguished and directly mapped by TOF-SIMS analysis. A semiquantitative approach in TOF-SIMS image can also provide variation of characteristic species at ROI under submicron scale. Example is shown in Figure 56.[152]

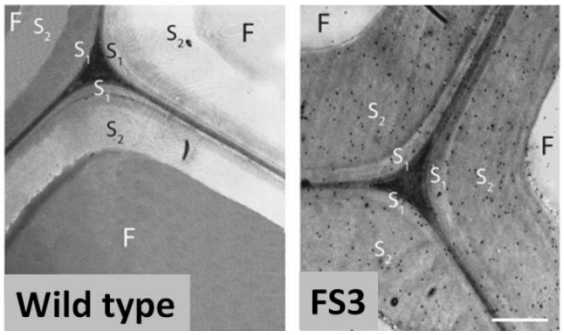

Figure 55 TEM of xylem sections of wild-Type and CCR-downregulated poplars and immunocytochemical localization of lignin epitopes.

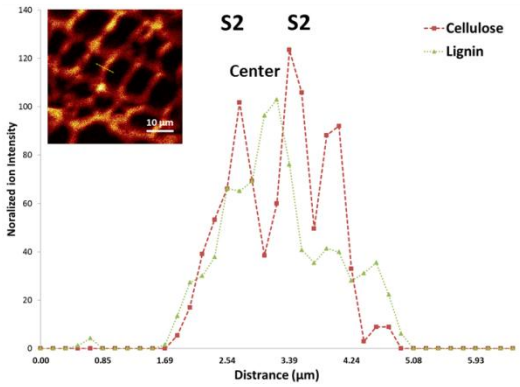

Figure 56 Line scan intensities of the characteristics ions of cellulose (red) and lignin (green) along the yellow dashed line indicated in the total ion image of cross-sections of extractive-free *Populu*s by TOF-SIMS (inset).

REFERENCES

[1] Ragauskas, A. J.; Williams, C. K.; Davison, B. H.; Britovsek, G.; Cairney, J.; Eckert, C. A.; Frederick, W. J.; Hallett, J. P.; Leak, D. J.; Liotta, C. L.; Mielenz, J. R.; Murphy, R.; Templer, R.; Tschaplinski, T., The Path Forward for Biofuels and Biomaterials. *Science* **2006,** *311* (5760), 484-489.

[2] Stöcker, M., Biofuels and Biomass-to-Liquid Fuels in the Biorefinery: Catalytic Conversion of Lignocellulosic Biomass Using Porous Materials. *Angew. Chem. Int. Ed.* **2008,** *47* (48), 9200-9211.

[3] Himmel, M. E.; Ding, S.-Y.; Johnson, D. K.; Adney, W. S.; Nimlos, M. R.; Brady, J. W.; Foust, T. D., Biomass Recalcitrance: Engineering Plants and Enzymes for Biofuels Production. *Science* **2007,** *315* (5813), 804-807.

[4] U.S. Department of Energy; 30 X 30 Workshop, Washington D.C, 1 to 2 August, **2006** (http://www.30x30workshop.Biomass.Govtools.Us/).

[5] Office of the Biomass Program (OBP), "Multi-Year Program Plan, 2007-2012" (OBP, U.S. Department of Energy, Washington, DC, **2005**) (http://www1.Eere.Energy.Gov/Biomass/Pdfs/Mypp.Pdf).

[6] Biofuels Research Advisory Council, Biofuels in the European Union: A Vision for 2030 and Beyond (http://www.Biomatnet.Org/Publications/1919rep.Pdf).

[7] Gomez, L. D.; Steele-King, C. G.; Mcqueen-Mason, S. J., Sustainable Liquid Biofuels from Biomass: The Writing's on the Walls. *New Phytol.* **2008,** *178* (3), 473-485.

[8] Tilman, D.; Hill, J.; Lehman, C., Carbon-Negative Biofuels from Low-Input High-Diversity Grassland Biomass. *Science* **2006,** *314* (5805), 1598-1600.

[9] Walker, G. M., *Bioethanol: Science and Technology of Fuel Alcohol*. Ventus Publishing ApS: Copenhagen, **2010**.

[10] Wyman, C. E., What Is (and Is Not) Vital to Advancing Cellulosic Ethanol. *Trends Biotechnol.* **2007,** *25* (4), 153-157.

[11] Scheffran, J., The Global Demand for Biofuels: Technologies, Markets and Policies. In *Biomass to Biofuels*, Blackwell Publishing Ltd. **2010**; pp 27-54.

[12] Pu, Y.; Zhang, D.; Singh, P. M.; Ragauskas, A. J., The New Forestry Biofuels Sector. *Biofpr* **2008,** *2* (1), 58-73.

[13] Sjöström, E., *Wood Chemistry: Fundamentals and Applications, Second Edition*. Gulf Professional Publishing, **1993**.

[14] Harris, P. J.; Stone, B. A., Chemistry and Molecular Organization of Plant Cell Walls. In *Biomass Recalcitrance*, Blackwell Publishing Ltd. **2009**; pp 61-93.

[15] Himmel, M. E.; Picataggio, S. K., Our Challenge Is to Acquire Deeper Understanding of Biomass Recalcitrance and Conversion. In *Biomass Recalcitrance*, Blackwell Publishing Ltd. **2009**; pp 1-6.

[16] Hoekman, S. K., Biofuels in the Us - Challenges and Opportunities. *Renew. Energ.* **2009,** *34* (1), 14-22.

[17] Keller, J. B.; Plath, P. B., Financing Biotechnology Projects - Lender Due Diligence Requirements and the Role of Independent Technical Consultants. *Appl. Biochem. Biotechnol.* **1999,** *77-9*, 641-648.

[18] Wooley, R.; Ruth, M.; Glassner, D.; Sheehan, J., Process Design and Costing of Bioethanol Technology: A Tool for Determining the Status and Direction of Research and Development. *Biotechnol. Progr.* **1999,** *15* (5), 794-803.

[19] Chen, F.; Dixon, R. A., Lignin Modification Improves Fermentable Sugar Yields for Biofuel Production. *Nat. Biotech.* **2007,** *25* (7), 759-761.

[20] Fu, C.; Mielenz, J. R.; Xiao, X.; Ge, Y.; Hamilton, C. Y.; Rodriguez, M., Jr.; Chen, F.; Foston, M.; Ragauskas, A.; Bouton, J.; Dixon, R. A.; Wang, Z.-Y., Genetic Manipulation of Lignin Reduces Recalcitrance and Improves Ethanol Production from Switchgrass. *PNAS* **2011,** *108* (9), 3803-3808.

[21] Mosier, N.; Wyman, C.; Dale, B.; Elander, R.; Lee, Y. Y.; Holtzapple, M.; Ladisch, M., Features of Promising Technologies for Pretreatment of Lignocellulosic Biomass. *Bioresour. Technol.* **2005,** *96* (6), 673-686.

[22] Yang, B.; Wyman, C. E., Pretreatment: The Key to Unlocking Low-Cost Cellulosic Ethanol. *Biofpr* **2008,** *2* (1), 26-40.

[23] Lynd, L. R.; Van Zyl, W. H.; Mcbride, J. E.; Laser, M., Consolidated Bioprocessing of Cellulosic Biomass: An Update. *Curr. Opin. Biotechnol.* **2005,** *16* (5), 577-583.

[24] Foston, M.; Ragauskas, A. J., Biomass Characterization: Recent Progress in Understanding Biomass Recalcitrance. *Industrial biotechnology* **2012,** *8* (4), 191-208.

[25] Davison, B. H., The Increasing Importance and Capabilities of Biomass Characterization. *Industrial Biotechnology* **2012,** *8* (4), 189-190.

[26] U.S. Department of Energy: Bioenergy Science Center (http://bioenergycenter.org/besc/index.cfm).

[27] Sanchez, O. J.; Cardona, C. A., Trends in Biotechnological Production of Fuel Ethanol from Different Feedstocks. *Bioresour. Technol.* **2008,** *99* (13), 5270-5295.

[28] U.S. Department of Energy: Office of the Biomass Program, *U.S. Billion-Ton Update* (http://www1.eere.energy.gov/biomass/billion_ton_update.html).

[29] Perlack, R. D.; Wright, L. L.; Turhollow, A. F.; Graham, R. L.; Stokes, B. J.; Erbach, D. C. Biomas as Feedstock for a Bioenergy and Bioproducts Industry: The Technical Feasibility of a Billion-Ton Annual Supply (http://feedstockreview.ornl.gov/pdf/billion_ton_vision.pdf).

[30] Fengel, D.; Wegener, G., *Wood—Chemistry, Ultrastructure, Reactions*. Walter de Gruyter: Berlin and New York, **1984**.

[31] Ding, S.-Y.; Himmel, M. E., Anatomy and Ultrastructure of Maize Cell Walls: An Example of Energy Plants. In *Biomass Recalcitrance*, Blackwell Publishing Ltd. **2009**; pp 38-60.

[32] Almkvist, G. 'The Chemistry of the Vasa - Iron, Acids and Degradation' PhD thesis, Swedish University of Agricultural Sciences, **2008**.

[33] Bassem, B. H. 'Fundamental Understanding of the Biochemical Conversion of Buddleja Davidii to Fermentable Sugras', PhD thesis Georgia Institute of Technology, **2011**.

[34] Bledzki, A. K.; Gassan, J., Composites Reinforced with Cellulose Based Fibres. *Prog. Polym. Sci.* **1999,** *24* (2), 221-274.

[35] Hon, D. N. Chemical Modification of Lignocellulosic Material. Marcel Dekker, Inc. New York, **1996**.

[36] Kamel, S.; Ali, N.; Jahangir, K.; Shah, S. M.; El-Gendy, A. A., Pharmaceutical Significance of Cellulose: A Review. *Express Polym. Lett.* **2008,** *2* (11), 758-778.

[37] Liang, C. Y.; Marchessault, R. H., Infrared Spectra of Crystalline Polysaccharides .1. Hydrogen Bonds in Native Celluloses. *J. Polym. Sci.* **1959,** *37* (132), 385-395.

[38] Marchessault, R. H.; Liang, C. Y., Infrared Spectra of Crystalline Polysaccharides .3. Mercerized Cellulose. *J. Polym. Sci.* **1960,** *43* (141), 71-84.

[39] Sarko, A.; Muggli, R., Packing Analysis of Carbohydrates and Polysaccharides .3. Valonia Cellulose and Cellulose-Ii. *Macromolecules* **1974,** *7* (4), 486-494.

[40] Gardner, K. H.; Blackwell, J., The Structure of Native Cellulose. *Biopolymers* **1974,** *13* (10), 1975-2001.

[41] Kroonbatenburg, L. M. J.; Kroon, J.; Northolt, M. G., Chain Modulus and Intramolecular Hydrogen-Bonding in Native and Regenerated Cellulose Fibers. *Polym. Commun.* **1986,** *27* (10), 290-292.

[42] Meyer, K. H.; Misch, L., Positions of Atoms in the New Spatial Model of Cellulose (on the Constitution of the Crystallized Part of the Cellulose Iv). *Helv. Chim. Acta* **1937,** *20*, 232-244.

[43] Atalla, R. H.; Vanderhart, D. L., Native Cellulose - a Composite of 2 Distinct Crystalline Forms. *Science* **1984,** *223* (4633), 283-285.

[44] Wickholm, K.; Larsson, P. T.; Iversen, T., Assignment of Non-Crystalline Forms in Cellulose I by CP/MAS 13C NMR Spectroscopy. *Carbohydr. Res.* **1998,** *312* (3), 123-129.

[45] Pu, Y. Q.; Ziemer, C.; Ragauskas, A. J., Cp/Mas C-13 Nmr Analysis of Cellulase Treated Bleached Softwood Kraft Pulp. *Carbohydr. Res.* **2006,** *341* (5), 591-597.

[46] Klemm, D.; Schmauder, H.; Heinze, T., Cellulose. In *Polysaccharides Ii: Polysaccharides from Eukaryotes*, Biopolymers Baets, S. D.; Vandamme, E., Wiley-VCH: Weinheim, **2003**, Vol. 6: Polysaccharides II, pp 275-287.

[47] Krässig, H. A., *Cellulose: Structure, Accessibility and Reactivity*. Gordon & Breach Science Publishers, Pennsylvania, **1993**, Vol. 36, p 101-101.

[48] Osullivan, A. C., Cellulose: The Structure Slowly Unravels. *Cellulose* **1997,** *4* (3), 173-207.

[49] Moon, R. J.; Martini, A.; Nairn, J.; Simonsen, J.; Youngblood, J., Cellulose Nanomaterials Review: Structure, Properties and Nanocomposites. *Chem. Soc. Rev.* **2011,** *40* (7), 3941-3994.

[50] Imai, T.; Putaux, J.-L.; Sugiyama, J., Geometric Phase Analysis of Lattice Images from Algal Cellulose Microfibrils. *Polymer* **2003,** *44* (6), 1871-1879.

[51] Foston, M.; Hubbell, C. A.; Davis, M.; Ragauskas, A. J., Variations in Cellulosic Ultrastructure of Poplar. *Bioenergy Research* **2009,** *2* (4), 193-197.

[52] Sannigrahi, P.; Ragauskas, A. J.; Miller, S. J., Effects of Two-Stage Dilute Acid Pretreatment on the Structure and Composition of Lignin and Cellulose in Loblolly Pine. *Bioenergy Research* **2008,** *1* (3-4), 205-214.

[53] Samuel, R.; Pu, Y.; Foston, M.; Ragauskas, A. J., Solid-State Nmr Characterization of Switchgrass Cellulose after Dilute Acid Pretreatment. *Biofuels* **2010,** *1* (1), 85-90.

[54] Sannigrahi, P.; Ragauskas, A. J.; Tuskan, G. A., Poplar as a Feedstock for Biofuels: A Review of Compositional Characteristics. *Biofpr* **2010,** *4* (2), 209-226.

[55] Freywyssling, A., The Fine Structure of Cellulose Microfibrils. *Science* **1954,** *119* (3081), 80-82.

[56] Heyn, A. N. J., Elementary Fibril Supermolecular Structure of Cellulose in Soft Wood Fiber. *J. Ultra. Mol. R.* **1969,** *26* (1-2), 52-&.

[57] Brown, R. M.; Saxena, I. M., Cellulose Biosynthesis: A Model for Understanding the Assembly of Biopolymers. *Plant Physiol. Bioch.* **2000,** *38* (1-2), 57-67.

[58] Sugiyama, J.; Vuong, R.; Chanzy, H., Electron Diffraction Study on the Two Crystalline Phases Occurring in Native Cellulose from an Algal Cell Wall. *Macromolecules* **1991,** *24* (14), 4168-4175.

[59] Nishiyama, Y.; Sugiyama, J.; Chanzy, H.; Langan, P., Crystal Structure and Hydrogen Bonding System in Cellulose Iα from Synchrotron X-Ray and Neutron Fiber Diffraction. *J. Am. Chem. Soc.* **2003,** *125* (47), 14300-14306.

[60] Peterlin, A.; Ingram, P., Morphology of Secondary Wall Fibrils in Cotton. *Text. Res. J.* **1970,** *40* (4), 345-&.

[61] Samir, M.; Alloin, F.; Dufresne, A., Review of Recent Research into Cellulosic Whiskers, Their Properties and Their Application in Nanocomposite Field. *Biomacromolecules* **2005,** *6* (2), 612-626.

[62] Ebringerova, A.; Hromadkova, Z.; Heinze, T., Hemicellulose. In *Polysaccharides 1: Structure, Characterization and Use*, Advances in Polymer ScienceHeinze, T., **2005**; Vol. 186, pp 1-67.

[63] Scheller, H. V.; Ulvskov, P., Hemicelluloses. In *Annual Review of Plant Biology, Vol 61*, Annual Review of Plant BiologyMerchant, S.; Briggs, W. R.; Ort, D., **2010**, Vol. 61, pp 263-289.

[64] Ragauskas, A. J.; Nagy, M.; Kim, D. H.; Eckert, C. A.; Hallett, J. P.; Liotta, C. L., From Wood to Fuels: Integrating Biofuels and Pulp Production. *Industrial Biotechnology* **2006,** *2* (1), 55-65.

[65] Willfor, S.; Sundberg, A.; Hemming, J.; Holmbom, B., Polysaccharides in Some Industrially Important Softwood Species. *Wood Sci. Technol.* **2005,** *39* (4), 245-258.

[66] Willfor, S.; Sundberg, A.; Pranovich, A.; Holmbom, B., Polysaccharides in Some Industrially Important Hardwood Species. *Wood Sci. Technol.* **2005,** *39* (8), 601-617.

[67] Johnson, J. M. F.; Barbour, N. W.; Weyers, S. L., Chemical Composition of Crop Biomass Impacts Its Decomposition. *Soil Sci. Soc. Am. J.* **2007,** *71* (1), 155-162.

[68] Dien, B. S.; Jung, H.-J. G.; Vogel, K. P.; Casler, M. D.; Lamb, J. F. S.; Iten, L.; Mitchell, R. B.; Sarath, G., Chemical Composition and Response to Dilute-Acid Pretreatment and Enzymatic Saccharification of Alfalfa, Reed Canarygrass, and Switchgrass. *Biomass Bioenergy* **2006,** *30* (10), 880-891.

[69] Feldman., D., Lignin and Its Polyblends - a Review. In *Chemical Modification, Properties, and Usage of Lignin* Hu, T. Q. New York, Kluwer Academic/Plenum Publishers: **2002**, pp 81-99.

[70] Sarkanen, K. V.; Ludwig, C. H., *Lignins: Occurrence, Formation, Structure and Reactions*. John Wiley & Sons, Inc. New York, **1971**.

[71] Freudenberg, K.; Neish, A. C., *Constitution and Biosynthesis of Lignin*. Springer, New York, **1968**, Vol. 2.

[72] Boerjan, W.; Ralph, J.; Baucher, M., Lignin Biosynthesis. *Annu. rev. plant biol.* **2003,** *54*, 519-546.

[73] Baucher, M.; Monties, B.; Montagu, M. V.; Boerjan, W., Biosynthesis and Genetic Engineering of Lignin. *Crit. Rev. Plant Sci.* **1998,** *17* (2), 125-197.

[74] Adler, E., Lignin Chemistry - Past, Present and Future. *Wood Sci. Technol.* **1977,** *11* (3), 169-218.

[75] Capanema, E. A.; Balakshin, M. Y.; Kadla, J. F., A Comprehensive Approach for Quantitative Lignin Characterization by Nmr Spectroscopy. *J. Agric. Food. Chem.* **2004,** *52* (7), 1850-1860.

[76] Capanema, E. A.; Balakshin, M. Y.; Kadla, J. F., Quantitative Characterization of a Hardwood Milled Wood Lignin by Nuclear Magnetic Resonance Spectroscopy. *J. Agric. Food. Chem.* **2005,** *53* (25), 9639-9649.

[77] David, K.; Ragauskas, A. J., Switchgrass as an Energy Crop for Biofuel Production: A Review of Its Ligno-Cellulosic Chemical Properties. *Energ .Environ. Sci.* **2010,** *3* (9), 1182-1190.

[78] Nagy, M. 'Biofuels from Lignin and Novel Biodiesel Analysis', PhD thesis,. Georgia Institute of Technology, **2009**.

[79] U.S. Department of Agriculture: Agricultural Research Service (http://ars.usda.gov/Services/docs.htm?docid=10443).

[80] Wallace, G.; Chesson, A.; Lomax, J. A.; Jarvis, M. C., Lignin-Carbohydrate Complexes in Graminaceous Cell Walls in Relation to Digestibility. *Anim. Feed Sci. Tech.* **1991,** *32* (1–3), 193-199.

[81] Azuma, J.; Takahashi, N.; Koshijima, T., Isolation and Characterization of Lignin-Carbohydrate Complexes from the Milled-Wood Lignin Fraction of Pinus-Densiflora Sieb Et Zucc. *Carbohydr. Res.* **1981,** *93* (1), 91-104.

[82] Mukoyoshi, S. I.; Azuma, J. I.; Koshijima, T., Lignin-Carbohydrate Complexes from Compression Wood of Pinus-Densiflora Sieb Et Zucc. *Holzforschung* **1981,** *35* (5), 233-240.

[83] Azuma, J.-I.; Tetsuo, K., Lignin-Carbohydrate Complexes from Various Sources. In *Methods Enzymol.*, Willis A. Wood, S. T. K., Ed.^Eds. Academic Press: **1988**; Vol. Volume 161, pp 12-18.

[84] Buranov, A. U.; Mazza, G., Lignin in Straw of Herbaceous Crops. *Ind. Crops Prod.* **2008,** *28* (3), 237-259.

[85] Ishii, T., Structure and Functions of Feruloylated Polysaccharides. *Plant Sci.* **1997,** *127* (2), 111-127.

[86] Koshijima, T.; Watanabe, T.; Azuma, J., Existence of Benzylated Carbohydrate Moiety in Lignin Carbohydrate Complex from Pine Wood. *Chem. Lett.* **1984,** (10), 1737-1740.

[87] Ramos, L. P., The Chemistry Involved in the Steam Treatment of Lignocellulosic Materials. *Quim. Nova* **2003,** *26* (6), 863-871.

[88] Kumar, S.; Singh, S. P.; Mishra, I. M.; Adhikari, D. K., Recent Advances in Production of Bioethanol from Lignocellulosic Biomass. *Chem. Eng. Technol.* **2009,** *32* (4), 517-526.

[89] Sangseethong, K.; Meunier-Goddik, L.; Tantasucharit, U.; Liaw, E. T.; Penner, M. H., Rationale for Particle Size Effect on Rates of Enzymatic Saccharification of Microcrystalline Cellulose. *J. Food Biochem.* **1998,** *22* (4), 321-330.

[90] Gharpuray, M. M.; Lee, Y. H.; Fan, L. T., Structural Modification of Lignocellulosics by Pretreatments to Enhance Enzymatic-Hydrolysis. *Biotechnol. Bioeng.* **1983,** *25* (1), 157-172.

[91] Park, S.; Baker, J. O.; Himmel, M. E.; Parilla, P. A.; Johnson, D. K., Cellulose Crystallinity Index: Measurement Techniques and Their Impact on Interpreting Cellulase Performance. *Biotechnol. Biofuels* **2010,** *3*.

[92] Foston, M.; Ragauskas, A. J., Changes in Lignocellulosic Supramolecular and Ultrastructure During Dilute Acid Pretreatment of Populus and Switchgrass. *Biomass. Bioenerg.* **2010,** *34* (12), 1885-1895.

[93] Mansfield, S. D.; Mooney, C.; Saddler, J. N., Substrate and Enzyme Characteristics That Limit Cellulose Hydrolysis. *Biotechnol. Progr.* **1999,** *15* (5), 804-816.

[94] Excoffier, G.; Toussaint, B.; Vignon, M. R., Saccharification of Steam-Exploded Poplar Wood. *Biotechnol. Bioeng.* **1991,** *38* (11), 1308-1317.

[95] Lu, Y. P.; Yang, B.; Gregg, D.; Saddler, J. N.; Mansfield, S. D., Cellulase Adsorption and an Evaluation of Enzyme Recycle During Hydrolysis of Steam-Exploded Softwood Residues. *Appl. Biochem. Biotechnol.* **2002,** *98*, 641-654.

[96] Kong, F. R.; Engler, C. R.; Soltes, E. J., Effects of Cell-Wall Acetate, Xylan Backbone, and Lignin on Enzymatic-Hydrolysis of Aspen Wood. *Appl. Biochem. Biotechnol.* **1992,** *34-5*, 23-35.

[97] Brosse, N.; Mohamad Ibrahim, M. N.; Abdul Rahim, A., Biomass to Bioethanol: Initiatives of the Future for Lignin. *ISRN Materials Science* **2011,** *2011*, 10.

[98] Qing, Q.; Yang, B.; Wyman, C. E., Xylooligomers Are Strong Inhibitors of Cellulose Hydrolysis by Enzymes. *Bioresour. Technol.* **2010,** *101* (24), 9624-9630.

[99] Kumar, R.; Wyman, C. E., Does Change in Accessibility with Conversion Depend on Both the Substrate and Pretreatment Technology? *Bioresour. Technol.* **2009,** *100* (18), 4193-4202.

[100] Alvira, P.; Tomas-Pejo, E.; Ballesteros, M.; Negro, M. J., Pretreatment Technologies for an Efficient Bioethanol Production Process Based on Enzymatic Hydrolysis: A Review. *Bioresour. Technol.* **2010,** *101* (13), 4851-4861.

[101] Chundawat, S. P. S.; Beckham, G. T.; Himmel, M. E.; Dale, B. E., Deconstruction of Lignocellulosic Biomass to Fuels and Chemicals. *Annu. Rev. Chem. Biomol. Eng.* **2011,** *2* (1), 121-145.

[102] Sanchez, C., Lignocellulosic Residues: Biodegradation and Bioconversion by Fungi. *Biotechnol. Adv.* **2009,** *27* (2), 185-194.

[103] Kumar, R.; Wyman, C. E., Effects of Cellulase and Xylanase Enzymes on the Deconstruction of Solids from Pretreatment of Poplar by Leading Technologies. *Biotechnol. Progr.* **2009,** *25* (2), 302-314.

[104] Jung, S.; Foston, M.; Sullards, M. C.; Ragauskas, A. J., Surface Characterization of Dilute Acid Pretreated Populus Deltoides by Tof-Sims. *Energ. Fuel.* **2010,** *24*, 1347-1357.

[105] Wyman, C. E.; Dale, B. E.; Elander, R. T.; Holtzapple, M.; Ladisch, M. R.; Lee, Y. Y.; Mitchinson, C.; Saddler, J. N., Comparative Sugar Recovery and Fermentation Data Following Pretreatment of Poplar Wood by Leading Technologies. *Biotechnol. Progr.* **2009,** *25* (2), 333-339.

[106] Kumar, R.; Wyman, C. E., Access of Cellulase to Cellulose and Lignin for Poplar Solids Produced by Leading Pretreatment Technologies. *Biotechnol. Progr.* **2009,** *25* (3), 807-819.

[107] Li, C.; Knierim, B.; Manisseri, C.; Arora, R.; Scheller, H. V.; Auer, M.; Vogel, K. P.; Simmons, B. A.; Singh, S., Comparison of Dilute Acid and Ionic Liquid Pretreatment of Switchgrass: Biomass Recalcitrance, Delignification and Enzymatic Saccharification. *Bioresour. Technol.* **2010,** *101* (13), 4900-4906.

[108] Digman, M. F.; Shinners, K. J.; Casler, M. D.; Dien, B. S.; Hatfield, R. D.; Jung, H.-J. G.; Muck, R. E.; Weimer, P. J., Optimizing on-Farm Pretreatment of Perennial Grasses for Fuel Ethanol Production. *Bioresour. Technol.* **2010,** *101* (14), 5305-5314.

[109] Xu, J.; Thomsen, M. H.; Thomsen, A. B., Pretreatment on Corn Stover with Low Concentration of Formic Acid. *J. Microbiol. Biotechnol.* **2009,** *19* (8), 845-850.

[110] Shuai, L.; Yang, Q.; Zhu, J. Y.; Lu, F. C.; Weimer, P. J.; Ralph, J.; Pan, X. J., Comparative Study of Sporl and Dilute-Acid Pretreatments of Spruce for Cellulosic Ethanol Production. *Bioresour. Technol.* **2010,** *101* (9), 3106-3114.

[111] Esteghlalian, A.; Hashimoto, A. G.; Fenske, J. J.; Penner, M. H., Modeling and Optimization of the Dilute-Sulfuric-Acid Pretreatment of Corn Stover, Poplar and Switchgrass. *Bioresour. Technol.* **1997,** *59* (2-3), 129-136.

[112] Nguyen, Q. A.; Tucker, M. P.; Keller, F. A.; Eddy, F. P., Two-Stage Dilute-Acid Pretreatment of Softwoods. *Appl. Biochem. Biotechnol.* **2000,** *84-6*, 561-576.

[113] Saha, B. C.; Iten, L. B.; Cotta, M. A.; Wu, Y. V., Dilute Acid Pretreatment, Enzymatic Saccharification and Fermentation of Wheat Straw to Ethanol. *Process Biochem.* **2005,** *40* (12), 3693-3700.

[114] Sun, Y.; Cheng, J. J., Dilute Acid Pretreatment of Rye Straw and Bermudagrass for Ethanol Production. *Bioresour. Technol.* **2005,** *96* (14), 1599-1606.

[115] Hu, F.; Jung, S.; Ragauskas, A., Pseudo-Lignin Formation and Its Impact on Enzymatic Hydrolysis. *Bioresour. Technol.* **2012,** *117*, 7-12.

[116] Sannigrahi, P.; Kim, D. H.; Jung, S.; Ragauskas, A., Pseudo-Lignin and Pretreatment Chemistry. *Energ. Environ. Sci.* **2011,** *4* (4), 1306-1310.

[117] Taherzadeh, M. J.; Karimi, K., Pretreatment of Lignocellulosic Wastes to Improve Ethanol and Biogas Production: A Review. *Int. J. .Mol. Sci.* **2008,** *9* (9), 1621-1651.

[118] Lloyd, T. A.; Wyman, C. E., Combined Sugar Yields for Dilute Sulfuric Acid Pretreatment of Corn Stover Followed by Enzymatic Hydrolysis of the Remaining Solids. *Bioresour. Technol.* **2005,** *96* (18), 1967-1977.

[119] Marzialetti, T.; Olarte, M. B. V.; Sievers, C.; Hoskins, T. J. C.; Agrawal, P. K.; Jones, C. W., Dilute Acid Hydrolysis of Loblolly Pine: A Comprehensive Approach. *Ind. Eng. Chem. Res.* **2008,** *47* (19), 7131-7140.

[120] Avellar, B. K.; Glasser, W. G., Steam-Assisted Biomass Fractionation. I. Process Considerations and Economic Evaluation. *Biomass Bioenerg.* **1998,** *14* (3), 205-218.

[121] Sun, Y.; Cheng, J. Y., Hydrolysis of Lignocellulosic Materials for Ethanol Production: A Review. *Bioresour. Technol.* **2002,** *83* (1), 1-11.

[122] Brownell, H. H.; Yu, E. K. C.; Saddler, J. N., Steam-Explosion Pretreatment of Wood - Effect of Chip Size, Acid, Moisture-Content and Pressure-Drop. *Biotechnol. Bioeng.* **1986,** *28* (6), 792-801.

[123] Mackie, K. L.; Brownell, H. H.; West, K. L.; Saddler, J. N., Effect of Sulphur Dioxide and Sulphuric Acid on Steam Explosion of Aspenwood. *J. Wood Chem. Technol.* **1985,** *5* (3), 405-425.

[124] Tengborg, C.; Stenberg, K.; Galbe, M.; Zacchi, G.; Larsson, S.; Palmqvist, E.; Hahn-Hagerdal, B., Comparison of So2 and H2so4 Impregnation of Softwood Prior to Steam Pretreatment on Ethanol Production. *Appl. Biochem. Biotechnol.* **1998,** *70-2*, 3-15.

[125] Soderstrom, J.; Pilcher, L.; Galbe, M.; Zacchi, G., Two-Step Steam Pretreatment of Softwood with So2 Impregnation for Ethanol Production. *Appl. Biochem. Biotechnol.* **2002,** *98*, 5-21.

[126] Teymouri, F.; Laureano-Perez, L.; Alizadeh, H.; Dale, B. E., Optimization of the Ammonia Fiber Explosion (Afex) Treatment Parameters for Enzymatic Hydrolysis of Corn Stover. *Bioresour. Technol.* **2005,** *96* (18), 2014-2018.

[127] Laureano-Perez, L.; Teymouri, F.; Alizadeh, H.; Dale, B. E., Understanding Factors That Limit Enzymatic Hydrolysis of Biomass. *Appl. Biochem. Biotechnol.* **2005,** *121*, 1081-1099.

[128] Holtzapple, M. T.; Lundeen, J. E.; Sturgis, R.; Lewis, J. E.; Dale, B. E., Pretreatment of Lignocellulosic Municipal Solid-Waste by Ammonia Fiber Explosion (Afex). *Appl. Biochem. Biotechnol.* **1992,** *34-5*, 5-21.

[129] Papatheofanous, M. G.; Billa, E.; Koullas, D. P.; Monties, B.; Koukios, E. G., Two-Stage Acid-Catalyzed Fractionation of Lignocellulosic Biomass in Aqueous Ethanol Systems at Low Temperatures. *Bioresour. Technol.* **1995,** *54* (3), 305-310.

[130] Zhao, X.; Cheng, K.; Liu, D., Organosolv Pretreatment of Lignocellulosic Biomass for Enzymatic Hydrolysis. *Appl. Microbiol. Biotechnol.* **2009,** *82* (5), 815-827.

[131] Sarkanen, K. V., Acid-Catalyzed Delignification of Lignocellulosics in Organic Solvents. *Progress in biomass conversion* **2009,** *2*, 127-144.

[132] Sánchez, Ó. J.; Cardona, C. A., Trends in Biotechnological Production of Fuel Ethanol from Different Feedstocks. *Bioresour. Technol.* **2008,** *99* (13), 5270-5295.

[133] Gremlich, H.-U., Infrared and Raman Spectroscopy. In *Ullmann's Encyclopedia of Industrial Chemistry*, Wiley-VCH Verlag GmbH & Co. KGaA, **2000**.

[134] Gierlinger, N.; Goswami, L.; Schmidt, M.; Burgert, I.; Coutand, C.; Rogge, T.; Schwanninger, M., In Situ FT-IR Microscopic Study on Enzymatic Treatment of Poplar Wood Cross-Sections. *Biomacromolecules* **2008,** *9* (8), 2194-2201.

[135] Gierlinger, N.; Schwanninger, M., Chemical Imaging of Poplar Wood Cell Walls by Confocal Raman Microscopy. *Plant Physiol.* **2006,** *140* (4), 1246-1254.

[136] Gierlinger, N.; Schwanninger, M., The Potential of Raman Microscopy and Raman Imaging in Plant Research. *Spectrosc.- Int. J.* **2007,** *21* (2), 69-89.

[137] Agarwal, U. P., Raman Imaging to Investigate Ultrastructure and Composition of Plant Cell Walls: Distribution of Lignin and Cellulose in Black Spruce Wood (Picea Mariana). *Planta* **2006,** *224* (5), 1141-1153.

[138] Zeng, Y.; Saar, B. G.; Friedrich, M. G.; Chen, F.; Liu, Y.-S.; Dixon, R. A.; Himmel, M. E.; Xie, X. S.; Ding, S.-Y., Imaging Lignin-Downregulated Alfalfa Using Coherent Anti-Stokes Raman Scattering Microscopy. *Bioenergy Research* **2010,** *3* (3), 272-277.

[139] Saar, B. G.; Zeng, Y.; Freudiger, C. W.; Liu, Y.-S.; Himmel, M. E.; Xie, X. S.; Ding, S.-Y., Label-Free, Real-Time Monitoring of Biomass Processing with Stimulated Raman Scattering Microscopy. *Angew. Chem. Int. Ed.* **2010,** *49* (32), 5476-5479.

[140] Yakovlev, V. V., Advanced Instrumentation for Non-Linear Raman Microscopy. *J. Raman Spectroscopy* **2003,** *34* (12), 957-964.

[141] Allison, G. G., *Application of Fourier Transform Mid-Infrared Spectroscopy (FTIR) for Research into Biomass Feed-Stocks, Fourier Transforms*. InTech, 2011, p 71-88.

[142] Dokken, K. M.; Davis, L. C.; Marinkovic, N. S., Use of Infrared Microspectroscopy in Plant Growth and Development. *Appl. Spectrosc. Rev.* **2005,** *40* (4), 301-326.

[143] Moore, A. K.; Owen, N. L., Infrared Spectroscopic Studies of Solid Wood. *Appl. Spectrosc. Rev.* **2001,** *36* (1), 65-86.

[144] Yin, Y.; Berglund, L.; Salmen, L., Effect of Steam Treatment on the Properties of Wood Cell Walls. *Biomacromolecules* **2011,** *12* (1), 194-202.

[145] Davies, L. M.; Harris, P. J., Atomic Force Microscopy of Microfibrils in Primary Cell Walls. *Planta* **2003,** *217* (2), 283-289.

[146] Kirby, A. R.; Gunning, A. P.; Waldron, K. W.; Morris, V. J.; Ng, A., Visualization of Plant Cell Walls by Atomic Force Microscopy. *Biophys. J.* **1996,** *70* (3), 1138-1143.

[147] Engel, A.; Lyubchenko, Y.; Muller, D., Atomic Force Microscopy: A Powerful Tool to Observe Biomolecules at Work. *Trends Cell Biol.* **1999,** *9* (2), 77-80.

[148] Atalla, R. H.; Brady, J. W.; Matthews, J. F.; Ding, S.-Y.; Himmel, M. E., Structures of Plant Cell Wall Celluloses. In *Biomass Recalcitrance*, Blackwell Publishing Ltd. **2009**, pp 188-212.

[149] Ding, S. Y.; Himmel, M. E., The Maize Primary Cell Wall Microfibril: A New Model Derived from Direct Visualization. *J. Agric. Food. Chem.* **2006,** *54* (3), 597-606.

[150] Tetard, L.; Passian, A.; Farahi, R. H.; Davison, B. H.; Jung, S.; Ragauskas, A. J.; Lereu, A. L.; Thundat, T., Nanometrology of Delignified Populus Using Mode Synthesizing Atomic Force Microscopy. *Nanotechnology* **2011,** *22* (46), 465702-465702.

[151] Tetard, L.; Passian, A.; Thundat, T., New Modes for Subsurface Atomic Force Microscopy through Nanomechanical Coupling. *Nat. Nanotechnol.* **2010,** *5* (2), 105-109.

[152] Tetard, L.; Passian, A.; Jung, S.; Ragauskas, A. J.; Davison, B. H., Development of New Methods in Scanning Probe Microscopy for Lignocellulosic Biomass Characterization. *Industrial Biotechnology* **2012,** *8* (4), 245-249.

[153] Kimura, S.; Laosinchai, W.; Itoh, T.; Cui, X. J.; Linder, C. R.; Brown, R. M., Immunogold Labeling of Rosette Terminal Cellulose-Synthesizing Complexes in the Vascular Plant Vigna Angularis. *Plant Cell* **1999,** *11* (11), 2075-2085.

[154] Jansen, S.; Choat, B.; Pletsers, A., Morphological Variation of Intervessel Pit Membranes and Implications to Xylem Function in Angiosperms. *Am. J. Botany* **2009,** *96* (2), 409-419.

[155] Hamm, M.; Debeire, P.; Monties, B.; Chabbert, B., Changes in the Cell Wall Network During the Thermal Dehydration of Alfalfa Stems. *J. Agric. Food. Chem.* **2002,** *50* (7), 1897-1903.

[156] Chundawat, S. P. S.; Donohoe, B. S.; Sousa, L. D. C.; Elder, T.; Agarwal, U. P.; Lu, F.; Ralph, J.; Himmel, M. E.; Balan, V.; Dale, B. E., Multi-Scale Visualization and Characterization of Lignocellulosic Plant Cell Wall Deconstruction During Thermochemical Pretreatment. *Energ. Environ. Sci.* **2011,** *4* (3), 973-984.

[157] Xu, P.; Donaldson, L. A.; Gergely, Z. R.; Staehelin, L. A., Dual-Axis Electron Tomography: A New Approach for Investigating the Spatial Organization of Wood Cellulose Microfibrils. *Wood Sci. Technol.* **2007,** *41* (2), 101-116.

[158] Cox, G., *Optical Imaging Techniques in Cell Biology, Second Edition* CRC Press, **2012** p 316.

[159] Huang, B.; Wang, W.; Bates, M.; Zhuang, X., Three-Dimensional Super-Resolution Imaging by Stochastic Optical Reconstruction Microscopy. *Science* **2008,** *319* (5864), 810-813.

[160] Ding, S.-Y.; Xu, Q.; Crowley, M.; Zeng, Y.; Nimlos, M.; Lamed, R.; Bayer, E. A.; Himmel, M. E., A Biophysical Perspective on the Cellulosome: New Opportunities for Biomass Conversion. *Curr. Opin. Biotechnol.* **2008,** *19* (3), 218-227.

[161] Ding, S. Y.; Xu, Q.; Ali, M. K.; Baker, J. O.; Bayer, E. A.; Barak, Y.; Lamed, R.; Sugiyama, J.; Rumbles, G.; Himmel, M. E., Versatile Derivatives of Carbohydrate-Binding Modules for Imaging of Complex Carbohydrates Approaching the Molecular Level of Resolution. *Biotechniques* **2006,** *41* (4), 435-+.

[162] Mcdonnell, L. A.; Heeren, R. M. A., Imaging Mass Spectrometry. *Mass Spectrom. Rev.* **2007,** *26* (4), 606-643.

[163] Rubakhin, S. S.; Jurchen, J. C.; Monroe, E. B.; Sweedler, J. V., Imaging Mass Spectrometry: Fundamentals and Applications to Drug Discovery. *Drug Discov. Today* **2005,** *10* (12), 823-837.

[164] Vickerman, J. C., Molecular Surface Mass Spectrometry by Sims. In *Surface Analysis – the Principal Techniques*, John Wiley & Sons, Ltd. **2009**, pp 113-203.

[165] Stump, M. J.; Fleming, R. C.; Gong, W. H.; Jaber, A. J.; Jones, J. J.; Surber, C. W.; Wilkins, C. L., Matrix-Assisted Laser Desorption Mass Spectrometry. *Appl. Spectrosc. Rev.* **2002,** *37* (3), 275-303.

[166] Macaleese, L.; Stauber, J.; Heeren, R. M. A., Perspectives for Imaging Mass Spectrometry in the Proteomics Landscape. *Proteomics* **2009,** *9* (4), 819-834.

[167] Hammond, J., Comparison of Sims and Maldi for Mass Spectrometric Imaging. In *Imaging Mass Spectrometry*, Setou, M., Springer Japan, **2010**, pp 235-257.

[168] Touboul, D.; Kollmer, F.; Niehuis, E.; Brunelle, A.; Laprevote, O., Improvement of Biological Time-of-Flight-Secondary Ion Mass Spectrometry Imaging with a Bismuth Cluster Ion Source. *J. Am. Soc. Mass. Spectrom.* **2005,** *16* (10), 1608-1618.

[169] Pacholski, M. L.; Winograd, N., Imaging with Mass Spectrometry. *Chem. Rev.* **1999,** *99* (10), 2977-+.

[170] Spengler, B.; Hubert, M., Scanning Microprobe Matrix-Assisted Laser Desorption Ionization (Smaldi) Mass Spectrometry: Instrumentation for Sub-Micrometer Resolved Ldi and Maldi Surface Analysis. *J. Am. Soc. Mass. Spectrom.* **2002,** *13* (6), 735-748.

[171] Fletcher, J. S.; Vickerman, J. C.; Winograd, N., Label Free Biochemical 2d and 3d Imaging Using Secondary Ion Mass Spectrometry. *Curr. Opin. Chem. Biol.* **2011,** *15* (5), 733-740.

[172] Crecelius, A. C.; Cornett, D. S.; Caprioli, R. M.; Williams, B.; Dawant, B. M.; Bodenheimer, B., Three-Dimensional Visualization of Protein Expression in Mouse Brain Structures Using Imaging Mass Spectrometry. *J. Am. Soc. Mass. Spectrom.* **2005,** *16* (7), 1093-1099.

[173] Kangas, H. 'Surface Chemical and Morphological Properties of Mechanical Pulps, Fibers and Fines', PhD thesis Helsinki University of Technology, **2007**.

[174] Sodhi, R. N. S., Time-of-Flight Secondary Ion Mass Spectrometry (Tof-Sims):-Versatility in Chemical and Imaging Surface Analysis. *Analyst* **2004,** *129* (6), 483-487.

[175] Castner, D. G., Surface Science - View from the Edge. *Nature* **2003,** *422* (6928), 129-130.

[176] Belu, A. M.; Graham, D. J.; Castner, D. G., Time-of-Flight Secondary Ion Mass Spectrometry: Techniques and Applications for the Characterization of Biomaterial Surfaces. *Biomaterials* **2003,** *24* (21), 3635-3653.

[177] rehl, T. 'Improvement in Tof-Sims Instrumentation for Analytical Application and Fundamental Research', PhD thesis, Westfälischen-Wilhelms Universität Münster, **2003**.

[178] Pól, J.; Strohalm, M.; Havlíček, V.; Volný, M., Molecular Mass Spectrometry Imaging in Biomedical and Life Science Research. *Histochem. Cell Biol.* **2010,** *134* (5), 423-443.

[179] IONTOF TOFSIMS5, (http://www.ion-tof.com).

[180] Luxembourg, S. L.; Mize, T. H.; Mcdonnell, L. A.; Heeren, R. M. A., High-Spatial Resolution Mass Spectrometric Imaging of Peptide and Protein Distributions on a Surface. *Anal. Chem.* **2004,** *76* (18), 5339-5344.

[181] Saito, K.; Kato, T.; Takamori, H.; Kishimoto, T.; Fukushima, K., A New Analysis of the Depolymerized Fragments of Lignin Polymer Using Tof-Sims. *Biomacromolecules* **2005,** *6* (5), 2688-2696.

[182] Saito, K.; Kato, T.; Tsuji, Y.; Fukushima, K., Identifying the Characteristic Secondary Ions of Lignin Polymer Using Tof-Sims. *Biomacromolecules* **2005,** *6* (2), 678-683.

[183] Tokareva, E. N.; Pranovich, A. V.; Fardim, P.; Danie, G.; Holmbom, B., Analysis of Wood Tissues by Time-of-Flight Secondary Ion Mass Spectrometry. *Holzforschung* **2007,** *61* (6), 647-655.

[184] Saito, K.; Mitsutani, T.; Imai, T.; Matsushita, Y.; Fukushima, K., Discriminating the Indistinguishable Sapwood from Heartwood in Discolored Ancient Wood by Direct Molecular Mapping of Specific Extractives Using Time-of-Flight Secondary Ion Mass Spectrometry. *Anal. Chem.* **2008,** *80* (5), 1552-1557.

[185] Goacher, R. E.; Jeremic, D.; Master, E. R., Expanding the Library of Secondary Ions That Distinguish Lignin and Polysaccharides in Time-of-Flight Secondary Ion Mass Spectrometry Analysis of Wood. *Anal. Chem.* **2010,** *83* (3), 804-812.

[186] Studer, M. H.; Demartini, J. D.; Davis, M. F.; Sykes, R. W.; Davison, B.; Keller, M.; Tuskan, G. A.; Wyman, C. E., Lignin Content in Natural Populus Variants Affects Sugar Release. *PNAS* **2011,** *108* (15), 6300-6305.

[187] Zhou, C.; Li, Q.; Chiang, V. L.; Lucia, L. A.; Griffis, D. P., Chemical and Spatial Differentiation of Syringyl and Guaiacyl Lignins in Poplar Wood Via Time-of-Flight Secondary Ion Mass Spectrometry. *Anal. Chem.* **2011,** *83* (18), 7020-7026.

[188] Saito, K.; Watanabe, Y.; Shirakawa, M.; Matsushita, Y.; Imai, T.; Koike, T.; Sano, Y.; Funada, R.; Fukazawa, K.; Fukushima, K., Direct Mapping of Morphological Distribution of Syringyl and Guaiacyl Lignin in the Xylem of Maple by Time-of-Flight Secondary Ion Mass Spectrometry. *Plant J.* **2012,** *69* (3), 542-552.

[189] Karas, M.; Bachmann, D.; Hillenkamp, F., Influence of the Wavelength in High-Irradiance Ultraviolet-Laser Desorption Mass-Spectrometry of Organic-Molecules. *Anal. Chem.* **1985,** *57* (14), 2935-2939.

[190] Tanaka, K.; Waki, H.; Ido, Y.; Akita, S.; Yoshida, Y.; Yoshida, T.; Matsuo, T., Protein and Polymer Analyses up to M/Z 100 000 by Laser Ionization Time-of-Flight Mass Spectrometry. *Rapid Commun. Mass Spectrom.* **1988,** *2* (8), 151-153.

[191] Dreisewerd, K., The Desorption Process in Maldi. *Chem. Rev.* **2003,** *103* (2), 395-425.

[192] Hillenkamp, F.; Karas, M.; Beavis, R. C.; Chait, B. T., Matrix-Assisted Laser Desorption Ionization Mass-Spectrometry of Biopolymers. *Anal. Chem.* **1991,** *63* (24), A1193-A1202.

[193] Ehring, H.; Karas, M.; Hillenkamp, F., Role of Photoionization and Photochemistry in Ionization Processes of Organic-Molecules and Relevance for Matrix-Assisted Laser Desorption Ionization Mass-Spectrometry. *Org. Mass Spectrom.* **1992,** *27* (4), 472-480.

[194] Knochenmuss, R.; Zenobi, R., Maldi Ionization: The Role of in-Plume Processes. *Chem. Rev.* **2003,** *103* (2), 441-452.

[195] Karas, M.; Kruger, R., Ion Formation in Maldi: The Cluster Ionization Mechanism. *Chem. Rev.* **2003,** *103* (2), 427-439.

[196] National Hihg Magneti Field Laboratory: Agricultural Research Service (http://www.magnet.fsu.edu/education/tutorials/tools/ionization_maldi.html).

[197] Caprioli, R. M.; Farmer, T. B.; Gile, J., Molecular Imaging of Biological Samples: Localization of Peptides and Proteins Using Maldi-Tof Ms. *Anal. Chem.* **1997,** *69* (23), 4751-4760.

[198] O'connor, P. B.; Hillenkamp, F., Maldi Mass Spectrometry Instrumentation. In *Maldi Ms*, Wiley-VCH Verlag GmbH & Co. KGaA, **2007**, pp 29-82.

[199] Sugiura, Y.; Setou, M.; Horigome, D., Methods of Matrix Application. In *Imaging Mass Spectrometry*, Setou, M., Springer Japan, **2010**, pp 71-85.

[200] Heeren, R. M. A.; Smith, D. F.; Stauber, J.; Kükrer-Kaletas, B.; Macaleese, L., Imaging Mass Spectrometry: Hype or Hope? *J. Am. Soc. Mass. Spectrom.* **2009,** *20* (6), 1006-1014.

[201] Karas, M.; Hillenkamp, F., Laser Desorption Ionization of Proteins with Molecular Masses Exceeding 10000 Daltons. *Anal. Chem.* **1988,** *60* (20), 2299-2301.

[202] Stoeckli, M.; Chaurand, P.; Hallahan, D. E.; Caprioli, R. M., Imaging Mass Spectrometry: A New Technology for the Analysis of Protein Expression in Mammalian Tissues. *Nat. Med.* **2001,** *7* (4), 493-496.

[203] Metzger, J. O.; Bicke, C.; Faix, O.; Tuszynski, W.; Angermann, R.; Karas, M.; Strupat, K., Matrix-Assisted Laser Desorption Mass-Spectrometry of Lignins. *Angew. Chem. Int. Ed.* **1992,** *31* (6), 762-764.

[204] Yoshioka, K.; Ando, D.; Watanabe, T., A Comparative Study of Matrix- and Nano-Assisted Laser Desorption/Ionisation Time-of-Flight Mass Spectrometry of Isolated and Synthetic Lignin. *Phytochem. Anal.* **2012,** *23* (3), 248-253.

[205] Sumi, T.; Sakaki, T.; Ohba, H.; Shibata, M., Application of Matrix-Assisted Laser Desorption/Ionization Time-of-Flight Mass Spectrometry to Insoluble Glucose Oligomers in Decomposed Cellulose. *Rapid Commun. Mass Spectrom.* **2000,** *14* (19), 1823-1827.

[206] Jung, S.; Chen, Y.; Sullards, M. C.; Ragauskas, A. J., Direct Analysis of Cellulose in Poplar Stem by Matrix-Assisted Laser Desorption/Ionization Imaging Mass Spectrometry. *Rapid Commun. Mass Spectrom.* **2010,** *24* (22), 3230-3236.

[207] Lunsford, K. A.; Peter, G. F.; Yost, R. A., Direct Matrix-Assisted Laser Desorption/Ionization Mass Spectrometric Imaging of Cellulose and Hemicellulose in Populus Tissue. *Anal. Chem.* **2011,** *83* (17), 6722-6730.

[208] Yamada, M.; Yao, I.; Hayasaka, T.; Ushijima, M.; Matsuura, M.; Takada, H.; Shikata, N.; Setou, M.; Kwon, A. H.; Ito, S., Identification of Oligosaccharides from Histopathological Sections by Maldi Imaging Mass Spectrometry. *Anal. Bioanal. Chem.* **2012,** *402* (5), 1921-1930.

[209] Burrell, M. M.; Earnshaw, C. J.; Clench, M. R., Imaging Matrix Assisted Laser Desorption Ionization Mass Spectrometry: A Technique to Map Plant Metabolites within Tissues at High Spatial Resolution. *J. Exp. Bot.* **2007,** *58* (4), 757-763.

[210] Tokareva, E. N.; Fardim, P.; Pranovich, A.; Fagerholm, H. P.; Daniel, G.; Holmbom, B., Imaging of Wood Tissue by Tof-Sims: Critical Evaluation and Development of Sample Preparation Techniques. *Appl. Surf. Sci.* **2007,** *253* (18), 7569-7577.

[211] Levitin, N., The Extractives of Birch Aspen, Elm and Maple: Review and Discussion. *Pulp Pap.-Canada* **1970,** *71* (16), 81.

[212] Zhang, D. C.; Pu, Y. Q.; Chai, X. S.; Naithani, V.; Jameel, H.; Ragauskas, A. J., Elucidating Carboxylic Acid Profiles for Extended Oxygen Delignification of High-Kappa Softwood Kraft Pulps. *Holzforschung* **2006,** *60* (2), 123-129.

[213] Vuorinen, T.; Alen, R., Carbohydrates. In *Analytical Methods in Wood Chemistry, Pulping and Paper Making*, Sjöström, E.; Alen, R., Springer-Verlag, Berlin: Berlin, **1998**.

[214] Liitia, T.; Maunu, S. L.; Hortling, B.; Tamminen, T.; Pekkala, O.; Varhimo, A., Cellulose Crystallinity and Ordering of Hemicelluloses in Pine and Birch Pulps as Revealed by Solid-State Nmr Spectroscopic Methods. *Cellulose* **2003,** *10* (4), 307-316.

[215] Tucker, M.; Farmer, J.; Keller, F.; Schell, D.; Nguyan, Q., Comparison of Yellow Poplar Pretreatment between Nrel Digester and Sunds Hydrolyzer. *Appl. Biochem. Biotechnol.* **1998,** *70-72* (1), 25-35.

[216] Söderström, J.; Pilcher, L.; Galbe, M.; Zacchi, G., Two-Step Steam Pretreatment of Softwood by Dilute H2so4 Impregnation for Ethanol Production. *Biomass Bioenerg.* **2003,** *24* (6), 475-486.

[217] Davis, M. W., A Rapid Modified Method for Compositional Carbohydrate Analysis of Lignocellulosics by High Ph Anion-Exchange Chromatography with Pulsed Amperometric Detection (Hpaec/Pad). *J. Wood Chem. Technol.* **1998,** *18* (2), 235-252.

[218] Feng, D.; Marshburn, D.; Jen, D.; Weinberg, R. J.; Taylor, R. M.; Burette, A., Stepping into the Third Dimension. *J. Neurosci.* **2007,** *27* (47), 12757-12760.

[219] Chen, Y. F.; Allegood, J.; Liu, Y.; Wang, E.; Cachon-Gonzalez, B.; Cox, T. M.; Merrill, A. H.; Sullards, M. C., Imaging Maldi Mass Spectrometry Using an Oscillating Capillary Nebulizer Matrix Coating System and Its Application to Analysis of Lipids in Brain from a Mouse Model of Tay-Sachs/Sandhoff Disease. *Anal. Chem.* **2008,** *80* (8), 2780-2788.

[220] Mohan, D.; Pittman, C. U.; Steele, P. H., Pyrolysis of Wood/Biomass for Bio-Oil: A Critical Review. *Energ. Fuel.* **2006,** *20* (3), 848-889.

[221] Palm, M.; Zacchi, G., Extraction of Hemicellulosic Oligosaccharides from Spruce Using Microwave Oven or Steam Treatment. *Biomacromolecules* **2003,** *4* (3), 617-623.

[222] Kataoka, Y.; Kondo, T., Ft-Ir Microscopic Analysis of Changing Cellulose Crystalline Structure During Wood Cell Wall Formation. *Macromolecules* **1998,** *31* (3), 760-764.

[223] Nishiyama, Y.; Sugiyama, J.; Chanzy, H.; Langan, P., Crystal Structure and Hydrogen Bonding System in Cellulose 1(Alpha), from Synchrotron X-Ray and Neutron Fiber Diffraction. *J. Am. Chem. Soc.* **2003,** *125* (47), 14300-14306.

[224] Laine, J.; Stenius, P.; Carlsson, G.; Strom, G., Surface Characterization of Unbleached Kraft Pulps by Means of Esca. *Cellulose* **1994,** *1* (2), 145-160.

[225] Whittaker, A. K.; Webb, G. A., *Modern Magnetic Resonance: The Structure of Polymer Networks*. **2006**, 583-589.

[226] Duchesne, I.; Daniel, G., Changes in Surface Ultrastructure of Norway Spruce Fibres During Kraft Pulping - Visualisation by Field Emission-Sem. *Nord. Pulp Pap. Res. J.* **2000,** *15* (1), 54-61.

[227] Kallavus, U.; Gravitis, J., A Comparative Investigation of the Ultrastructure of Steam Exploded Wood with Light, Scanning and Transmission Electron-Microscopy. *Holzforschung* **1995,** *49* (2), 182-188.

[228] Singh, A. P.; Daniel, G., The S2 Layer in the Tracheid Walls of Picea Abies Wood: Inhomogeneity in Lignin Distribution and Cell Wall Microstructure. *Holzforschung* **2001,** *55* (4), 373-378.

[229] Fardim, P.; Gustafsson, J.; Von Schoultz, S.; Peltonen, J.; Holmbom, B., Extractives on Fiber Surfaces Investigated by Xps, Tof-Sims and Afm. *Colloid. Surface. A.* **2005,** *255* (1-3), 91-103.

[230] Fardim, P.; Duran, N., Modification of Fibre Surfaces During Pulping and Refining as Analysed by SEM, XPS and ToF-SIMS. *Colloid. Surface. A.* **2003,** *223* (1-3), 263-276.

[231] Gou, J. Y.; Park, S.; Yu, X. H.; Miller, L. M.; Liu, C. J., Compositional Characterization and Imaging of "Wall-Bound" Acylesters of Populus Trichocarpa Reveal Differential Accumulation of Acyl Molecules in Normal and Reactive Woods. *Planta* **2008,** *229* (1), 15-24.

[232] Teleman, A.; Lundqvist, J.; Tjerneld, F.; Stalbrand, H.; Dahlman, O., Characterization of Acetylated 4-O-Methylglucuronoxylan Isolated from Aspen Employing H-1 and C-13 NMR Spectroscopy. *Carbohydr. Res.* **2000,** *329* (4), 807-815.

[233] Robert, P.; Marquis, M.; Barron, C.; Guillon, F.; Saulnier, L., Ft-Ir Investigation of Cell Wall Polysaccharides from Cereal Grains. Arabinoxylan Infrared Assignment. *J. Agric. Food. Chem.* **2005,** *53* (18), 7014-7018.

[234] Philippe, S.; Robert, P.; Barron, C.; Saulnier, L.; Guillon, F., Deposition of Cell Wall Polysaccharides in Wheat Endosperm During Grain Development: Fourier Transform-Infrared Microspectroscopy Study. *J. Agric. Food. Chem.* **2006,** *54* (6), 2303-2308.

[235] Li, J. B.; Henriksson, G.; Gellerstedt, G., Lignin Depolymerization / Repolymerization and Its Critical Role for Delignification of Aspen Wood by Steam Explosion. *Bioresour. Technol.* **2007,** *98* (16), 3061-3068.

[236] Kleen, Internation Symposium on Cellulose and Lignocellulosics Chemistry: Kunming, China, **2000**; pp 290-294.

[237] Kleen, M., Surface Lignin and Extractives on Hardwood Rdh Kraft Pulp Chemically Characterized by Tof-Sims. *Holzforschung* **2005,** *59* (5), 481-487.

[238] Gilmore, I. S.; Seah, M. P., Static Sims Inter-Laboratory Study. *Surf. Interface Anal.* **2000,** *29* (9), 624-637.

[239] Kumar, P.; Barrett, D. M.; Delwiche, M. J.; Stroeve, P., Methods for Pretreatment of Lignocellulosic Biomass for Efficient Hydrolysis and Biofuel Production. *Ind. Eng. Chem. Res.* **2009,** *48* (8), 3713-3729.

[240] Brunecky, R.; Vinzant, T. B.; Porter, S. F.; Donohoe, B. S.; Johnson, D. K.; Himmel, M. E., Redistribution of Xylan in Maize Cell Walls During Dilute Acid Pretreatment. *Biotechnol. Bioeng.* **2009,** *102* (6), 1537-1543.

[241] Awano, T.; Takabe, K.; Fujita, M., Localization of Glucuronoxylans in Japanese Beech Visualized by Immunogold Labelling. *Protoplasma* **1998,** *202* (3-4), 213-222.

[242] Ruel, K.; Chevalier-Billosta, V.; Guillemin, F.; Berrio-Sierra, J.; Joseleau, J.-P., The Wood Cell Wall at the Ultrastructural Scale - Formation and Topochemical Organization. *Maderas-Cienc. tecnol.* **2006,** *8*, 107-116.

[243] Claassen, P. a. M.; Van Lier, J. B.; Lopez Contreras, A. M.; Van Niel, E. W. J.; Sijtsma, L.; Stams, A. J. M.; De Vries, S. S.; Weusthuis, R. A., Utilisation of Biomass for the Supply of Energy Carriers. *Appl. Microbiol. Biotechnol.* **1999,** *52* (6), 741-755.

[244] Bobleter, O.; Niesner, R.; Röhr, M., The Hydrothermal Degradation of Cellulosic Matter to Sugars and Their Fermentative Conversion to Protein. *J. Appl. Polym. Sci.* **1976,** *20* (8), 2083-2093.

[245] Liu, C. G.; Wyman, C. E., The Effect of Flow Rate of Compressed Hot Water on Xylan, Lignin, and Total Mass Removal from Corn Stover. *Ind. Eng. Chem. Res.* **2003,** *42* (21), 5409-5416.

[246] Yang, B.; Wyman, C. E., Effect of Xylan and Lignin Removal by Batch and Flowthrough Pretreatment on the Enzymatic Digestibility of Corn Stover Cellulose. *Biotechnol. Bioeng.* **2004,** *86* (1), 88-95.

[247] Chandra, R. P.; Bura, R.; Mabee, W. E.; Berlin, A.; Pan, X.; Saddler, J. N., Substrate Pretreatment: The Key to Effective Enzymatic Hydrolysis of Lignocellulosics? In *Biofuels*, Advances in Biochemical Engineering-BiotechnologyOlsson, L., **2007**; Vol. 108, pp 67-93.

[248] Donohoe, B. S.; Decker, S. R.; Tucker, M. P.; Himmel, M. E.; Vinzant, T. B., Visualizing Lignin Coalescence and Migration through Maize Cell Walls Following Thermochemical Pretreatment. *Biotechnol. Bioeng.* **2008,** *101* (5), 913-925.

[249] Biofuels Research Advisory Council, Biofuels in the European Union: A Vision for 2030 and Beyond (http://www.Biomatnet.Org/Publications/1919rep.Pdf).

[250] Roger, P.; Mandla, T.; James, H.; Roger, R.; Jeffrey, R., Cell Wall Chemistry. In *Handbook of Wood Chemistry and Wood Composites*, CRC Press, **2005**.

[251] Hendriks, A. T. W. M.; Zeeman, G., Pretreatments to Enhance the Digestibility of Lignocellulosic Biomass. *Bioresour. Technol.* **2009,** *100* (1), 10-18.

[252] Breitenstein, D.; Rommel, C. E.; Möllers, R.; Wegener, J.; Hagenhoff, B., The Chemical Composition of Animal Cells and Their Intracellular Compartments Reconstructed from 3d Mass Spectrometry. *Angew. Chem. Int. Ed.* **2007,** *46* (28), 5332-5335.

[253] Chang, V.; Holtzapple, M., Fundamental Factors Affecting Biomass Enzymatic Reactivity. *Appl. Biochem. Biotechnol.* **2000,** *84-86* (1), 5-37.

[254] Plomion, C.; Leprovost, G.; Stokes, A., Wood Formation in Trees. *Plant Physiology* **2001,** *127* (4), 1513-1523.

[255] Pilate, G.; Dejardin, A.; Laurans, F.; Leple, J. C., Tension Wood as a Model for Functional Genomics of Wood Formation. *New Phytol.* **2004,** *164* (1), 63-72.

[256] Pilate, G.; Chabbert, B.; Cathala, B.; Yoshinaga, A.; Leplé, J.-C.; Laurans, F.; Lapierre, C.; Ruel, K., Lignification and Tension Wood. *C. R. Biol.* **2004,** *327* (9–10), 889-901.

[257] Sluiter, A.; Hames, B.; Ruiz, R.; Scarlata, C.; Sluiter, J.; Templeton, D.; Crocker, D. Determination of Structural Carbohydrates and Lignin in Biomass (http://www.nrel.gov/biomass/pdfs/42618.pdf (accessed TP-510-42618)).

[258] Mellerowicz, E. J.; Gorshkova, T. A., Tensional Stress Generation in Gelatinous Fibres: A Review and Possible Mechanism Based on Cell-Wall Structure and Composition. *J. Exp. Bot.* **2012,** *63* (2), 551-565.

[259] Foston, M.; Hubbell, C. A.; Samuel, R.; Jung, S.; Fan, H.; Ding, S.-Y.; Zeng, Y.; Jawdy, S.; Davis, M.; Sykes, R.; Gjersing, E.; Tuskan, G. A.; Kalluri, U.; Ragauskas, A. J., Chemical, Ultrastructural and Supramolecular Analysis of Tension Wood in Populus Tremula X Alba as a Model Substrate for Reduced Recalcitrance. *Energ. Environ. Sci.* **2011,** *4* (12), 4962-4971.

[260] Mohan, D.; Pittman, C. U.; Steele, P. H., Pyrolysis of Wood/Biomass for Bio-Oil: A Critical Review. *Energ. Fuel.* **2006,** *20* (3), 848-889.

[261] Perlack, R. D.; Wright, L. L.; Turhollow, A. F.; Graham, R. L.; Stokes, B. J.; Erbach, D. C., Biomas as Feedstock for a Bioenergy and Bioproducts Industry: The Technical Feasibility of a Billion-Ton Annual Supply **2005**. (http://feedstockreview.ornl.gov/pdf/billion_ton_vision.pdf).

[262] Harvey, D. J.; Naven, T. J. P.; Küster, B., Identification of Oligosaccharides by Matrix-Assisted Laser Desorption Ionization and Electrospray Ms. *Biochem. Soc. Trans.* **1996,** *24* (3), 905-912.

[263] Stahl, B.; Linos, A.; Karas, M.; Hillenkamp, F.; Steup, M., Analysis of Fructans from Higher Plants by Matrix-Assisted Laser Desorption/Ionization Mass Spectrometry. *Anal. Biochem.* **1997,** *246* (2), 195-204.

[264] Harvey, D. J., Matrix-Assisted Laser Desorption/Ionization Mass Spectrometry of Carbohydrates. *Mass Spectrom. Rev.* **1999,** *18* (6), 349-450.

[265] Khatib-Shahidi, S.; Andersson, M.; Herman, J. L.; Gillespie, T. A.; Caprioli, R. M., Direct Molecular Analysis of Whole-Body Animal Tissue Sections by Imaging Maldi Mass Spectrometry. *Anal. Chem.* **2006,** *78* (18), 6448-6456.

[266] Ng, K. M.; Liang, Z. T.; Lu, W.; Tang, H. W.; Zhao, Z. Z.; Che, C. M.; Cheng, Y. C., In Vivo Analysis and Spatial Profiling of Phytochemicals in Herbal Tissue by Matrix-Assisted Laser Desorption/Ionization Mass Spectrometry. *Anal. Chem.* **2007,** *79* (7), 2745-2755.

[267] Mullen, A. K.; Clench, M. R.; Crosland, S.; Sharples, K. R., Determination of Agrochemical Compounds in Soya Plants by Imaging Matrix-Assisted Laser Desorption/Ionisation Mass Spectrometry. *Rapid Commun. Mass Spectrom.* **2005,** *19* (18), 2507-2516.

[268] Anderson, D. M. G.; Carolan, V. A.; Crosland, S.; Sharples, K. R.; Clench, M. R., Examination of the Distribution of Nicosulfuron in Sunflower Plants by Matrix-Assisted Laser Desorption/Ionisation Mass Spectrometry Imaging. *Rapid Commun. Mass Spectrom.* **2009,** *23* (9), 1321-1327.

[269] Robinson, S.; Warburton, K.; Seymour, M.; Clench, M.; Thomas-Oates, J., Localization of Water-Soluble Carbohydrates in Wheat Stems Using Imaging Matrix-Assisted Laser Desorption Ionization Mass Spectrometry. *New Phytol.* **2007,** *173* (2), 438-444.

[270] Momcilovic, D.; Schagerlof, H.; Wittgren, B.; Wahlund, K. G.; Brinkmalm, G., Improved Chemical Analysis of Cellulose Ethers Using Dialkylamine Derivatization and Mass Spectrometry. *Biomacromolecules* **2005,** *6* (5), 2793-2799.

[271] Klemm, D.; Heublein, B.; Fink, H. P.; Bohn, A., Cellulose: Fascinating Biopolymer and Sustainable Raw Material. *Angew. Chem. Int. Ed.* **2005,** *44* (22), 3358-3393.

[272] Broberg, S.; Koch, K.; Andersson, R.; Kenne, L., A Comparison between Maldi-Tof Mass Spectrometry and Hpaec-Pad Analysis of Debranched Starch. *Carbohydr. Polym.* **2000,** *43* (3), 285-289.

[273] Sporns, P.; Wang, J., Exploring New Frontiers in Food Analysis Using Maldi-Ms. *Food Res. Int.* **1998,** *31* (3), 181-189.

[274] Zhang, W.; Liang, M.; Lu, C., Morphological and Structural Development of Hardwood Cellulose During Mechanochemical Pretreatment in Solid State through Pan-Milling. *Cellulose* **2007,** *14* (5), 447-456.

[275] Leple, J.-C.; Dauwe, R.; Morreel, K.; Storme, V.; Lapierre, C.; Pollet, B.; Naumann, A.; Kang, K.-Y.; Kim, H.; Ruel, K.; Lefebvre, A.; Joseleau, J.-P.; Grima-Pettenati, J.; De Rycke, R.; Andersson-Gunneras, S.; Erban, A.; Fehrle, I.; Petit-Conil, M.; Kopka, J.; Polle, A.; Messens, E.; Sundberg, B.; Mansfield, S. D.; Ralph, J.; Pilate, G.; Boerjan, W., Downregulation of Cinnamoyl-Coenzyme a Reductase in Poplar: Multiple-Level Phenotyping Reveals Effects on Cell Wall Polymer Metabolism and Structure. *Plant Cell* **2007,** *19* (11), 3669-3691.

JOHN WILEY AND SONS LICENSE
TERMS AND CONDITIONS

Nov 07, 2012

This is a License Agreement between Seokwon Jung ("You") and John Wiley and Sons ("John Wiley and Sons") provided by Copyright Clearance Center ("CCC"). The license consists of your order details, the terms and conditions provided by John Wiley and Sons, and the payment terms and conditions.

All payments must be made in full to CCC. For payment instructions, please see information listed at the bottom of this form.

License Number	3023820387121
License date	Nov 07, 2012
Licensed content publisher	John Wiley and Sons
Licensed content publication	Angewandte Chemie International Edition
Book title	
Licensed content author	Seokwon Jung,Marcus Foston,Udaya C. Kalluri,Gerald A. Tuskan,Arthur J. Ragauskas
Licensed content date	Oct 25, 2012
Start page	n/a
End page	n/a
Type of use	Dissertation/Thesis
Requestor type	Author of this Wiley article
Format	Electronic
Portion	Full article
Will you be translating?	No
Order reference number	
Total	0.00 USD

Terms and Conditions

TERMS AND CONDITIONS

This copyrighted material is owned by or exclusively licensed to John Wiley & Sons, Inc. or one of its group companies (each a "Wiley Company") or a society for whom a Wiley Company has exclusive publishing rights in relation to a particular journal (collectively WILEY"). By clicking "accept" in connection with completing this licensing transaction, you agree that the following terms and conditions apply to this transaction (along with the billing and payment terms and conditions established by the Copyright Clearance Center Inc., ("CCC's Billing and Payment terms and conditions"), at the time that you opened your Rightslink account (these are available at any time at http://myaccount.copyright.com)

Terms and Conditions

JOHN WILEY AND SONS LICENSE
TERMS AND CONDITIONS

Oct 09, 2012

This is a License Agreement between Seokwon Jung ("You") and John Wiley and Sons ("John Wiley and Sons") provided by Copyright Clearance Center ("CCC"). The license consists of your order details, the terms and conditions provided by John Wiley and Sons, and the payment terms and conditions.

All payments must be made in full to CCC. For payment instructions, please see information listed at the bottom of this form.

License Number	3004590583053
License date	Oct 09, 2012
Licensed content publisher	John Wiley and Sons
Licensed content publication	Rapid Communications in Mass Spectrometry
Book title	
Licensed content author	Seokwon Jung,Yanfeng Chen,M. Cameron Sullards,Arthur J. Ragauskas
Licensed content date	Oct 19, 2010
Start page	3230
End page	3236
Type of use	Dissertation/Thesis
Requestor type	Author of this Wiley article
Format	Print and electronic
Portion	Full article
Will you be translating?	No
Order reference number	
Total	0.00 USD

Terms and Conditions

TERMS AND CONDITIONS

This copyrighted material is owned by or exclusively licensed to John Wiley & Sons, Inc. or one of its group companies (each a "Wiley Company") or a society for whom a Wiley Company has exclusive publishing rights in relation to a particular journal (collectively WILEY"). By clicking "accept" in connection with completing this licensing transaction, you agree that the following terms and conditions apply to this transaction (along with the billing and payment terms and conditions established by the Copyright Clearance Center Inc., ("CCC's Billing and Payment terms and conditions"), at the time that you opened your Rightslink account (these are available at any time at http://myaccount.copyright.com)

Terms and Conditions

JOHN WILEY AND SONS LICENSE
TERMS AND CONDITIONS

Nov 08, 2012

This is a License Agreement between Seokwon Jung ("You") and John Wiley and Sons ("John Wiley and Sons") provided by Copyright Clearance Center ("CCC"). The license consists of your order details, the terms and conditions provided by John Wiley and Sons, and the payment terms and conditions.

All payments must be made in full to CCC. For payment instructions, please see information listed at the bottom of this form.

License Number	3024070511843
License date	Nov 08, 2012
Licensed content publisher	John Wiley and Sons
Licensed content publication	Helvetica Chimica Acta
Book title	
Licensed content author	Kurt H. Meyer,Lore Misch
Licensed content date	Oct 24, 2004
Start page	232
End page	244
Type of use	Dissertation/Thesis
Requestor type	University/Academic
Format	Electronic
Portion	Figure/table
Number of figures/tables	1
Number of extracts	
Original Wiley figure/table number(s)	Figure 2
Will you be translating?	No
Order reference number	
Total	0.00 USD

Terms and Conditions

TERMS AND CONDITIONS

This copyrighted material is owned by or exclusively licensed to John Wiley & Sons, Inc. or one of its group companies (each a "Wiley Company") or a society for whom a Wiley Company has exclusive publishing rights in relation to a particular journal (collectively WILEY"). By clicking "accept" in connection with completing this licensing transaction, you agree that the following

ELSEVIER LICENSE
TERMS AND CONDITIONS

Nov 08, 2012

This is a License Agreement between Seokwon Jung ("You") and Elsevier ("Elsevier") provided by Copyright Clearance Center ("CCC"). The license consists of your order details, the terms and conditions provided by Elsevier, and the payment terms and conditions.

All payments must be made in full to CCC. For payment instructions, please see information listed at the bottom of this form.

Supplier	Elsevier Limited The Boulevard,Langford Lane Kidlington,Oxford,OX5 1GB,UK
Registered Company Number	1982084
Customer name	Seokwon Jung
Customer address	500 10th street NW Atlanta, GA 30332
License number	3024351340756
License date	Nov 08, 2012
Licensed content publisher	Elsevier
Licensed content publication	Polymer
Licensed content title	Geometric phase analysis of lattice images from algal cellulose microfibrils
Licensed content author	Tomoya Imai,Jean-Luc Putaux,Junji Sugiyama
Licensed content date	March 2003
Licensed content volume number	44
Licensed content issue number	6
Number of pages	9
Start Page	1871
End Page	1879
Type of Use	reuse in a thesis/dissertation
Portion	figures/tables/illustrations
Number of figures/tables/illustrations	1
Format	electronic
Are you the author of this Elsevier article?	No

Will you be translating?	No
Order reference number	
Title of your thesis/dissertation	SURFACE CHARACTERIZATION OF BIOMASS BY IMAGING MASS SPECTROMETRY
Expected completion date	Dec 2012
Estimated size (number of pages)	200
Elsevier VAT number	GB 494 6272 12
Permissions price	0.00 USD
VAT/Local Sales Tax	0.0 USD / 0.0 GBP
Total	0.00 USD
Terms and Conditions	

INTRODUCTION

1. The publisher for this copyrighted material is Elsevier. By clicking "accept" in connection with completing this licensing transaction, you agree that the following terms and conditions apply to this transaction (along with the Billing and Payment terms and conditions established by Copyright Clearance Center, Inc. ("CCC"), at the time that you opened your Rightslink account and that are available at any time at http://myaccount.copyright.com).

GENERAL TERMS

2. Elsevier hereby grants you permission to reproduce the aforementioned material subject to the terms and conditions indicated.

3. Acknowledgement: If any part of the material to be used (for example, figures) has appeared in our publication with credit or acknowledgement to another source, permission must also be sought from that source. If such permission is not obtained then that material may not be included in your publication/copies. Suitable acknowledgement to the source must be made, either as a footnote or in a reference list at the end of your publication, as follows:

"Reprinted from Publication title, Vol /edition number, Author(s), Title of article / title of chapter, Pages No., Copyright (Year), with permission from Elsevier [OR APPLICABLE SOCIETY COPYRIGHT OWNER]." Also Lancet special credit - "Reprinted from The Lancet, Vol. number, Author(s), Title of article, Pages No., Copyright (Year), with permission from Elsevier."

4. Reproduction of this material is confined to the purpose and/or media for which permission is hereby given.

5. Altering/Modifying Material: Not Permitted. However figures and illustrations may be altered/adapted minimally to serve your work. Any other abbreviations, additions, deletions and/or any other alterations shall be made only with prior written authorization of Elsevier Ltd. (Please contact Elsevier at permissions@elsevier.com)

6. If the permission fee for the requested use of our material is waived in this instance, please be advised that your future requests for Elsevier materials may attract a fee.

SPRINGER LICENSE
TERMS AND CONDITIONS

Nov 08, 2012

This is a License Agreement between Seokwon Jung ("You") and Springer ("Springer") provided by Copyright Clearance Center ("CCC"). The license consists of your order details, the terms and conditions provided by Springer, and the payment terms and conditions.

All payments must be made in full to CCC. For payment instructions, please see information listed at the bottom of this form.

License Number	3024380966858
License date	Nov 08, 2012
Licensed content publisher	Springer
Licensed content publication	Springer eBook
Licensed content title	Hemicellulose
Licensed content author	Anna Ebringerová
Licensed content date	Sep 1, 2005
Type of Use	Thesis/Dissertation
Portion	Figures
Author of this Springer article	No
Order reference number	62
Title of your thesis / dissertation	SURFACE CHARACTERIZATION OF BIOMASS BY IMAGING MASS SPECTROMETRY
Expected completion date	Dec 2012
Estimated size(pages)	200
Total	0.00 USD
Terms and Conditions	

Introduction

The publisher for this copyrighted material is Springer Science + Business Media. By clicking "accept" in connection with completing this licensing transaction, you agree that the following terms and conditions apply to this transaction (along with the Billing and Payment terms and conditions established by Copyright Clearance Center, Inc. ("CCC"), at the time that you opened your Rightslink account and that are available at any time at http://myaccount.copyright.com).

Limited License

With reference to your request to reprint in your thesis material on which Springer Science and Business Media control the copyright, permission is granted, free of charge, for the use indicated in your enquiry.

Copyright Clearance Center

1 PAYMENT 2 REVIEW 3 CONFIRMATION

Step 3: Order Confirmation

Thank you for your order! A confirmation for your order will be sent to your account email address. If you have questions about your order, you can call us at 978-646-2600, M-F between 8:00 AM and 6:00 PM (Eastern), or write to us at info@copyright.com.

Confirmation Number: 11044037
Order Date: 11/08/2012

If you pay by credit card, your order will be finalized and your card will be charged within 24 hours. If you pay by invoice, you can change or cancel your order until the invoice is generated.

Payment Information

Seokwon Jung
hansom1007@gmail.com
+1 (404)6062814
Payment Method: n/a

Order Details

Annual Review of Chemical and Biomolecular Engineering

Order detail ID:	63168569
Order License Id:	3024400179023
ISSN:	1947-5438
Publication Type:	Journal
Volume:	
Issue:	
Start page:	
Publisher:	Annual Reviews

Permission Status: Granted

Permission type: Republish or display content
Type of use: Republish in a thesis/dissertation

Requestor type	Academic institution
Format	Electronic
Portion	image/photo
Number of images/photos requested	1
Title or numeric reference of the portion(s)	Figure 3
Editor of portion(s)	n/a
Author of portion(s)	n/a
Volume of serial or monograph	n/a
Page range of portion	1 page in total 200pp
Publication date of portion	1 data in total 100
Rights for	Main product
Duration of use	Life of current edition
Creation of copies for the disabled	no
With minor editing privileges	no
For distribution to	Worldwide
In the following language(s)	Original language of publication

With incidental promotional use	no
Lifetime unit quantity of new product	0 to 499
Made available in the following markets	n/a
The requesting person/organization	Georgia Institute of Technology
Order reference number	
Author/Editor	Seokwon Jung
The proposed price	n/a
Title	SURFACE CHARACTERIZATION OF BIOMASS BY IMAGING MASS SPECTROMETRY
Publisher	Georgia Institute of Technology
Expected publication date	Dec 2012
Estimated size (pages)	200

Note: This item will be invoiced or charged separately through CCC's **RightsLink** service. More info $ 0.00

Total order items: 1 **Order Total: $ 0.00**

Copyright Clearance Center

1 PAYMENT 2 REVIEW 3 CONFIRMATION

Step 3: Order Confirmation

Thank you for your order! A confirmation for your order will be sent to your account email address. If you have questions about your order, you can call us at 978-646-2600, M-F between 8:00 AM and 6:00 PM (Eastern), or write to us at info@copyright.com.

Confirmation Number: 11044020
Order Date: 11/08/2012

If you pay by credit card, your order will be finalized and your card will be charged within 24 hours. If you pay by invoice, you can change or cancel your order until the invoice is generated.

Payment Information

Seokwon Jung
hansom1007@gmail.com
+1 (404)6062814
Payment Method: n/a

Order Details

Annual review of plant biology

Order detail ID:	63168497
Order License Id:	3024390264321
ISSN:	1543-5008
Publication Type:	Journal
Volume:	
Issue:	
Start page:	
Publisher:	ANNUAL REVIEWS

Permission Status: Granted

Permission type: Republish or display content
Type of use: Republish in a thesis/dissertation

Requestor type	Academic institution
Format	Electronic
Portion	chart/graph/table/figure
Number of charts/graphs/tables/figures	1
Title or numeric reference of the portion(s)	Table 1
Editor of portion(s)	n/a
Author of portion(s)	n/a
Volume of serial or monograph	n/a
Page range of portion	1 page in total 200pp
Publication date of portion	1 data in total 100
Rights for	Main product
Duration of use	Life of current edition
Creation of copies for the disabled	no
With minor editing privileges	no
For distribution to	Worldwide
In the following language(s)	Original language of publication

With incidental promotional use	no
Lifetime unit quantity of new product	0 to 499
Made available in the following markets	n/a
The requesting person/organization	Georgia Institute of Technology
Order reference number	
Author/Editor	Seokwon Jung
The proposed price	n/a
Title	SURFACE CHARACTERIZATION OF BIOMASS BY IMAGING MASS SPECTROMETRY
Publisher	Georgia Institute of Technology
Expected publication date	Dec 2012
Estimated size (pages)	200

Note: This item will be invoiced or charged separately through CCC's **RightsLink** service. More info $ 0.00

Total order items: 1 **Order Total: $ 0.00**

JOHN WILEY AND SONS LICENSE
TERMS AND CONDITIONS

Nov 08, 2012

This is a License Agreement between Seokwon Jung ("You") and John Wiley and Sons ("John Wiley and Sons") provided by Copyright Clearance Center ("CCC"). The license consists of your order details, the terms and conditions provided by John Wiley and Sons, and the payment terms and conditions.

All payments must be made in full to CCC. For payment instructions, please see information listed at the bottom of this form.

License Number	3024410182838
License date	Nov 08, 2012
Licensed content publisher	John Wiley and Sons
Licensed content publication	Wiley Books
Book title	Surface Analysis: The Principal Techniques, 2nd Edition
Licensed content author	John C. Vickerman (Editor), Ian Gilmore (Co-Editor)
Licensed content date	May 1, 2009
Type of use	Dissertation/Thesis
Requestor type	University/Academic
Format	Electronic
Portion	Figure/table
Number of figures/tables	1
Number of extracts	
Original Wiley figure/table number(s)	Table 4.1
Will you be translating?	No
Order reference number	
Total	0.00 USD

Terms and Conditions

TERMS AND CONDITIONS

This copyrighted material is owned by or exclusively licensed to John Wiley & Sons, Inc. or one of its group companies (each a "Wiley Company") or a society for whom a Wiley Company has exclusive publishing rights in relation to a particular journal (collectively WILEY"). By clicking "accept" in connection with completing this licensing transaction, you agree that the following terms and conditions apply to this transaction (along with the billing and payment terms and conditions established by the Copyright Clearance Center Inc., ("CCC's Billing and Payment terms and conditions"), at the time that you opened your Rightslink account (these are available at any time at http://myaccount.copyright.com)